Technische Universität München
Institut für Molekulare Immunologie

DISSERTATION

LIVER-RESIDENT CD8$^+$ T CELLS IN RESOLVED AND PERSISTENT VIRAL INFECTION OF THE LIVER

MIRIAM BOSCH

Technische Universität München

Fakultät für Medizin

Liver-resident CD8$^+$ T cells in resolved and persistent viral infection of the liver

Miriam Bosch

Vollständiger Abdruck der von der Fakultät für Medizin der Technischen Universität München zur Erlangung des akademischen Grades einer Doktorin der Naturwissenschaften (Dr. rer. nat.) genehmigten Dissertation.

Vorsitz: Prof. Dr. Jürgen Ruland

Prüfer*innen der Dissertation:

1. Prof. Dr. Percy A. Knolle
2. Prof. Dr. Dietmar Zehn

Die Dissertation wurde am 04.02.2021 bei der Technischen Universität München eingereicht und durch die Fakultät für Medizin am 13.07.2021 angenommen.

Abstract

Tissue-resident memory T cells (T_{RM}) and effector memory T cells (T_{EM}) emerge after resolved viral infections and remain in the organism for long-term protection against subsequent infections with the same virus. In contrast to circulating T_{EM} cells, T_{RM} cells stay at the infection site to support efficient immune surveillance of the respective tissue and provide more rapid immune responses during a second infection. Due to their fast reaction towards pathogen re-encounter, T_{RM} cells have been described as “first responders” in tissues, releasing granzymes to kill infected cells and cytokines to recruit further immune cells to the site of infection. Hence, T_{RM} cells are considered potent effector T cells in local immunity during secondary immune responses. In contrast, virus-specific T cell responses during persistent viral infection, such as chronic Hepatitis B virus (HBV) infection, are described as weak and are characterized by low numbers of antigen-specific T cells with reduced effector functions.

Here, liver-resident T cells and T_{EM} cells were analyzed after persistent compared to resolved viral infection of the liver in experimental model systems with the aim to determine also mechanisms leading to weak T cell responses during chronic HBV infection and identify potential therapeutic targets. T_{RM} and T_{EM} cells were analyzed in preclinical adenovirus-based infection model systems, where either the nominal antigen ovalbumin or the entire HBV genome were delivered into murine hepatocytes. For both models, a persistent infection was compared to an acute-resolving infection course.

After resolved viral infections of the liver, I detected T_{RM}-like cells marked by CXCR6 expression and T_{EM} cells expressing CX_3CR1. Of note, $CXCR6^{hi}$ T cells were only detected in the liver, whereas CX_3CR1^+ T cells were similarly present in liver, spleen and circulation. Only T_{RM}-like $CXCR6^{hi}$ T cells co-expressed other residency markers such as CD69, CD11a, and CD49a. CX_3CR1^+ T_{EM} cells did not express residency markers but partially co-expressed KLRG-1. Of note, both T_{RM}-like $CXCR6^{hi}$ and CX_3CR1^+ T_{EM} cells were highly functional regarding their re-stimulatory capacity when exposed to their cognate antigen after the infection was resolved. However, T_{RM}-like $CXCR6^{hi}$ T cells killed significantly more antigen-bearing hepatocytes, coinciding with their large intracellular granzyme B pools. Transcriptome analysis of ovalbumin-specific $CD8^+$ T cells revealed a residency-associated gene signature in $CXCR6^{hi}$ T cells, whereas CX_3CR1^+ T cell indeed resembled circulating T_{EM} cells.

Strikingly, during persistent viral infection only antigen-specific $CXCR6^{hi}$, but not CX_3CR1^+ $CD8^+$ T cells were present. Importantly, antigen-specific $CXCR6^{hi}$ T cells were localized almost exclusively in the liver and were charactizered by residency-mediating CD69 and CD11a expression. During persistent infection, liver $CXCR6^{hi}CD8^+$ T cells did not exert any effector functions but, instead, expressed high levels of inhibitory receptors, compatible with a dysfunctional state. These clear-cut differences in T cell phenotype and function during persistent compared to after

resolved infection were observed in both model systems, i.e. for ovalbumin-specific as well as for HBV-specific $CD8^+$ T cells.

A transcriptome analysis revealed a similar residency-associated gene signature in dysfunctional hepatic ovalbumin-specific $CXCR6^{hi}$ T cells as in their functional counterparts, i.e. $CXCR6^{hi}$ T cells after resolved infection. Transcription factor network analysis revealed regulation of dysfunctional $CXCR6^{hi}$ T cells through the transcription factor CREM (cAMP-responsive element modulator) or its isoform ICER (inducible cAMP early repressor). Consequently, in $ICER^{fl/fl}$xCD4-Cre mice, a partial rescue of IFNγ production by $CXCR6^{hi}$ T cells was observed despite persistent viral infection of the liver, pointing towards an important role of cAMP signaling and gene regulation by CREM/ICER for loss of function in hepatic $CXCR6^{hi}$ T cells during persistent infection.

In conclusion, antigen-specific liver $CD8^+$ T cells were separated into liver-resident $CXCR6^{hi}$ and circulating CX_3CR1^+ T cells after resolved viral infection. During persistent viral infection of the liver, only liver-resident $CXCR6^{hi}$ antigen-specific $CD8^+$ T cells were present. However, these cells lacked effector functions and showed evidence for increased cAMP signaling. Hence, targeting cAMP signaling might be a promising strategy to re-invigorate resident but dysfunctional virus-specific T cells during persistent infection.

Zusammenfassung

Geweberesidente T-Gedächtniszellen (T_{RM}; engl.: *tissue resident memory T cell*) und Effektor-Gedächtnis-T-Zellen (T_{EM}; engl.: *effector memory T cell*) bilden sich nach ausgeheilten viralen Infektionen und bleiben zum Langzeitschutz vor erneunten Infektionen mit demselben Virus im Organismus. Im Gegensatz zu zirkulierenden T_{EM} Zellen bleiben T_{RM} Zellen zur Unterstützung der Immunüberwachung im zuvor infizierten Gewebe für den Fall einer Sekundärinfektion. Da T_{RM} Zellen im Fall einer Sekundärinfektion sehr schnell reagieren, wurden diese Zellen als „Ersthelfer" beschrieben. In diesem Fall schütten T_{RM} Zellen Granzyme aus, um infizierte Zellen zu eliminieren und rekrutieren mittels Zytokinausschüttung weitere Immunzellen zum Ort der Infektion. Folglich gelten T_{RM} Zellen während Sekundärinfektionen als leistungsfähige Effektor-T-Zellen.

Im Gegensatz zu T_{RM} Zellen mit ausgeprägter Funktionalität ist die T-Zell-vermittelte Immunität während persistierenden viralen Infektionen wie chronischer Hepatitis B Virus (HBV) Infektion geschwächt. Die Zahl der antigen-spezifischen T-Zellen ist vermindert und deren Funktionalität eingeschränkt.

In dieser Arbeit werden Leber-residente T-Zellen und T_{EM} Zellen sowohl während einer persistierenden viralen Leberinfektion als auch nach ausgeheilter viraler Leberinfektion untersucht. Dabei soll der Mechanismus, der während einer chronischen HBV Infektion zu verminderter T-Zell-vermittelten Immunität führt, bestimmt werden. Dies kann wiederum potenzielle therapeutische Zielmoleküle für die Stärkung der T-Zell-basierten Immunabwehr identifizieren. Leber-residente T-Zellen und T_{EM} Zellen werden in dieser Studie in einem präklinischen adenoviralen Modellsystem untersuch, in dem das nominalen Antigen Ovalbumin oder das gesamte HBV-Genom in murine Hepatozyten eingebracht wird. In beiden Modellsystemen kann ein akut-ausheilender mit einem persistierenden Infektionsverlauf verglichen werden.

Nach einer ausgeheilten viralen Leberinfektion wurden CXCR6-exprimierende T_{RM}-ähnliche Zellen und CX_3CR1-experimierende T_{EM} Zellen gefunden. Interessanterweise waren $CXCR6^{hi}$ T-Zellen ($CXCR6^{hoch}$ von engl.: *high*) ausschließlich in der Leber lokalisiert, wohingegen CX_3CR1^+ T-Zellen sowohl in der Leber als auch in der Milz und im Blut detektiert wurden. Ausschließlich $CXCR6^{hi}$ T-Zellen ko-exprimierten weitere Marker für Geweberesidenz wie CD69, CD11a und CD49a. CX_3CR1^+ T-Zellen exprimierten keine Marker für Geweberesidenz, sondern teilweise den Effektormarker KLRG-1. Sowohl T_{RM}-ähnliche als auch T_{EM} Zellen reagierten auf Antigenreexposition mit Zytokinproduktion, was der Reaktion funktioneller Gedächtnis-T-Zellen entspricht. Allerdings eliminierten $CXCR6^{hi}$ T_{RM}-ähnliche Zellen signifikant mehr Antigen-beladene Hepatozyten, was mit der große Mengen an intrazellularem GranzymB intrazellular übereinstimmte. Durch eine Transkriptomanalyse dieser Ovalbumin-spezifischen Zellen konnte gezeigt werden, dass ausschließlich $CXCR6^{hi}$ und nicht CX_3CR1^+ Zellen Gene für Gewebeständigkeit exprimieren. Das Transkriptom von CX_3CR1^+ Zellen hingegen war dem von T_{EM} Zellen sehr ähnlich.

Besonders interessant war die Detektion von CXCR6^{hi}, nicht aber CX_3CR1^+ $CD8^+$ T-Zellen auch während einer persistierender Virusinfektion. Bemerkenswert war, dass Antigen-spezifische CXCR6^{hi} T-Zellen beinahe ausschließlich in der Leber lokalisiert und durch die Expression der Geweberesidenz-vermittelnden Moleküle CD69 und CD11a charakterisiert waren. Allerdings hatten CXCR6^{hi} $CD8^+$ T-Zellen während einer persistierenden Virusinfektion keinerlei Effektorfunktionen und wiesen stattdessen eine hohe Oberflächenexpression von inhibitorischen Rezeptoren auf, was einem dysfunktionalen Status der Zellen entspricht. Diese eindeutigen Unterschiede bei Phenotyp und Funktion zwischen einer persistierenden und einer ausgeheilten Infektion wurden in beiden Modellsystemen beobachtet, d.h. für Ovalbumin-spezifische und für HBV-spezifische $CD8^+$ T-Zellen.

Die Transkriptomanalyse zeigte, dass diese dysfunktionalen Leber-residenten CXCR6^{hi} T-Zellen eine ähnliche Gensignatur für Gewebeständigkeit exprimierten wie funktionellen CXCR6^{hi} T_{RM} Zellen nach einer ausgeheilten Infektion. Eine Transkriptionsfaktor-Netzwerkanalyse zeigte die Regulation von dysfunktionalen CXCR6^{hi} T-Zellen durch den Transkriptionsfaktor CREM (von engl. *cAMP-responsive element modulator*, cAMP-reagierendes Element Modulator) oder dessen Isoform ICER (von engl. *inducible cAMP early repressor*, cAMP-induzierbarer früher Repressor) während einer persistierenden Virusinfektion. Dementsprechend wurde vermehrte IFNγ-Expression in CXCR6^{hi} T-Zellen nach Restimulierung in ICER$^{fl/fl}$xCD4-Cre T-Zellen mit einer T-Zell-spezifische Deletion von ICER trotz einer persistierenden Virusinfektion beobachtet. Dies wies auf eine wichtige Rolle des cAMP-Signalwegs und der Genregulierung durch CREM/ICER bei dem Funktionsverlust Leber-residenter CXCR6^{hi} T-Zellen hin.

Abschließend ist festzuhalten, dass sich Antigen-spezifische $CD8^+$ T-Zellen nach einer ausgeheilten Leberinfektion in Leber-residente CXCR6^{hi} und zirkulierende CX_3CR1^+ T-Zellen aufteilen. Während einer persistierenden viralen Leberinfektion hingegen wurden ausschließlich CXCR6^{hi} Antigen-spezifische T-Zellen in der Leber gefunden. Allerdings hatten diese Zellen keine Funktionalität und wiesen Evidenz für vermehrtes cAMP-Signaling auf. Folglich ist der cAMP-Signalweg ein vielversprechendes therapeutisches Ziel, um die Immunanwort von dysfunktionalen Leber-residenten T-Zellen zu stärken.

Table of Contents

1 Introduction

1.1 The liver's tolerogenic micro-environment

The liver is an exceptional organ regarding (1) its location between the intestine and the systemic circulation, leading to an accumulation of gut-derived bacterial degradation products[1], (2) slow blood flow in the liver's sinusoids facilitating interactions between immune cells and the endothelium[2] and (3) liver-resident immune cells, sensing threats, eliminating pathogens and therefore, maintaining tissue homeostasis[3]. Tissue homeostasis needs to be controlled tightly as the liver is continuously exposed to gut-derived inflammatory cues. To outweigh this constant stimulation, the liver is prone to induce tolerance towards foreign antigens[4]. Hepatic antigen-presenting cells (APCs) are the rheostats controlling the balance between immunity and tolerance[5]. Here, several hepatic cell populations can present antigens: liver sinusoidal endothelial cells (LSECs), Kupffer cells, hepatic stellate cells, and dendritic cells (DCs). These cells can release anti-inflammatory molecules such as IL-10, TGF-β and prostaglandins[6,7]. Moreover, hepatic APCs dampen the adaptive immune response by providing only low co-stimulation and co-inhibitory signals, as summarized in **Fig. 1**[5]. Anti-inflammatory TGF-β and stellate cell-derived retinoic acid induce regulatory T cells (Tregs), further contributing to liver-mediated tolerance[8].

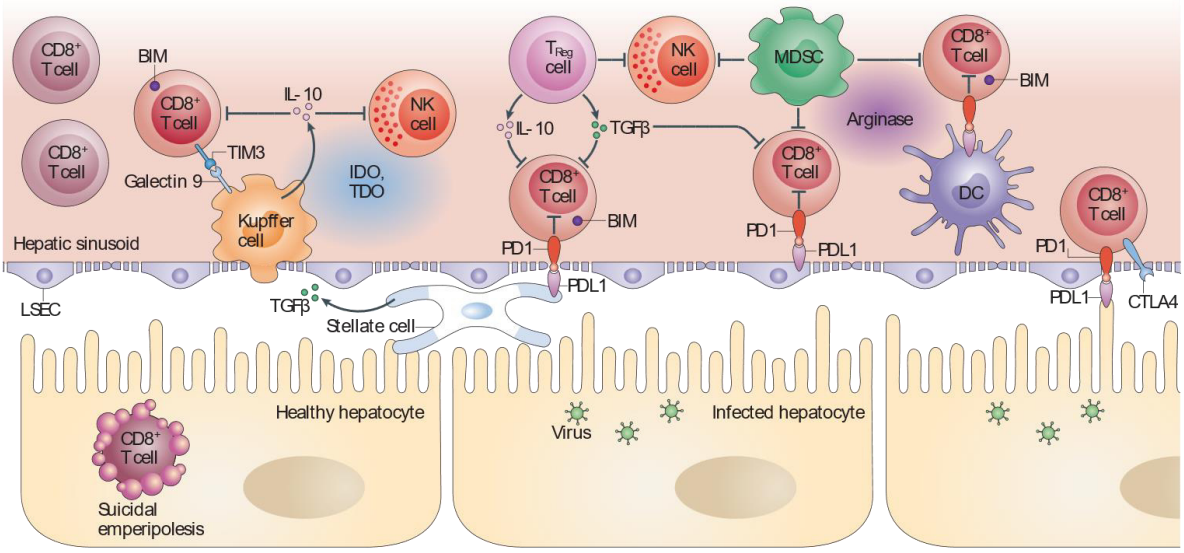

Fig. 1: Liver microanatomy.
Hepatocytes are loosely separated from the blood by Kupffer cells, liver sinusoidal endothelial cells (LSECs), and stellate cells. Soluble factors such as IL-10, TGF-β, arginase, and co-inhibitory molecules on APCs such as Galectin-9 and PDL1, induce T cell tolerance towards foreign antigens instead of immune responses, thereby avoiding tissue damage [illustration from 4].

1.2 CD8+ T cell activation upon liver infection

At the beginning of an infection, naïve CD8+ T cells are primed in lymphoid organs such as lymph nodes and spleen by DCs presenting their cognate antigen peptide. In addition to antigen presentation (signal 1), APCs provide co-stimulation (signal 2) and inflammatory cytokines (signal 3). These signals result in activation and expansion of

the respective T cell[9]. Once primed, activated T cells migrate to the infection site, irrespective of the initial location of antigen recognition[10]. Upon recognizing infected cells, cytolytic T lymphocytes (CTLs) secrete cytokines such as TNF and IFNγ or direct target cell lysis through secretion of perforins and granzymes[11].

Besides T cell priming in secondary lymphoid organs, naïve CD8 T cells can also be activated directly *in situ* following liver infections. Due to endothelial fenestrae, slow hepatic blood flow, and the lack of a basement membrane, T cells can detect peptide-MHC I complexes directly on hepatocytes without leaving the circulation[12,13]. A preclinical study by Bénéchet *et al*. (2019) in a model system for viral liver infection with hepatocyte-restricted antigen presentation showed that naïve $CD8^+$ T cells expand upon antigen presentation by hepatocytes. However, this process was not as efficient as upon DC- or Kupffer cell-restricted antigen presentation. Of note, these hepatocyte-primed T cells are dysfunctional due to the lack of IL-2 signaling during priming[14]. Besides antigen presentation by hepatocytes, also antigen presentation by LSECs tolerizes T cells, as LSECs upregulate co-inhibitory B7-H1 instead of costimulatory molecules upon cognate interaction with T cells[15]. Furthermore, the liver may be a "graveyard" during the peripheral deletion of T cells[16–18]. In summary, the liver's tolerogenic microenvironment favors the development of dysfunctional T cells, creating a loophole for liver-targeting pathogens.

1.3 Functionally impaired $CD8^+$ T cells in chronic viral infection

Memory T cells are formed during pathogen clearance and survive for several years in the absence of antigen. Some pathogens, however, persist and thereby establish a chronic infection. As antigen is continuously presented to T cells, T cell receptor (TCR) signaling is triggered repetitively, resulting in TCR downregulation, and reduced cytotoxicity[19]. In addition to a loss of functionality, peripheral T cells are partly deleted depending on T cell epitope specificity in persisting LCMV infection[20].

1.3.1 Mechanisms of T cell exhaustion

These initial findings of T cell dysfunctionality during chronic viral infections were extended, and the underlying molecular mechanisms are being unraveled since[21]. First, exhaustion of T cells develops in a hierarchical fashion: $CD8^+$ T cells during chronic infections lose effector functions gradually, starting with the loss of IL-2 production and impaired survival. With increasing exhaustion, T cells no longer proliferate and finally lose their cytotoxic potential (**Fig. 2**)[22]. Second, in addition to constant TCR stimulation by high antigen load, diminished help from $CD4^+$ T cells contributes to more severe $CD8^+$ T cell exhaustion[23]. Third, the local cytokine milieu is skewed towards anti-inflammatory cytokines in chronic infection. For instance, higher IL-10 levels have been observed in chronic LCMV Clone 13 infections[24].

Exhausted T cells are prone to apoptosis, as they express low levels of CD122 (β-chain of IL-2 and IL-15 receptor) and CD127 (α-chain of IL-7 receptor) and thereby respond poorly to longevity-mediating pro-survival IL-15 and IL-7 signaling[25]. In

addition to altered population maintenance, triggering of inhibitory receptors downregulates the functionality of T cells. Expression of inhibitory receptors is upregulated after T cell activation to reduce tissue damage through an excessive immune reaction, i.e., immunopathology. During chronic infection, inhibitory receptors like PD-1 and CTLA-4 are constitutively and highly expressed by T cells[26]. Notably, both the multiplicity and expression levels of these inhibitory receptors distinguish between recently activated functional T cells and dysfunctional T cells in chronic infection, as reviewed in[27].

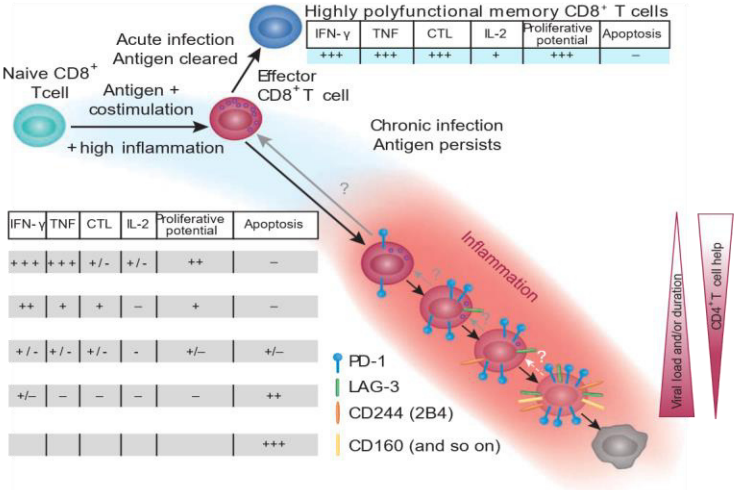

Fig. 2 Hallmarks of functional memory T cells and exhausted T cells.
Antigen-presenting cells prime naïve T cells and provide co-stimulation. Effector CD8+ T cells eliminate infected cells during the acute phase, followed by the establishment of a functional memory population. Contrastingly, exhausted T cells gradually lose effector functions and express inhibitory receptors during chronic infections with persisting antigen. Viral load and duration of the infection increase the exhausted phenotype marked by co-expression of inhibitory receptors and lack of cytokine production Illustration from [22].

1.3.2 Regulation of T cell exhaustion

T cell exhaustion is often analyzed by surface expression patterns but rooted and regulated by transcription factors. The transcription factor TOX (thymocyte selection-associated high mobility group box protein) maintains exhausted T cell populations. TCR signaling induces TOX expression, and in turn, TOX positively regulates PD-1 expression[28]. Moreover, Martinez *et al.* (2015) induced T cells with an exhausted phenotype on both protein and transcriptomic levels in an *in vivo* model system by constitutively active transcription factor NFAT (nuclear factor of activated T cells)[29].

In conclusion, exhausted T cells in chronic viral infection are a distinct population compared to memory T cells formed after acutely resolving infections. They differ by surface phenotype, functionality, and transcriptional regulation. However, T cells in chronic infections are not an entirely homogenous population[30]. A fraction of dysfunctional T cells expressing the transcription factor TCF-1 (T cell factor 1), PD-1, and CD127, shows central memory-like and exhaustion-related characteristics and can give rise to the expansion of T cells that then develop into terminally exhausted T cells[31,32].

1.4 Regulation of CD8+ T cells by cAMP signaling

Persistent TCR signaling and lack of co-stimulation cause T cell exhaustion, as illustrated in **Fig. 2**. However, more mechanisms regulate T cell responses, amongst them, cyclic adenosine monophosphate (cAMP) signaling. Increased intracellular cAMP levels in T cells can originate from (1) regulatory T cells (Tregs), which can transfer cAMP into T cells via gap junctions, or (2) via Treg-derived adenosine, which induces increased cAMP levels in T cells[33]. Moreover, (3) prostaglandin E_2 binding to its receptors EP_2 and EP_4 on T cells activates adenylyl cyclase, which synthesizes cAMP in T cells[34].

Increased cAMP signaling in $CD8^+$ T cells can dampen cytotoxicity and cause loss of IL-2 production[35]. Moreover, cAMP signaling counteracts TCR signaling-induced T cell activation and proliferation[36,37]. In more detail, cAMP binds to the regulatory subunit of protein kinase A (PKA), which dissociates upon binding and thereby activates PKA via phosphorylation. Phosphorylated PKA translocates into the nucleus and phosphorylates transcription factors such as CREM (cAMP-responsive element modulator) and its inducible homolog ICER[38]. ICER (inducible cAMP-responsive element) represses target gene expression as it lacks a transactivation domain, whereas CREM can regulate target gene expression either positively or negatively. In contrast to constitutively expressed CREM, cAMP can induce ICER expression[39]. Notably, ICER can interfere with CREM binding to its target sites via heterodimerization or binding to CRE-responsive DNA sites. Thereby, CREM and other Cre-binding proteins cannot induce target gene transcription[40]. Competitive binding of ICER is crucial in T cell activation, as they do not express transactivation domain-containing isoforms of CREM[41].

In conclusion, cAMP signaling and downstream gene regulation influence T cell immunity depending on the microenvironment's signals acting on T cells.

1.5 Immune response towards Hepatitis B virus infection

In the following, the relevance of chronic Hepatitis B virus infections on global health, the immune system's response towards the infection, and model systems to investigate both the virus and the immune response are laid out.

1.5.1 Health impact of Hepatitis B virus infections

Worldwide, 257 million patients were persistently infected with the hepatitis B virus (HBV) in 2015, with African and Western Pacific regions mainly affected. Patients with chronic hepatitis B virus infection are prone to develop fibrosis, cirrhosis, and hepatocellular carcinoma[42]. In 2015, viral hepatitis caused 1.34 million deaths and thereby represents a severe health threat[43]. However, in adults, HBV infection is mostly resolved (>95%), whereas more than 90% of children develop chronic hepatitis[44]. The available prophylactic vaccine can prevent neonatal transmission from mother to child, but vaccination during chronic infection has not shown success[42].

1.5.2 Persistence form of the Hepatitis B virus

HBV is an enveloped noncytopathic virus of the *hepadnaviridae* family that infects humans and chimpanzees[45]. Its genome consists of a partially double-stranded DNA of 3 kbp length in a relaxed circular (rcDNA) structure[46]. After HBV enters hepatocytes through binding to the sodium taurocholate cotransporting polypeptide (NTCP)[47], it establishes an episomal covalently closed circular DNA (cccDNA), which persists in host cells and serves as a template for viral RNA synthesis[48]. The cccDNA, therefore, is key to the persistence of the virus in infected hepatocytes[42] and is the main reason why direct antiviral agents fail to eliminate HBV infection. HBV DNA can integrate into the host genome and can thereby promote cancerogenesis[49]. Although HBV genomes can be delivered into hepatocytes of mice via viral vectors and thus overcome the species barrier, cccDNA is not formed in murine hepatocytes. However, persistent HBV infection is observed after AAV or adenoviral transfer of HBV genomes into mice, demonstrating the involvement of hepatic immune tolerance rather than viral persistence mechanisms[50].

1.5.3 Immune response towards Hepatitis B virus infection

Infection with HBV can lead to acute hepatitis and resolved infection or persistent infection and chronic viral hepatitis. Of note, the lack of an innate immune response towards HBV infection might facilitate persistent infection[51–53]. However, the molecular mechanisms causing the absence of an immune response are discussed controversially in the existing literature. HBV might actively suppress the innate immune response[54]. Others contradict an active suppression mechanism and instead suggest intrinsically lower levels of DNA sensing machinery in hepatocytes, which are targeted by HBV and could mediate viral stealth[55].

The adaptive immune response, precisely virus-specific $CD8^+$ T cells, is crucial to control HBV infections, as depletion of $CD8^+$ T cells delays viral clearance in HBV-infected chimpanzees[56]. $CD8^+$ T cells engage in viral clearance both in a cytolytic and non-cytolytic fashion, as illustrated in **Fig. 3**: granzymes and perforins lyse infected cells, whereas INFα, IFNγ, and TNF deaminate and thereby reduce viral cccDNA without killing hepatocytes[57,58]. Therefore, a robust polyclonal T cell response, accompanied by seroconversion from the viral antigens HBeAg and HBsAg to protective anti-HBe and anti-HBs antibodies characterize a functional immune response[59].

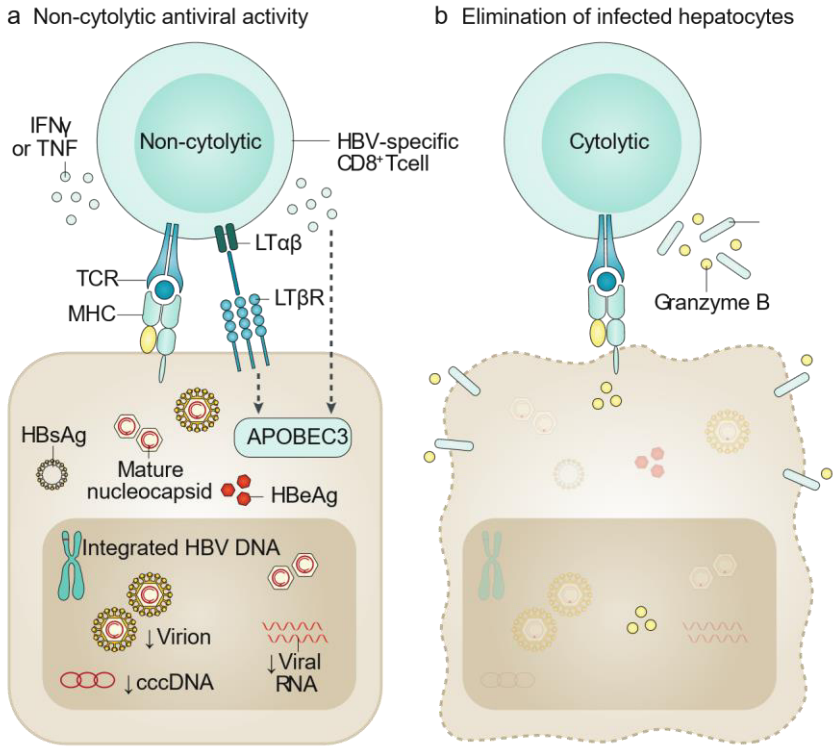

Fig. 3. Immune response by CD8⁺ T cells towards HBV infected hepatocytes.
A Non-cytolytic reduction of the covalently closed circular DNA (cccDNA) via cytokines and induction of APOBEC3.
B Cytolytic elimination of infected hepatocytes leads to complete removal of HBV DNA Illustration from [44].

However, even after successfully gaining control over HBV infection by the immune system, HBV is probably not completely cleared, as cccDNA and genome-integrated DNA may persist in hepatocytes and give rise to re-emergence of infection, which is indeed observed after immune-suppressive therapies[59,60]. Most hepatocytes (75 %) are infected in acute viral hepatitis, and thereby not every infected hepatocyte can be eliminated[61].

As stated above (p.14), HBV is a noncytopathic virus. However, chronic hepatitis, fibrosis, cirrhosis, and hepatocellular carcinoma occur in patients with chronic HBV infection. The liver damage leading to these diseases is caused by the immune response towards the virus[42]. Persistence of HBV in the liver causes chronic hepatitis B (CHB)[62], characterized by a weak T cell response to viral antigens[52]. HBV-specific T cells are rare in CHB patients and mostly unable to produce IFNγ after activation, a functional deficit that correlates with high expression of the inhibitory receptor PD-1[63]. Moreover, T cells in CHB patients show high expression levels of the inhibitory receptor CTLA-4, marking exhausted T cells prone to cell death[64]. These alterations in phenotype and functionality coincide with altered expression of the transcription factor T-bet, as T-bet deficiency marks T cells lacking IFNγ production and failing to proliferate[65]. Moreover, transcriptome analysis identified the existence of dysfunctional mitochondria in HBV-specific T cells of CHB patients that may further contribute to the dysfunctional T cell phenotype[66].

In summary, results from preclinical models of persistent HBV infection and patients with chronic hepatitis B indicate that virus-specific T cells in chronic HBV infections are exhausted and that this dysfunctional phenotype contributes to the persistence of infection in hepatocytes.

1.5.4 Murine model systems for Hepatitis B virus infection

HBV selectively infects humans and chimpanzees[48], limiting the analysis of the immune response towards HBV infection. Therefore, alternatives were required to investigate the pathogenesis of HBV infection. Mice are well-characterized model organisms that are susceptible to genetic modification, which greatly benefits the elucidation of molecular mechanisms of disease pathogenesis. However, to study HBV infections in mice, HBV specificity for human hepatocyte infection had to be overcome. To this end, transgenic mice expressing the 1.3-fold overlength genome were created. These mice express the entire HBV genome as 1.3 overlength construct and, therefore, all viral proteins but lack the cccDNA formed in human hepatocytes. Despite high copy numbers of 100-200 replicates per hepatocyte corresponding to serum concentrations as observed in humans, HBV-transgenic mice do not develop significant liver histopathology[67], supporting the notion that liver damage is mediated by virus-specific immunity but not viral replication. Of note, viral clearance cannot be studied in HBV-transgenic mice as all hepatocytes express the HBV genome stably.

An alternative approach to achieving HBV genome expression in murine hepatocytes is viral vectors as a gene shuttle for the HBV genome. Therefore, the 1.3-fold overlength HBV genome was cloned into recombinant replication-deficient adenoviral vectors. Adenoviruses deliver DNA to proliferating and non-proliferating cells of various species, including mice, and guarantee efficient liver targeting in defined quantities[68]. The HBV genome (genotype D, subtype *ayw*) was cloned into the Adenovirus serotype 5 after the E1 and E3 region were deleted to make space for the HBV genome and render the adenoviral vector replication-deficient. Injection of mice with the Adeno-HBV1.3 construct led to the synthesis of all viral nucleic acids from an extrachromosomal DNA template, protein translation, and eventually to the release of virions[69]. This model system provokes an immune response toward the HBV antigens and allows for the investigation of HBV-specific T cells[70]. AdHBV vectors were used to study acutely-resolving and persistent infections[50,71]. To follow HBcore-specific $CD8^+$ T cells *in vivo*, TCR-transgenic $CD45.1^+CD8^+$ T cells recognizing the HBCor93-100 peptide in the context of $H\text{-}2K^b$ molecules were generated[72]. Thus, a toolbox of recombinant viral vectors for transferring HBV genomes to establish infection in mice and HBV-specific TCR transgenic mice was generated to allow following antigen-specific CD8 T cell immunity to HBV infection in mice.

1.6 Memory $CD8^+$ T cells

Antigen-presenting cells prime antigen-specific T cells during infections. Subsequently, T cells mediate cytotoxicity to clear virus-infected cells[73]. After successful clearance,

the number of pathogen-specific T cells is reduced during a contraction phase, as most of them are short-lived effector T cells. A fraction of the T cells activated during infection persists even after the antigen is cleared. These cells are termed memory T cells[74], that survive in the absence of their cognate antigen. Upon a second infection with the same pathogen, memory T cells provide a qualitatively and quantitatively enhanced immune response that controlling infections faster[75].

1.6.1 Different memory T cells subsets

In 1999, Sallusto *et al*. described two distinct subsets of memory T cells: central memory T cells (T_{CM}) and effector memory T cells (T_{EM}). T_{CM} and T_{EM} differ in their phenotype, migration pattern as well as functional and proliferative potential. T_{CM} cells express the lymph node homing receptor CCR7, lack effector functions, but proliferate upon secondary infections. Instead of CCR7, T_{EM} cells express β1 and β2 integrins enabling migration to inflamed tissues in case of secondary infections. There, T_{EM} cells rapidly induce inflammation and execute cytotoxic effector functions[76]. The fractalkine receptor CX_3CR1 allows for discrimination of T_{EM} cells with cytotoxic effector function from T_{CM} cells with the potential for proliferation[77,78].

Over the last decade, a third category of memory T cells was discovered: tissue-resident memory T cells (T_{RM} cells). T_{RM} cells are not part of the pool of circulating memory T cells but establish long-term residency at the site of infection (**Fig. 4**).

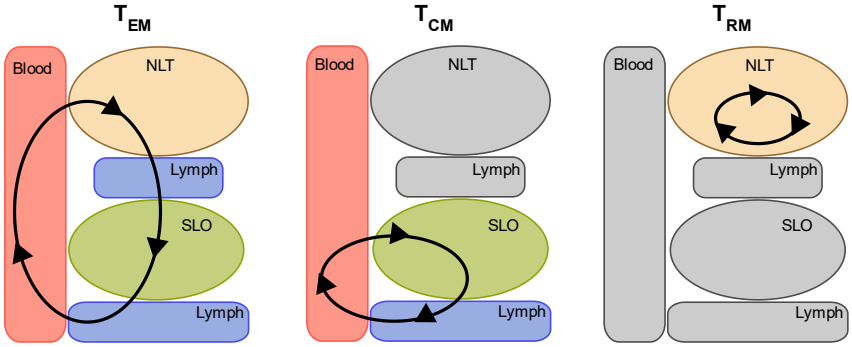

Fig. 4: Subsets of memory T cells and their respective circulating patterns.
T_{EM} cells continuously circulate between NLT and lymphoid organs via lymph and blood. T_{CM} cells only circulate within the lymphoid compartment, whereas T_{RM} cells stay in one peripheral organ. Abbreviations: nonlymphoid tissue (NLT), secondary lymphoid organ (SLO), Effector memory T cells (T_{EM}), central memory T cells (T_{CM}), Tissue-resident memory T cells (T_{RM}) Illustration from [79].

Two studies proved the residency of T_{RM} cells in formerly infected tissues and their protective capacities during secondary challenges using transplantation models of sensory ganglia and skin[80] or the small intestine[81] in infected mice. Later on, T_{RM} cells were described in many other organs/tissues such as the lung after influenza infection[82], the brain after lymphocytic choriomeningitis virus (LCMV) infection[83], the female reproductive tract after LCMV infection[84], and the liver after infection with malaria sporozoites[85].

1.6.2 Phenotype of T_{RM} cells

T_{RM} cells differ from T_{CM} cells and T_{EM} cells by their localization and migration patterns (**Fig. 4**). Besides, the phenotype and functionality of these T cell categories are different. A hallmark of T_{RM} cells in different organs and infection models is the surface expression of CD69[86–88]. CD69 competes with tissue egress-mediating $S1P_1$ (sphingosine 1-phosphate receptor) for surface expression on T cells. $S1P_1$, in turn, mediates tissue egress via S1P ligand detection in blood and lymph vessels and is positively regulated by the transcription factor KLF2. In T_{RM} cells, tissue-specific cues like TGFβ downregulate KLF2. Hence, CD69 being essential for tissue retention, makes it a *bona fide* T_{RM} marker[89]. In addition to CD69, the α-chain of the integrin $\alpha_E\beta_7$ (CD103) is widely used to identify T_{RM} cells in epithelial tissues[80,90,91].

In contrast, hepatic T_{RM} cells do not express CD103[92,93]. Instead, hepatic T_{RM} cells express high levels of integrin αL (also termed CD11a and leukocyte adhesion glycoprotein-1, LFA-1) to mediate adhesion to endothelial cell-expressed ICAM-I[92]. A third surface molecule used for T_{RM} cell identification is CD49a (also termed VLA-1). CD49a protects T_{RM} cells from apoptosis during the contraction phase in the lung[94]. Besides, CD49a identifies tumor-infiltrating lymphocytes with a T_{RM} phenotype and an increased activation status[95]. Also, in human skin, CD49a identifies highly cytotoxic T_{RM} cells[96].

In addition to these global T_{RM} markers, human and murine liver T_{RM} cells express the chemokine receptors CXCR6 and CXCR3[93,97]. The ligand of CXCR6 is CXCL16, a membrane-bound chemokine expressed by LSECs, macrophages, monocytes, DCs, and B cells. CXCR6 might play a role in interactions with antigen-presenting cells or migration to inflamed liver tissues[98]. However, the lack of CXCR6 expression does not affect the primary infection clearance or T cell accumulation in the liver. Instead, long-term T cell maintenance is impaired in CXCR6-deficient mice[99]. In addition to CXCR6, the chemokine receptor CXCR3 is highly expressed on liver-infiltrating T cells. Its ligands, CXCL9, -10, and -11, are induced by IFNγ on LSECs in the liver[100,101]. After engagement of CXCR3 with its ligands, T cell surface-expressed β1 and β2 integrins bind their endothelial ligands and thereby mediate adhesion[100]. Although CXCR3-deficient cells are still functional and migrate to infected skin, they move around faster in the tissue and eventually fail to engage with infected cells[102]. As a result, viral clearance is hampered but not erased[101,102].

1.6.3 Functionality of T_{RM} cells

Strikingly, T_{RM} cells differ from T_{EM} and T_{CM} cells regarding functionality as they are highly alert and protective in secondary infections. In detail, T_{RM} cells express high levels of granzyme B and cytokines to control pathogen re-infection and recruit other immune cells in case of a secondary infection. Lung T_{RM} cells clear viral challenges, with higher numbers of antigen-specific T_{RM} cells correlating with faster clearance[82]. Fernandez-Ruiz *et al*. (2016) confirmed this protective effect for malaria-specific liver T_{RM} cells generated by a prime-and-pull approach: antigen-specific cells were primed

in the spleen, recruited to the liver via local antigen recognition, and were protective in case of a challenge with sporozoites[93].

In summary, T_{RM} cells are distinguishable by surface expression of the markers CD69, CD49a, CD11a, and, in some tissues, also CD103. These markers have been associated with tissue residency in parabiosis studies. The unique functional properties of T_{RM} cells make them promising targets for prophylactic and therapeutic vaccines.

1.7 Aim of this study

This study aimed at a comprehensive characterization of liver-resident $CD8^+$ T cells during viral infections of the liver. For this, an adenoviral gene transfer model was employed that coded for the nominal antigen ovalbumin, which allowed to define the phenotype and functionality of resident T_{RM} and circulating T_{EM} cells after resolved and during persistent viral infections of the liver.

This model system allowed to inquire (1) the transcriptional response of antigen-specific T cells and to (2) differentiate between resident and circulating T cells and (3) between T cells after resolved and during persistent infection. This analysis aimed to identify regulatory mechanisms of antigen-specific T cells in the liver, which could constitute potential therapeutical targets to improve T cell functionality during persistent viral infection. Finally, this study aimed at transferring the findings gained with the ovalbumin-based model system to a clinically relevant infection, namely, persistent HBV infection in a preclinical murine model.

2 Results

2.1 Acute-resolving Ad-CMV-GOL and persistent Ad-TTR-GOL infection of the liver

At first, a characterization of the differences between antigen-specific CD8$^+$ T cells in acute-resolving and persistent viral infections of the liver was performed. Therefore, two adenoviral infection models were used as previously described[103]. These models employ ovalbumin as nominal antigen and two reporter genes, luciferase and GFP, to enable antigen detection both *in vivo* and in tissue sections, respectively. Both adenoviruses express the transgenes GFP, ovalbumin, and luciferase (GOL) separated by 2A sequences. However, transgene expression is controlled by the ubiquitous CMV promoter (Ad-CMV-GOL), leading to transgene expression in all infected cells or by the hepatocyte-specific transthyretin promoter (Ad-TTR-GOL). In addition to different promoters, viral load was the second setscrew to define the infection outcome. As shown by Manske *et al.*, injection of 10^7 PFU Ad-CMV-GOL led to acutely resolving infections, whereas 100-fold higher doses of the same construct resulted in persistent infections. In contrast, injection of Ad-TTR-GOL always led to persisting transgene expression, irrespective of the injected dosage[103]. To infect enough hepatocytes and match initial antigen expression levels in both infection models, 10^8-10^9 PFU Ad-TTR-GOL were administered.

2.1.1 Establishment of an acute-resolved and persistent adenoviral infection model

For this, the infection kinetics and outcome of Ad-CMV-GOL and Ad-TTR-GOL infections were monitored over time. Real-time *in vivo* monitoring of the infection kinetic was performed using *in vivo* bioluminescence imaging of the liver and complemented by determination of serum alanine transaminase (sALT), indicating antigen expression and liver damage (**Fig. 5**), respectively.

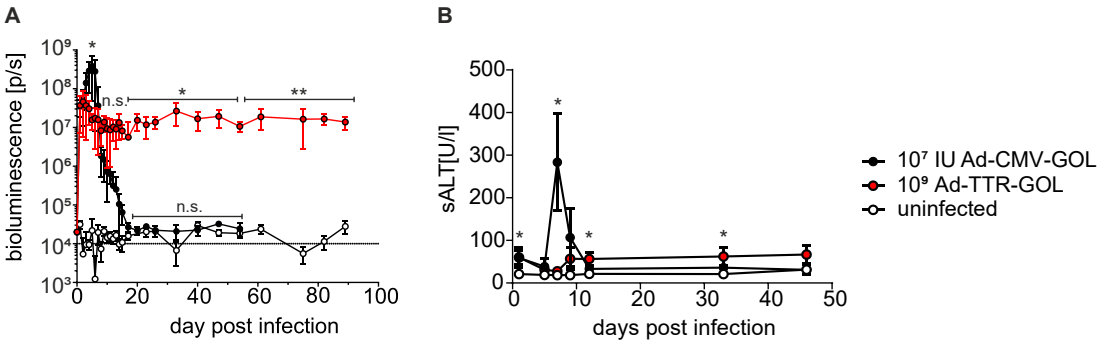

Fig. 5 *In vivo* infection monitoring of Ad-CMV-GOL and Ad-TTR-GOL infected mice.
A Bioluminescence imaging with the *in vivo* imaging system (IVIS) indicating transgene expression. **B** Serum ALT measurement of blood withdrawn from the V. facialis indicating tissue damage caused by the immune system.

Bioluminescence of Ad-CMV-GOL infected mice peaked on d5 post infection (p.i.), followed by a drop until day 20 when the signal intensity was back to background

levels. In contrast, the bioluminescence signal of Ad-TTR-GOL infected mice was stable over the whole monitoring period (**Fig. 5A**). Coinciding, sALT of Ad-CMV-GOL infected mice peaked on d7 p.i., indicating a robust immune response towards the transgenes. In Ad-TTR-GOL infected mice, contrastingly, sALT levels were always slightly above background. sALT elevation might be caused by low-level inflammation over a prolonged period (**Fig. 5B**).

In addition to *in vivo* infection monitoring, the reporter gene GFP expression was analyzed in histological tissue sections.

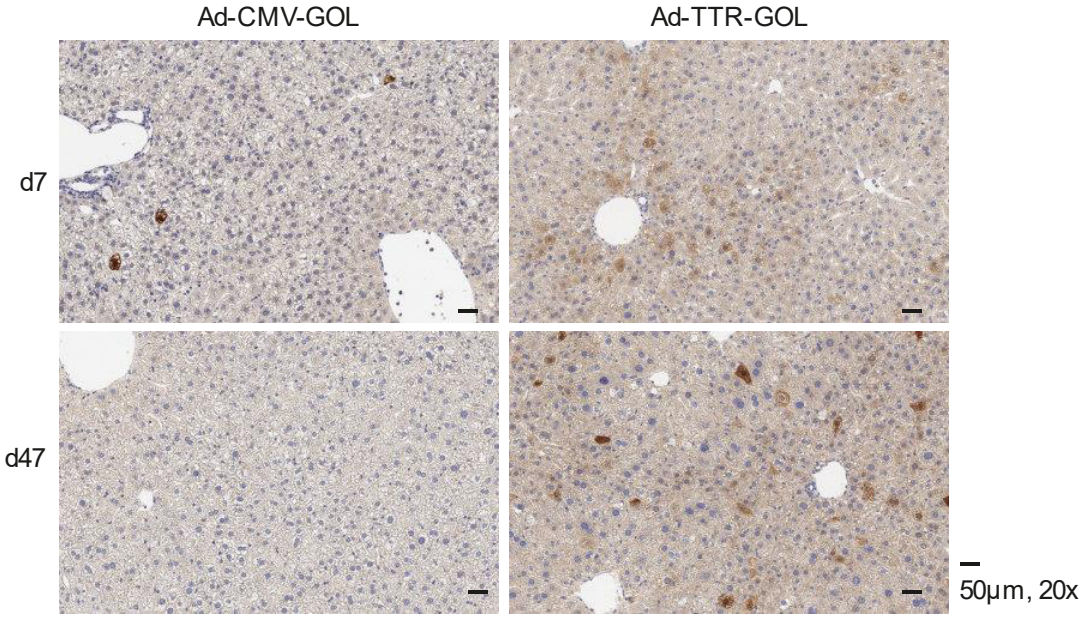

Fig. 6 Hepatic expression of the reporter gene GFP after Ad-CMV-GOL and Ad-TTR-GOL infection.
Histological liver sections of mice infected with either Ad-CMV-GOL (left panels) or Ad-TTR-GOL (right panels) on d7 (upper panels) and d47 (lower panels) p.i. GFP signal was enhanced by anti-GFP antibody staining (brown). Liver tissue is shown in 20x magnification.

In Ad-CMV-GOL infected mice, GFP^+ hepatocytes were detected on d7 p.i. (**Fig. 6**, upper left panel). On d47 p.i., no more GFP^+ hepatocytes were detected in liver sections (**Fig. 6**, lower left panel), coinciding with the decrease in the measured bioluminescence signal. Contrastingly, in Ad-TTR-GOL infected mice, GFP^+ hepatocytes were detectable equally well on early time points and d 47 p.i. (**Fig. 6**, right panels), consistent with a persistent infection.

Summarizing, expression levels of both reporter genes indicated an acute-resolved infection upon injection of Ad-CMV-GOL, whereas Ad-TTR-GOL injection led to persistent transgene expression in the liver.

2.1.2 Antigen-specific $CD8^+$ T cells stay in the liver after resolved and during persistent viral infection

Throughout the time course of infection, antigen-specific $CD8^+$ T cells were isolated from the liver and spleen and characterized via flow cytometry. Days 3, 5, 7, 18, 45, and 98 p.i. were chosen for T cell analysis. In both Ad-CMV-GOL and Ad-TTR-GOL

infections, T cells specific for the ovalbumin peptide SIINFEKL (ovalbumin 257-264) were analyzed. As the H-2k^b-restricted peptide SIINFEKL is the most immunogenic ovalbumin peptide[104], a significant number of virus-specific T cells was expected to be SIINFEKL-specific.

2.1.2.1 Adoptively transferred antigen-specific CD45.1$^+$CD8$^+$ T cells

All mice received 100 naïve TCR-transgenic SIINFEKL-specific CD45.1$^+$CD8$^+$ T cells before infection, a dose shown not to alter the course of endogenous T cell immunity[105]. T cell transfer facilitated the monitoring of antigen-specific T cells, as these cells were detected via the congenic marker CD45.1 in addition to streptamer staining. Detection of CD45.1 by antibody staining is more robust than streptamer staining, especially if staining protocols involve fixation. Moreover, adoptive transfer of antigen-specific T cells allowed for following T cell expansion and contraction. In both infection models, CD45.1$^+$CD8$^+$ T cells expanded upon infection (**Fig. 7**). In Ad-CMV-GOL infection, CD45.1$^+$ CD8$^+$ T cells were detected in both liver and spleen on all days analyzed (**Fig. 7A, B**). Of note, a high accumulation of CD45.1$^+$CD8$^+$ T cells was observed in the liver during infection clearance, followed by a contraction phase (**Fig. 7C**). After Ad-TTR-GOL infection, CD45.1$^+$ T cells initially expanded, but at a lower magnitude. Moreover, a contraction phase was not observed in Ad-TTR-GOL infected mice (**Fig. 7D**). Of note, the frequency of CD45.1$^+$CD8$^+$ T cells in spleens of Ad-TTR-GOL infected mice was very low (**Fig. 7B, D**).

In resolving Ad-CMV-GOL infections, T cells contributed to viral clearance[103]. In contrast, T cell kinetics in Ad-TTR-GOL infected mice suggested a dysfunctional T cell response, as CD45.1$^+$CD8$^+$ T cells were firstly mainly observed at the site of infection, secondly failed to expand as strong as in Ad-CMV-GOL, infected mice and thirdly did not undergo a contraction phase but persisted at constant cell numbers.

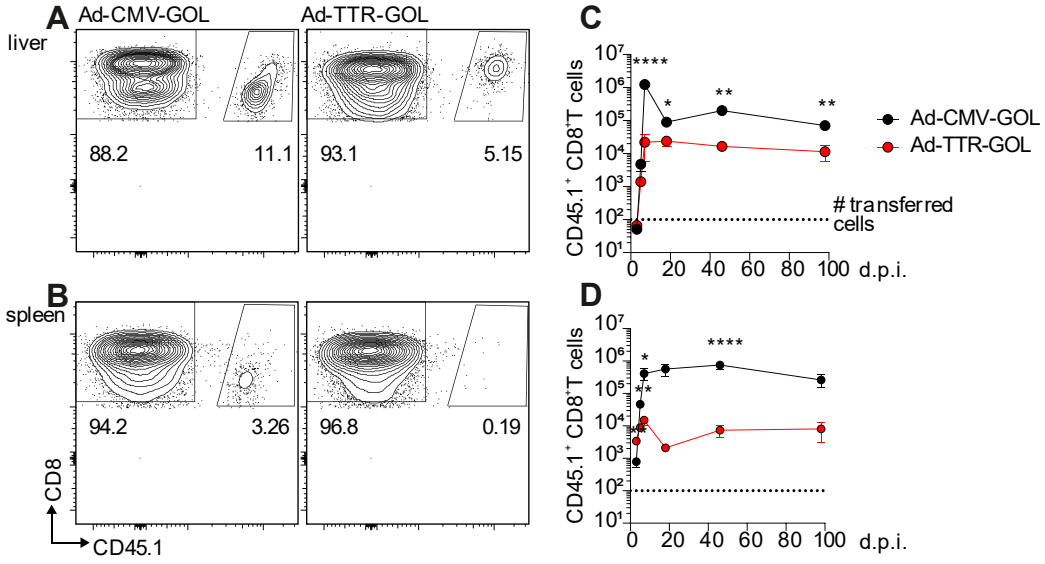

Fig. 7 Kinetics of antigen-specific CD45.1$^+$CD8$^+$ T cells in the liver and spleen after acute-resolving Ad-CMV-GOL or persistent Ad-TTR-GOL infection.
A Hepatic and **B** splenic CD8$^+$ T cells on d45 p.i. were gated into CD45.1$^+$ and CD45.1^{neg} populations. **C** Hepatic and **D** splenic lymphocytes were quantified on days 3, 5, 7, 18, 45, and 98 after Ad-CMV-GOL (black) and Ad-TTR-GOL (red) infection.

2.1.2.2 Endogenous antigen-specific CD8⁺ T cells

Before focusing on the analysis of adoptively transferred CD45.1⁺CD8⁺ T cells, they were compared to endogenous SIINFEKL-specific CD8⁺ T cells to ensure transgenic CD45.1⁺CD8⁺ T cells reflect the endogenous CD8⁺ T cell response. Endogenous SIINFEKL-specific CD8⁺ T cells were identified by streptamer staining (**Fig. 8A, B**). Reflecting the results observed for CD45.1⁺CD8⁺ T cells, streptamer⁺CD8⁺ T cells were detected in the liver and spleen of Ad-CMV-GOL infected mice at all time points analyzed. After the initial expansion of streptamer⁺ T cells in the liver and spleen, T cell numbers decreased (**Fig. 8C**). In Ad-TTR-GOL infected mice, endogenous streptamer⁺ T cells expanded as well, albeit at lower levels than in Ad-CMV-GOL infected mice. However, these cells were rare in spleens, and no contraction phase was observed (**Fig. 8B, D**).

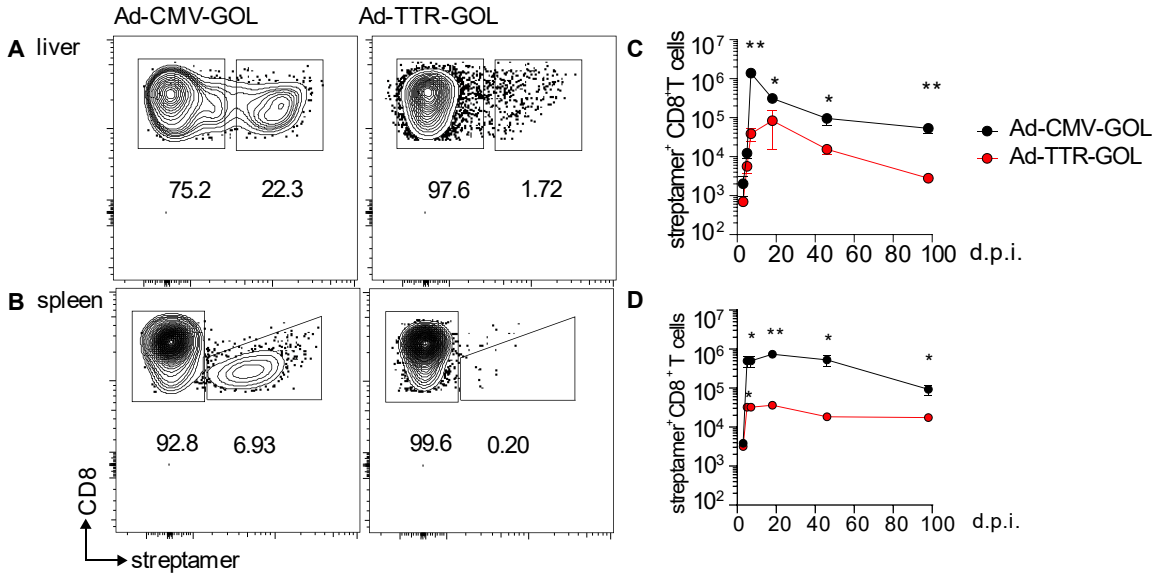

Fig. 8 Kinetics of endogenous streptamer⁺CD8⁺ T cells after acute-resolving Ad-CMV-GOL or persistent Ad-TTR-GOL infection.
A-B Endogenous CD45.1^{neg} SIINFEKL-specific CD8⁺ T cells were identified by streptamer staining. CD45.1^{neg}CD8⁺ T cells were isolated from Ad-CMV-GOL and Ad-TTR-GOL infected mice from the liver (**A**) and spleen (**B**) on day 45 post infection. **C-D** Hepatic (**C**) and splenic (**D**) lymphocytes were isolated on days 3, 5, 7, 18, 45, and 98 p.i. to monitor the endogenous T cell response's kinetics.

Comparison of the results for CD45.1⁺CD8⁺ T cells (**Fig. 7**) and CD45.1^{neg}streptamer⁺ T cells (**Fig. 8**) led to the conclusion that CD45.1⁺CD8⁺ T cells reflect the course of the endogenous CD8⁺ T cell response toward viral infection, which justified focusing on the CD45.1⁺CD8⁺ T cells for characterization of the virus-specific T cell response.

2.1.3 Antigen-specific CD8⁺ T cells in the liver and spleen differ between resolved and persistent viral infection

To understand the differences between antigen-specific T cells in resolving and persistent Ad-GOL infections, the phenotype of these cells was characterized in detail.

2.1.3.1 Effector and memory T cell marker

First, the expression of CD44 and CD62L was analyzed. CD44 is expressed on all antigen-experienced T cells and thereby a useful marker for previous T cell priming. The lymph node homing marker CD62L is expressed on naïve T cells and T_{CM} cells. Used in combination, these markers can distinguish naïve T cells, $T_{CM,}$ and effector/effector memory T cell (T_{EFF}/T_{EM}) cells[106].

The adoptively transferred antigen-specific CD45.1$^+$ T cells expressed CD44 uniformly in the liver (**Fig. 9A, C**) and spleen (**Fig. 9B, D**) of Ad-CMV-GOL infected mice. Hence, all transferred CD45.1$^+$ T cells had been primed. In splenic endogenous CD45.1^{neg}CD8$^+$ T cells, also CD44$^+$CD62L$^+$ T_{CM} and CD62L$^+$ naïve T cells were detected (**Fig. 9B,D**), reflecting diverse T cell populations. Likewise, in hepatic CD45.1^{neg}CD8$^+$ T cells, naïve T cells, and low frequencies of T_{CMs} were detected (**Fig. 9A, C**). Of note, CD45.1$^+$ T cells and endogenous CD45.1^{neg} T cells in Ad-TTR-GOL infected mice did not differ from their counterparts in resolved infections concerning CD44 and CD62L expression (**Fig. 9A, B**; right panels). As observed previously (**Fig. 7**), CD45.1$^+$ cells in spleens of Ad-TTR-GOL infected mice were rare and at the detection limit (**Fig. 9B**, right panel).

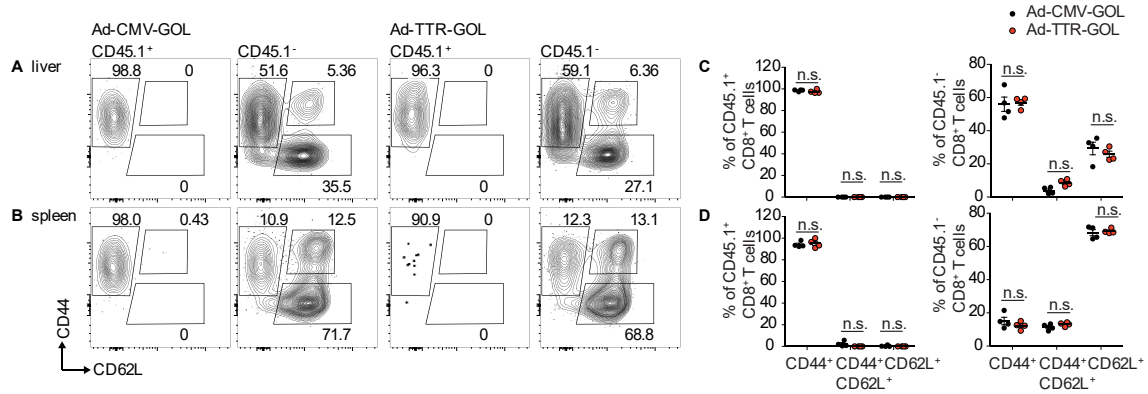

Fig. 9 Expression of CD44 and CD62L on antigen-specific CD45.1$^+$ and polyclonal CD45.1^{neg} CD8$^+$ T cells on d45 after resolved Ad-CMV-GOL or persistent Ad-TTR-GOL infection.
A-B CD44 and CD62L expression on CD45.1$^+$ and CD45.1^{neg} CD8$^+$ T cells from liver (**A**) and spleen (**B**) of Ad-CMV-GOL and Ad-TTR-GOL infected mice. **C-D** Frequencies of CD44$^+$, CD44$^+$CD62L$^+$, and CD62L$^+$ T cells in liver (**C**) and spleen (**D**) are depicted in black for Ad-CMV-GOL infected mice and in red for Ad-TTR-GOL infected mice.

In summary, all CD45.1$^+$ T cells uniformly expressed CD44 independently of infection outcome. However, the analysis of CD44 and CD62L expression did not explain the differences observed in T cell and infection kinetics between Ad-CMV-GOL and Ad-TTR-GOL infected mice. Besides, no differences were observed regarding CD127 expression (**Fig. S 1**).

2.1.3.2 Transiting and resident hepatic CD8$^+$ T cells in resolved and persistent viral infection of the liver

To elucidate differences in antigen-specific T cell populations after resolved and during persisting liver infection, markers for effector memory T cells (T_{EM} cells) and tissue-resident memory T cells (T_{RM} cells) were analyzed from the activation phase (d3) on until memory phase (d98, **Fig. 10**). Therefore, expression of the liver T_{RM} marker CXCR6[93,97] and the T_{EM} marker CX_3CR1[77,78] on CD45.1$^+$ CD8$^+$ T cells were analyzed

in the liver (**Fig. 10A**) and spleen (**Fig. 10B**). Hepatic CD45.1$^+$ T cells separated into a CXCR6^{hi} and a CX$_3$CR1$^+$ population from as early as d18 p.i. with Ad-CMV-GOL. These populations were maintained at least up to d98 p.i. (**Fig. 10A**). Of note, this was not observed for CD45.1$^+$ T cells in Ad-TTR-GOL infected livers. Here, only CXCR6^{hi} cells, but not CXCR6^{neg}CX$_3$CR1$^+$ cells, were detected. A fraction of CXCR6^{hi} cells in persistently infected livers co-expressed CX$_3$CR1$^+$, as observed on d7 in both infection models, hinting at an insufficient T_{EM} cell development. CD45.1$^+$ T cells in spleens of Ad-CMV-GOL infected mice developed into a substantial CX$_3$CR1$^+$ population, likely representing circulating T_{EM} cells (**Fig. 10B**). Of note, no profound CD45.1$^+$ population was maintained in spleens of Ad-TTR-GOL infected mice.

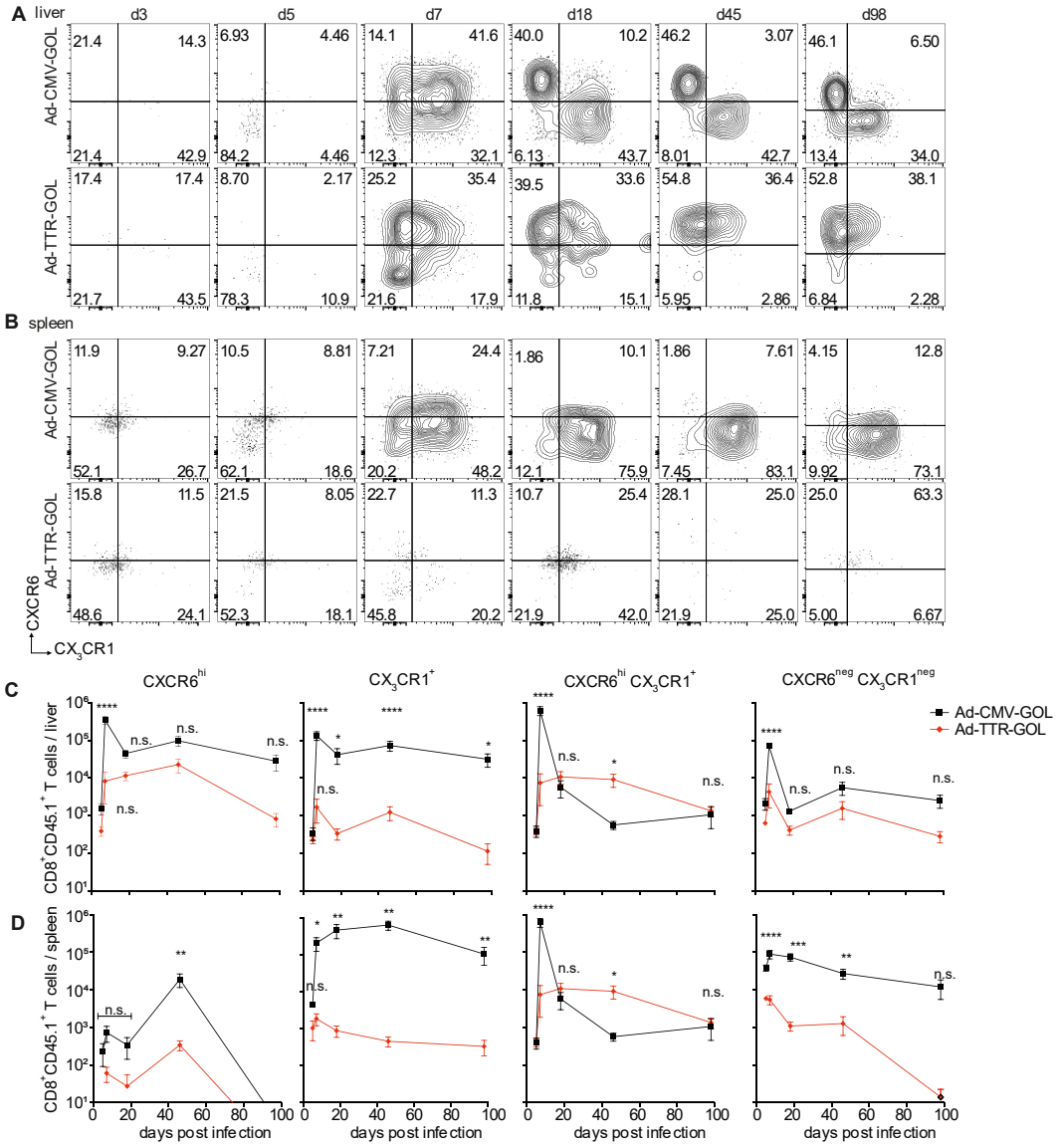

Fig. 10 Time kinetics of CXCR6^{hi} and CX$_3$CR1$^+$ CD45.1$^+$ CD8$^+$ T cells in the liver and spleen after Ad-CMV-GOL and Ad-TTR-GOL infection.
A-B Expression of CXCR6 and CX$_3$CR1 was monitored during acute resolving Ad-CMV-GOL and persistent Ad-TTR-GOL infection. CD45.1$^+$ CD8$^+$ T cells from the liver (**A**) and spleen (**B**) were analyzed on days 3, 5, 7, 28, 45, and 98 p.i. **C-D** Gated populations (A, B) were quantified in the liver (**C**) and spleen (**D**).

Absolute numbers of CXCR6^{hi}, CXCR6^{hi}CX$_3$CR1$^+$, CX$_3$CR1$^+$, and CXCR6^{neg}CX$_3$CR1^{neg} CD45.1$^+$ T cells were quantified in both liver (**Fig. 10C**) and spleen

(**Fig. 10D**), showing the development of CXCR6^{hi} in the liver and CX$_3$CR1$^+$ cells in the liver and spleen after resolved infections. CXCR6^{hi} and CXCR6^{hi}CX$_3$CR1$^+$ cells were maintained during persistent infection in the liver. Using rectangular gates instead of quadrants for a more accurate population definition, I quantified the exact frequencies of CXCR6^{hi}, CXCR6^{hi}CX$_3$CR1$^+$, CX$_3$CR1$^+$, and CXCR6^{neg}CX$_3$CR1^{neg} CD45.1$^+$ and CD45.1^{neg} T cells in the liver (**Fig. 11A**) and spleen (**Fig. 11B**) on day 45 p.i. Comparing frequencies instead of absolute cell numbers resulted in the observation of the same distribution, namely hepatic CXC6^{hi}, hepatic and splenic CX$_3$CR1$^+$ CD45.1$^+$CD8$^+$ T cells after resolved infection and hepatic CXCR6^{hi} and CXCR6^{hi}CX$_3$CR1$^+$ CD45.1$^+$CD8$^+$ T cells during persistent infection.

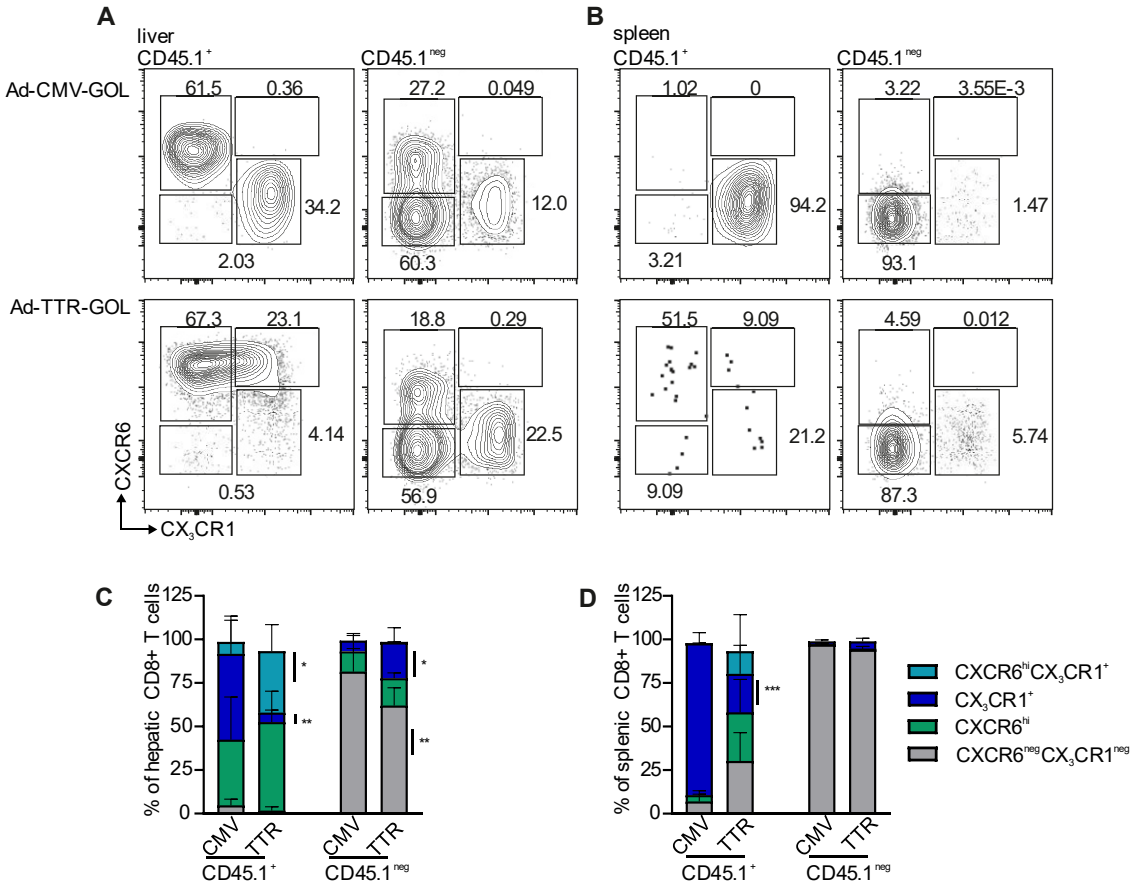

Fig. 11 Frequencies of CXCR6^{hi} and CX$_3$CR$^+$ CD8$^+$ T cells in the liver and spleen on day 45 post resolved Ad-CMV-GOL or persistent Ad-CMV-GOL infection.
A-B CD45.1$^+$ and CD45.1^{neg} CD8$^+$ T cells were gated according to their CXCR6 and CX3CR1 expression in liver (**A**) and spleen (**B**). **C-D** Frequencies of hepatic (**C**) and splenic (**D**) T cell populations were quantified for Ad-CMV-GOL (CMV) and Ad-TTR-GOL (TTR) infection.

These results were further corroborated by t-distributed stochastic neighbor embedding (t-SNE) analysis (**Fig. 12A, B**). CD45.1$^+$CD8$^+$ T cells were separated into CXCR6^{hi} and CX$_3$CR1^{hi} cells after resolved infection (**Fig. 12A**), whereas all CD45.1$^+$ cells were CXCR6^{hi} and CX$_3$CR1^{low} during persistent infection (**Fig. 12B**). In contrast, the activation marker CD44 and naïve T cell/T$_{CM}$ marker CD62L did not separate

antigen-specific T cells (**Fig. 12 A, B**). Therefore, the subsequent analyses focussed on CXCR6^{hi} and CX$_3$CR1$^+$ populations.

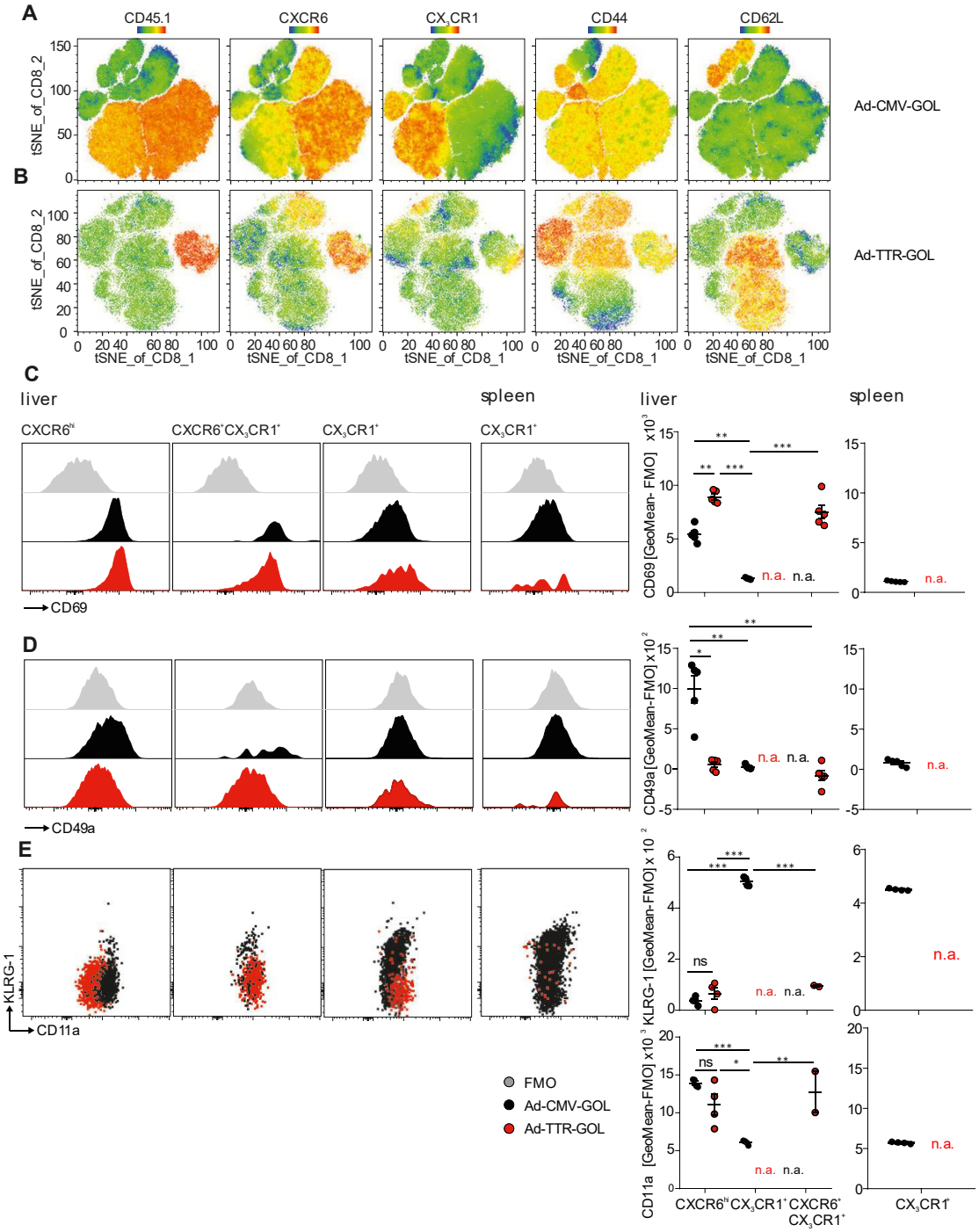

Fig. 12 Phenotype of hepatic and splenic CXCR6^{hi} and CX$_3$CR1$^+$ CD45.1$^+$CD8$^+$ T cells on d45 after resolved Ad-CMV-GOL or persistent Ad-TTR-GOL infection.
A-B t-Distributed stochastic neighbor embedding of hepatic CD8$^+$ T cells in Ad-CMV-GOL (**A**) and Ad-TTR-GOL (**B**) infection of a panel consisting of CD8, CD45.1, CXCR6, CX$_3$CR1, CD127, CD11a, KLRG-1, GzmB. **C-E** CD45.1$^+$CD8$^+$ T Cells were pre-gated according to their CXCR6 and CX$_3$CR1 expression. Geometric means of fluorescence intensities were normalized to FMO controls for quantification.

First, hepatic and splenic T$_{RM}$-like antigen-specific CD8$^+$ T cells were examined regarding other tissue-residency markers besides CXCR6. Indeed, hepatic CXCR6^{hi} but not CX$_3$CR1$^+$ CD45.1$^+$CD8$^+$ T cells in both resolved and persistent liver infection

expressed the universal tissue residency marker CD69 (**Fig. 12C**) as well as the adhesion-mediating integrin αL (CD11a, **Fig. 12E**). Of note, only CXCR6^{hi}CD8^{+} T cell after resolved but not during persistent infection expressed CD49a (**Fig. 12D**), a marker described for identifying T_{RM} cells with high cytotoxic potential[96]. Importantly, antigen-specific $CX_3CR1^{+}CD8^{+}$ T cells in the liver or spleen were only present after resolved infection and did not express residency markers. However, approximately 50% of $CX_3CR1^{+}CD8^{+}$ T cells expressed the effector marker KLRG1 (**Fig. 12E**), suggesting these cells were effector T cells and that $CX_3CR1^{+}CD8^{+}$ T cells were only present after a resolved infection. CD103, a marker described for epithelial T_{RM} cells, was not expressed on liver CXCR6^{hi} T cells (**Fig. S 2**).

Taken together, all antigen-specific CD8^{+} T cells were antigen-experienced in the liver and spleen after resolved infection. Of note, these cells separated clearly into CXCR6^{hi} cells resembling T_{RM} cells and CX_3CR1^{+} cells with an effector/effector memory phenotype. In contrast, antigen-specific CD8^{+} T cells were mainly CXCR6^{hi} in the liver during persistent Ad-TTR-GOL infection. These CXCR6^{hi}CD8^{+} T cells expressed the residency markers CD69 and CD11a but failed to express the functionality-associated T_{RM} marker CD49a. This prompted me to analyze the population maintenance of antigen-specific CD8^{+} T cells after resolved or during persistent infection.

2.1.3.3 Proliferation of antigen-specific CD8^{+} T cell in liver and spleen

Antigen-specific CXCR6^{hi}CD8^{+} T cells persisted in livers after resolved and during persistent viral infection for at least 98 days, raising the question of whether these T cells were maintained by proliferation or longevity. To answer the question of population maintenance, BrdU incorporation and Ki-67 expression were measured in antigen-specific hepatic CD8^{+} T cells. Significantly more antigen-specific CXCR6^{hi} CD45.1^{+}CD8^{+} T cells during persistent viral infections incorporated BrdU and were Ki-67^{+} than CXCR6^{hi} CD45.1^{+}CD8^{+} T cells after resolved infection (**Fig. 13 A, B**). Of note, there was no difference between CXCR6^{hi} and CXCR6$^{hi}CX_3CR1^{+}$ T cells during persistent infection. Significantly more CXCR6^{hi} cells compared to CX_3CR1^{+} cells were BrdU^{neg}Ki-67^{+} (**Fig. 13 A** left side, **B**). However, there was no significant difference in BrdU incorporation.

In summary, antigen-specific CD8^{+} T cells after resolved infection were likely long-lived and slow-cycling, contrasting antigen-specific CXCR6^{hi}CD8^{+} T cells in a persistent infection presumably maintained by proliferation. This difference in population maintenance led me to characterize exhaustion markers expression on antigen-specific CD8^{+} T cells in persistent and resolved liver infection.

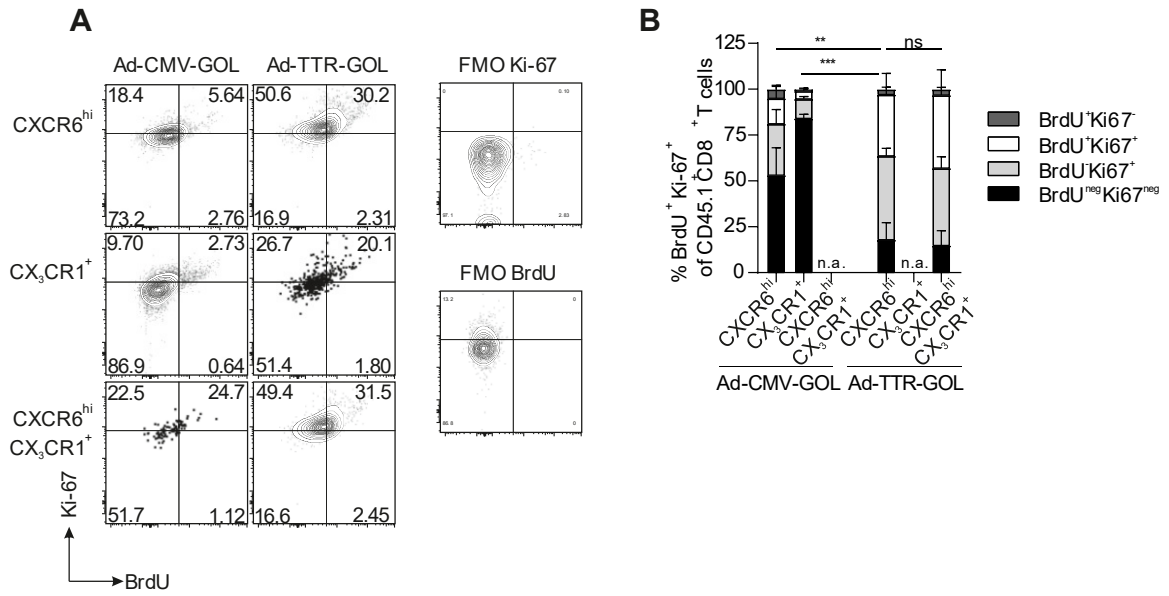

Fig. 13 Proliferation of antigen-specific CD8⁺ T cells in the liver.
A Proliferation of CD45.1⁺CD8⁺ T cell after resolved Ad-CMV-GOL and during persistent Ad-TTR-GOL infection was assessed by BrdU incorporation and Ki-67 expression analysis in the liver. **B** CD45.1⁺CD8⁺ T Cells were pre-gated according to their CXCR6 and CX_3CR1 expression**.** Frequencies of BrdU and Ki-67 expressing T cells in the liver.

2.1.3.4 Inhibitory receptors and exhaustion markers

To elucidate further differences between antigen-specific $CXCR6^{hi}CD8^+$ T cells in resolved and persistent Ad-GOL infections, expression of inhibitory receptors and exhaustion markers was analyzed. First, I compared PD-1 and TIGIT expression in different CD8⁺ T cell populations from resolved Ad-CMV-GOL and persistent Ad-TTR-GOL infection (**Fig. 14**). $CXCR6^{hi}$ and $CXCR6^{hi}CX_3CR1^+$ antigen-specific $CD45.1^+CD8^+$ T cells during persistent infection co-expressed PD-1 and TIGIT at significantly higher levels as $CXCR6^{hi}$ $CD45.1^+CD8^+$ T cells after resolved infection (**Fig. 14 A, B**). In addition to lower PD-1 levels, $CXCR6^{hi}CD8^+$ T cells after resolved infection only partially co-expressed TIGIT. Of note, $CXCR6^{hi}$ cells after resolved infection expressed more PD-1 than CX_3CR1^+ $CD45.1^+CD8^+$ T cells from the same liver, in line with PD-1 expression being described for T_{RM} cells[107]. $CD45.1^+$ and $CD45.1^{neg}$ $CD8^+$ T cells in the spleen did not express PD-1 or TIGIT (**Fig. 14 A, C**). Polyclonal endogenous $CD45.1^{neg}CD8^+$ T cells in the liver and spleen mirrored the antigen-specific $CD45.1^+CD8^+$ T cells partially, as presumably only a fraction of these cells responded toward the viral infection.

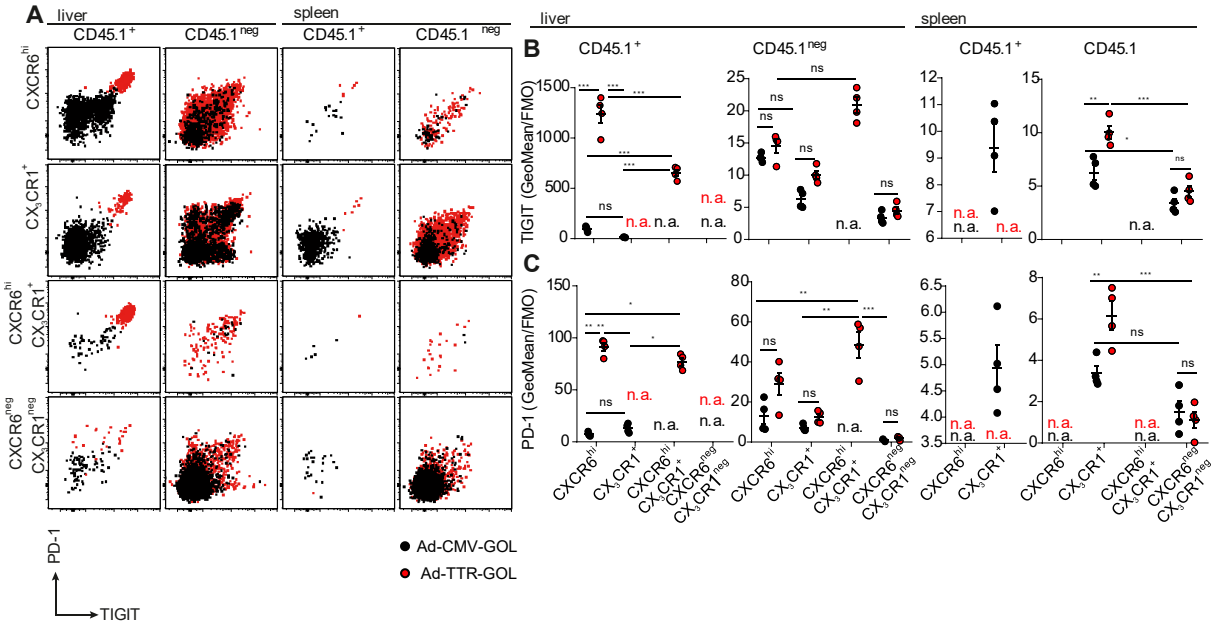

Fig. 14 CD8⁺ T cell exhaustion in persistent Ad-TTR-GOL infection compared to resolved Ad-CMV-GOL infection on d>30.
A CD45.1⁺ and CD45.1^{neg} CD8⁺ T Cells were pre-gated according to their CXCR6 and CX_3CR1 expression**.** Expression of PD-1 and TIGIT on CD45.1⁺ and CD45.1^{neg} CD8⁺ T cells in the liver and spleen. **B-C** Geometric means of fluorescence intensities were normalized to the respective FMO control for liver (**B**) and spleen (**C**).

Furthermore, expression of the exhaustion-associated transcription factor TOX coincided with PD-1 expression and was significantly increased on CXCR6^{hi} CD45.1⁺CD8⁺ T cells during persistent infection compared to CXCR6^{hi} cells after resolved infection (**Fig. 15 A, B**). As observed for PD-1, splenic CD45.1⁺ and CD45.1^{neg}CD8⁺ T cells expressed very low levels of TOX (**Fig. 15 A, C**).

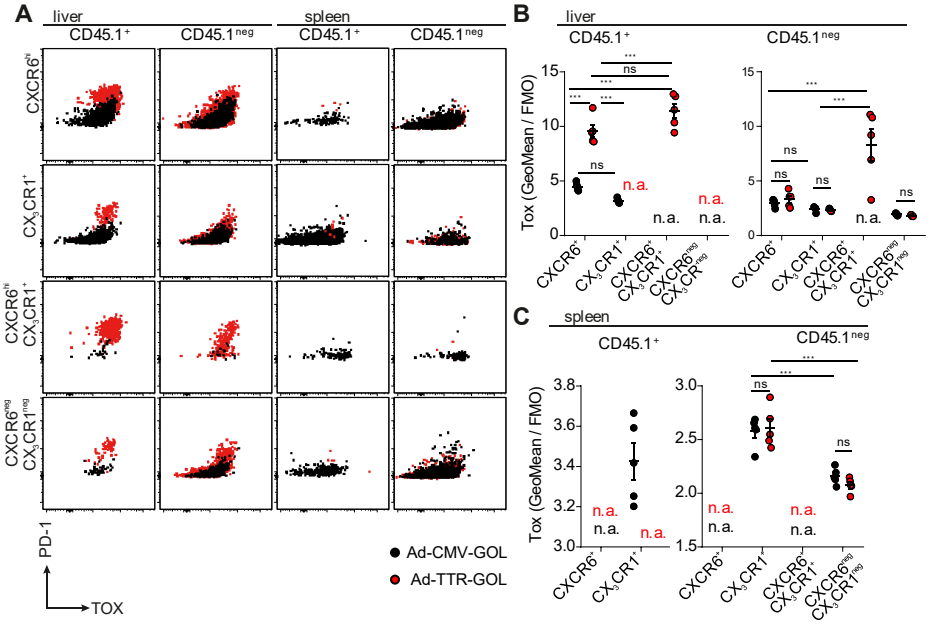

Fig. 15 CD8⁺ T cell exhaustion in persistent Ad-TTR-GOL infection compared to resolved Ad-CMV-GOL infection on d>30.
A CD45.1⁺ and CD45.1^{neg} CD8⁺ T Cells were pre-gated according to their CXCR6 and CX_3CR1 expression**.** Expression of the inhibitory receptors PD-1 and the exhaustion-related transcription factor TOX on CD45.1⁺ and CD45.1^{neg} CD8⁺ T cells in the liver and spleen. **B-C** Geometric means of fluorescence intensities were normalized to the respective FMO control for liver (**B**) and spleen (**C**).

Additionally, expression of the inhibitory receptors Lag-3 and Tim-3 was analyzed, as both expression level and the multitude of inhibitory receptors determine the degree of T cell exhaustion. CXCR6^{hi} CD45.1^{+}CD8^{+} T cells during persistent liver infection co-expressed significantly more Lag-3 and Tim-3 than CXCR6^{hi} cells after resolved infection (**Fig. 16 A, C**). As observed for PD-1, CXCR6^{hi} CD45.1^{+}CD8^{+} T cells after resolved infection expressed more Lag-3 and Tim-3 than CX$_3$CR1^{+} T cells. Interestingly, polyclonal CD45.1^{neg}CD8^{+} T cells expressed Tim-3 during persistent liver infection, albeit at lower levels than CD45.1^{+} cells. Polyclonal splenic CX$_3$CR1^{+} CD45.1^{neg}CD8^{+} T cells during persistent infection expressed more Lag-3 than polyclonal splenic CX$_3$CR1^{+} T cells after resolved infection (**Fig. 16D**).

Taken together, antigen-specific CXCR6^{hi}CD8^{+} T cells during persistent infection were characterized by co-expression of several inhibitory receptors and the exhaustion-associated transcription factor TOX. Contrastingly, antigen-specific CXCR6^{hi}CD8^{+} T cells after resolved infection expressed significantly lower levels of inhibitory receptors than their counterparts in persistent infection, but more than CX$_3$CR1^{+} T cells after resolved infection, which did not express inhibitory receptors or TOX.

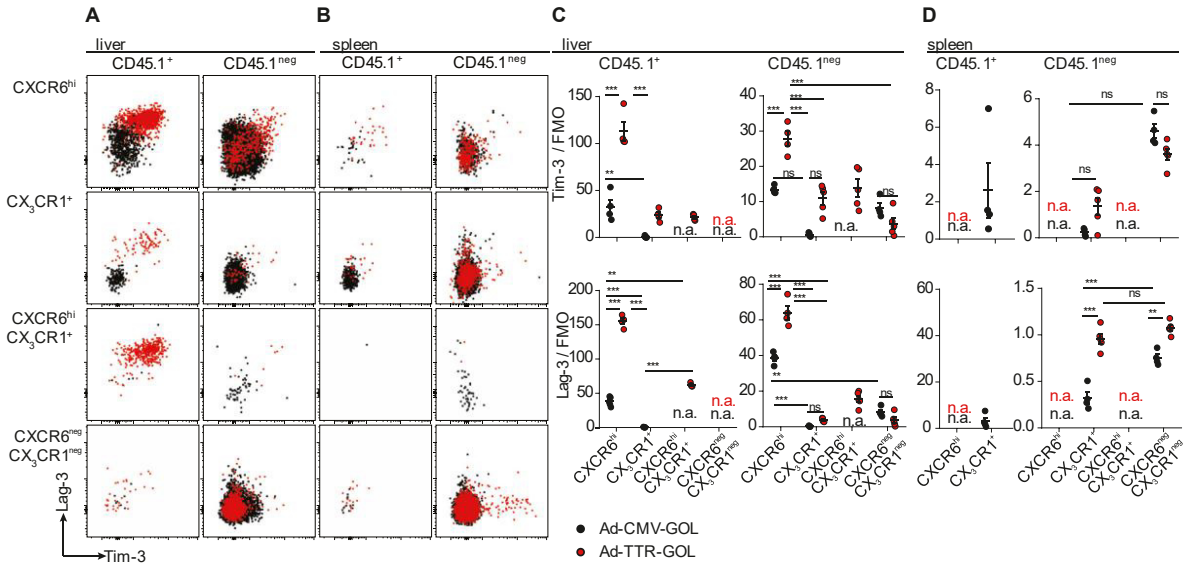

Fig. 16 Exhaustion marker expression of CD8^{+} T cells after resolved or during persistent infection on d>30. **A-B** Representative dot plots of Lag-3 and Tim-3 surface expression on CD45.1^{+} and CD45.1^{neg} CD8^{+} T cells in the liver (**A**) and spleen (**B**). **C-D** Geometric means of fluorescence intensities were normalized to the respective FMO control for liver (**C**) and spleen (**D**).

2.1.4 Functionality of antigen-specific CD8^{+} T cells

T$_{RM}$ cells are described as highly alert cells reacting fast upon re-exposure to previously encountered pathogens, and potent T cell effector functions are considered a hallmark of T$_{RM}$ cells. Therefore, I analyzed the expression of the target cell lysis-mediating effector molecule granzyme B (GzmB). Antigen-specific hepatic CXCR6^{hi} CD45.1^{+}CD8^{+} T cells after resolved infection expressed significantly more GzmB compared to all other CD8^{+} T cell populations analyzed (**Fig. 17 A, C**). Of note, hepatic or splenic antigen-specific CX$_3$CR1^{+} T cells after resolved infection expressed levels

comparable to those of CXCR6^{hi} T cells during persistent infection (**Fig. 17 A, C**). Interestingly, polyclonal CXCR6^{hi} CD45.1^{neg}CD8^{+} T cells during persistent infection expressed more GzmB than CX$_3$CR1^{+} CD45.1^{neg}CD8^{+} T cells after resolved infection (**Fig. 17 B, C**), indicating only antigen-specific T cells failed to express GzmB.

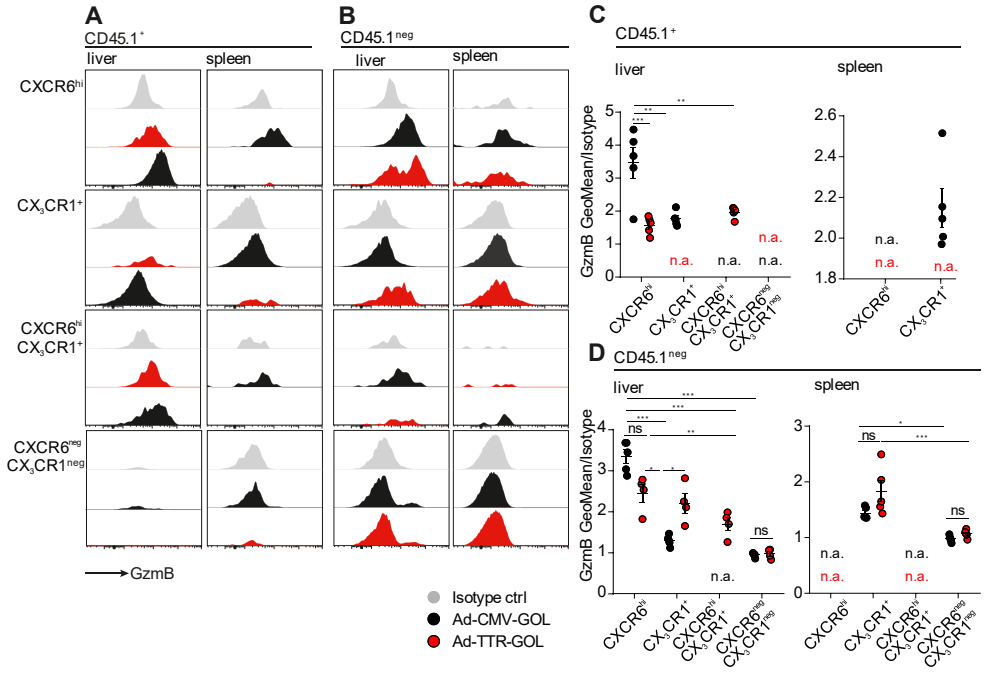

Fig. 17 Intracellular Granzyme B expression in CD8^{+} T cells in resolved Ad-CMV-GOL or persistent Ad-TTR-GOL infection on d>30.
A-B Representative histogram plots of Granzyme B (GzmB) expression are shown for hepatic and splenic CD45.1^{+} (**A**) and polyclonal CD45.1^{neg} **(B)** CD8^{+} T cells. Isotype control (grey), resolved Ad-CMV-GOL infection (black), and persistent Ad-TTR-GOL infection (red) are depicted in one plot. **C-D** Geometric means of fluorescence intensities were normalized to the respective isotype control for the liver and spleen (**C, D**).

In addition to GzmB expression, cytokine production was analyzed in CD8^{+} T cells upon antigen re-exposure via peptide re-stimulation *ex vivo*. Liver CXCR6^{hi} and CX$_3$CR1^{+} CD45.1^{+}CD8^{+} T cells after resolved infection produced TNF and IFNγ upon peptide re-stimulation, whereas CXCR6^{hi} and CXCR6^{hi}CX$_3$CR1^{+} CD45.1^{+}CD8^{+} T cells during persistent infection failed to produce cytokines upon peptide re-stimulation or PMA/Ionomycin stimulation (**Fig. 18 A, B**). Of note, polyclonal CD45.1^{neg}CD8^{+} T cells produced cytokines when stimulated with PMA/Ionomycin (**Fig. 18 C, D**), demonstrating that T cell dysfunction was limited to antigen-specific T cells during persistent liver infection.

Next, I aimed at measuring actual target cell killing capacities of antigen-specific CD8^{+} T cells *ex vivo*. Therefore, primary murine hepatocytes were loaded with cognate peptide (SIINFEKL), and real-time killing by sorted antigen-specific CD8^{+} T cell populations was monitored (**Fig. 19**). Strikingly, CXCR6^{hi}CD8^{+} T cells after resolved infection killed SIINFEKL-loaded hepatocytes within 5 h, whereas CX$_3$CR1^{+}CD8^{+} T cells from livers or spleens after a resolved infection started killing hepatocytes delayed and were significantly less efficient. CXCR6^{hi}CD8^{+} T cells during persistent infection

completely failed at killing SIINFEKL-loaded hepatocytes, coinciding with the lack of GzmB and cytokine expression.

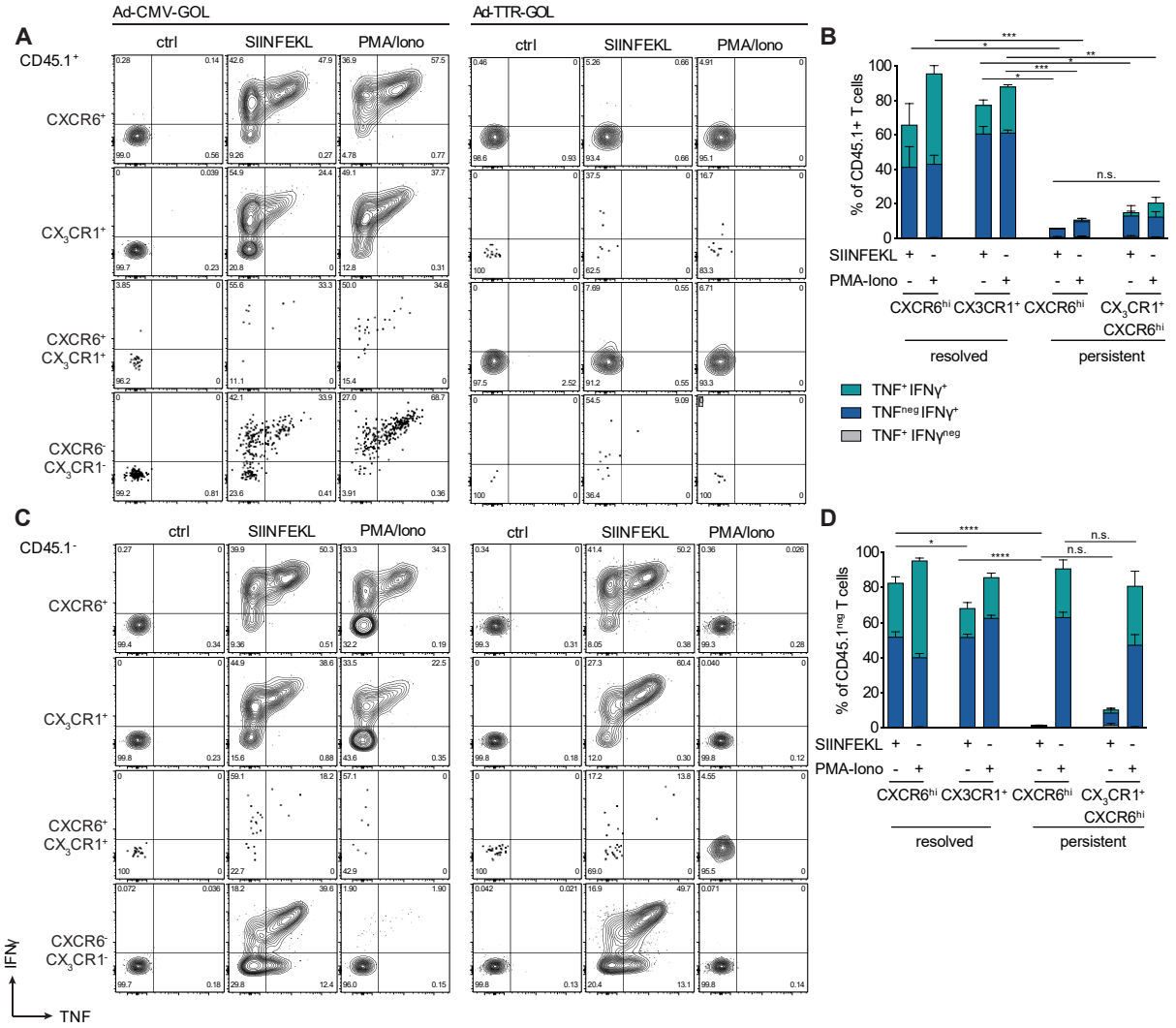

Fig. 18 Cytokine production in CD8⁺ T cells from resolved Ad-CMV-GOL or persistent Ad-TTR-GOL infection upon re-stimulation on d>30.
A-D Liver-associated lymphocytes isolated from mice with resolved Ad-CMV-GOL (**A, C**) or persistent Ad-TTR-GOL infection (**B, D**) were re-stimulated with SIINFEKL peptide or PMA-/Ionomycin for 15 h. CD45.1⁺ and CD45.1^{neg} CD8⁺ T Cells were pre-gated according to their CXCR6 and CX_3CR1 expression**.** TNF and IFNγ expression was analyzed by intracellular cytokine staining in CD45.1⁺ (**A, B**) and CD45.1^{neg} CD8⁺ T cells (**C, D**).

In summary, antigen-specific $CX_3CR1^+CD8^+$ T cells from the liver and spleen after resolved infection expressed GzmB, produced cytokines upon re-stimulation, and killed target cells. $CXCR6^{hi}CD8^+$ T cells after resolved infection were even more functional, reacting faster and stronger towards antigen re-exposure. In sharp contrast, antigen-specific $CXCR6^{hi}CD8^+$ T cells during persistent infection completely lacked effector functions, corresponding to high expression levels of inhibitory receptors.

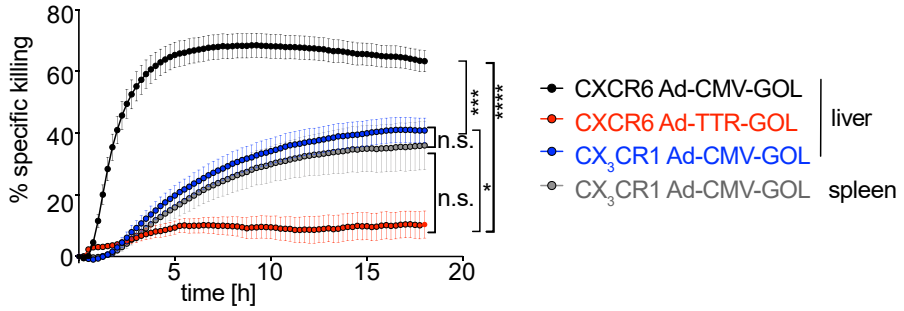

Fig. 19 Real-time killing assay of peptide-loaded primary murine hepatocytes by antigen-specific CD8⁺ T cells at d>30 p.i.
Sorted CD45.1⁺CD8⁺ T cell populations from liver and spleen after resolved infection and liver during persistent infection were incubated for 20 h with SIINFEKL-loaded primary murine hepatocytes or control hepatocytes. xCelligence technology was used for real-time impedance measurements to determine the killing kinetics of the T cell populations. Statistical analysis: Ordinary One-way ANOVA on AUCs.

2.2 Relevance of the chemokine receptor CXCR6 for T_{RM} cell formation in the Ad-GOL model system

In the experiments described so far, I used CXCR6 to identify liver-resident T cells. However, the role of this chemokine receptor for liver-resident T cell formation was not analyzed. Therefore, I infected CXCR6$^{GFP/GFP}$ mice with Ad-CMV-GOL to characterize whether antigen-specific T cells in the liver and spleen differed from those of CXCR6$^{WT/WT}$ mice.

First, I examined infection kinetics via bioluminescence measurements. CXCR6$^{WT/WT}$ and CXCR6$^{GFP/GFP}$ mice controlled the infection with the same kinetic (**Fig. 20**), suggesting that either CXCR6^{neg} cells clear the infection in wild-type mice or CXCR6$^{GFP/GFP}$ cells were still able to migrate to the liver and exert anti-viral immunity.

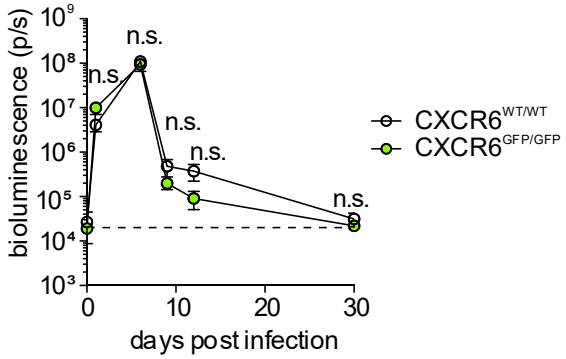

Fig. 20 Infection kinetics of Ad-CMV-GOL infected CXCR6$^{WT/WT}$ and CXCR6$^{GFP/GFP}$ mice.
In vivo bioluminescence of the liver was measured *via* IVIS to monitor hepatic antigen expression on d0, d1, d6, d9, d12, and d30 after Ad-CMV-GOL infection in CXCR6$^{WT/WT}$ as well as CXCR6$^{GFP/GFP}$ mice, where the CXCR6 gene was replaced by GFP and therefore lacked functional CXCR6 expression.

Next, antigen-specific CD8⁺ T cells in CXCR6$^{GFP/GFP}$ and CXCR6$^{WT/WT}$ mice were quantified after resolved infection. Antigen-specific CD8⁺ T cells in the liver were identified via streptamer labeling (**Fig. 21A**). Interestingly, the lack of CXCR6 in these mice did not reduce the number of antigen-specific CD8⁺ T cells in the liver (**Fig. 21B**).

Instead, the proportion of GFP^{hi} antigen-specific T cells was increased compared to CXCR6^{hi} cells (**Fig. 21 C-D**). Within CXCR6$^{GFP/GFP}$ CD8^{+} T cells, I distinguished CX$_3$CR1^{+}GFP^{neg} and CX$_3$CR1^{+}GFP^{+} cells, which was impossible by antibody labeling before. Of note, CX$_3$CR1^{+} cells were less abundant in CXCR6$^{GFP/GFP}$ mice compared to CXCR6$^{WT/WT}$ mice. This difference was not compensated by CX$_3$CR1^{+}GFP^{+} cells (**Fig. 21 C-D**). Hence, the ratio of liver-resident cells and T_{EM} cells was altered in CXCR6$^{GFP/GFP}$ CD8^{+} T cells (**Fig. 21E**).

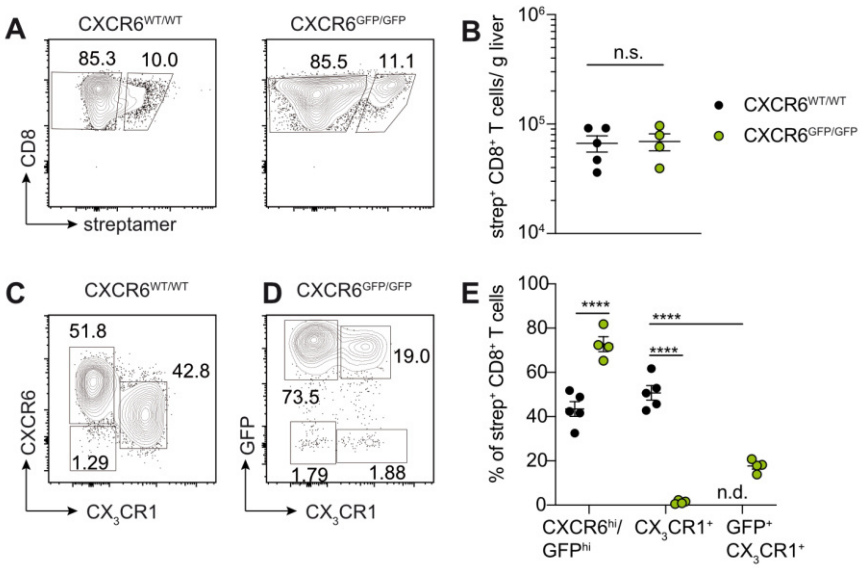

Fig. 21. CXCR6$^{WT/WT}$ and CXCR6$^{GFP/GFP}$ CD8^{+} T cells after resolved Ad-CMV-GOL infection.
A Antigen-specific CD8^{+} T cells were identified by streptamer labeling in CXCR6$^{WT/WT}$ (left) and CXCR6$^{GFP/GFP}$ (right) mice. **B** Quantification of antigen-specific streptamer^{+} CD8^{+} T cells in the liver. **C-D** Expression of CXCR6 or GFP and CX$_3$CR1 on antigen-specific CD8^{+} T cells in the liver. **E** Quantification of antigen-specific liver CXCR6^{hi} or GFP^{+} CD8^{+} T cells from CXCR6$^{WT/WT}$ and CXCR6$^{GFP/GFP}$ mice, respectively, and CX$_3$CR1^{+} CD8^{+} T cells from both CXCR6$^{WT/WT}$ and CXCR6$^{GFP/GFP}$ mice, and GFP^{+}CX$_3$CR1^{+} CD8^{+} T cells from CXCR6$^{GFP/GFP}$ mice.

Loss of CXCR6 expression did not affect migration to the liver or maintenance of liver-resident CD8^{+} T cells. Still, I aimed at analyzing whether their functionality was affected. Therefore, hepatic T cells were re-exposed to cognate peptide antigen. Indeed, GFP^{hi}CD8^{+} T cells produced fewer cytokines upon peptide re-stimulation when compared to CXCR6^{hi}CD8^{+} T cells (**Fig. 22 A-B**)

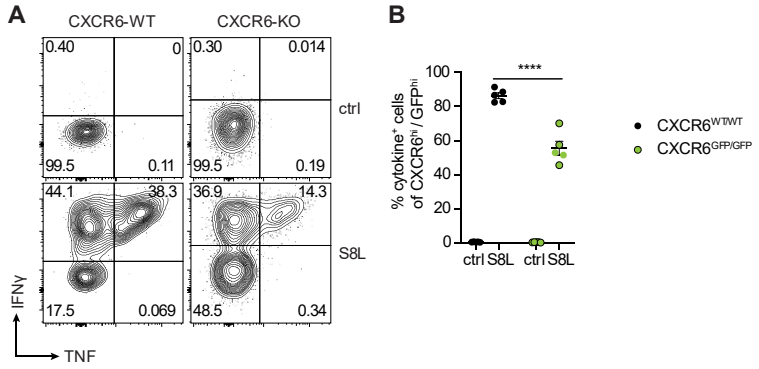

Fig. 22 Cytokine expression of CXCR6$^{WT/WT}$ and CXCR6$^{GFP/GFP}$ CD8^{+} T cells.
A CXCR6$^{WT/WT}$ and CXCR6$^{GFP/GFP}$ T cells were isolated from livers after resolved infection and re-stimulated with cognate SIINFEKL (S8L) peptide. Expression of IFNγ and TNF was measured. **B** Cytokine expressing CXCR6^{hi} and GFP^{hi} cells, respectively, were quantified.

In summary, a lack of CXCR6 expression did not hamper the clearance of Ad-CMV-GOL infection of hepatocytes nor the maintenance of hepatic antigen-specific CD8$^+$ T cells within the time frame monitored. However, responsiveness towards antigen re-exposure was reduced in CXCR6-deficient CD8$^+$ T cells, indicating a so far not fully clarified role of CXCR6 in the effector function of T cells.

2.3 Transcriptional analysis of antigen-specific CD8$^+$ T cells after resolved and during persistent liver infection

Antigen-specific CD8$^+$ T cells after resolved or during persistent infection differ fundamentally regarding their phenotype and functionality. To decipher the regulatory mechanisms causing these effects, RNA sequencing was performed. For this, liver CXCR6^{hi} and CX$_3$CR1$^+$ CD45.1$^+$CD8$^+$ T cells and splenic CX$_3$CR1$^+$ T cells after resolved infection (d40 p.i.) and liver CXCR6^{hi} and CXCR6^{hi}CX$_3$CR1$^+$ CD45.1$^+$CD8$^+$ T cells during persistent infection (d40 p.i.) were sorted. The resulting insights are set out in the following.

2.3.1 Differential gene expression in hepatic and splenic CD45.1$^+$CD8$^+$ T cell populations

Transcriptome profiling by RNAseq generates a vast data set, which generates new hypotheses, allows for comparison with other data sets, and provides valuable insights into cellular regulation. **Fig. 23A** delineates the workflow of the bioinformatic analyses. Differentially expressed genes (DEGs) are shown in Table 1 - Table 5 in section 6.2 (p.99). First, principal component analysis (PCA) was performed to examine population separation based on DEGs (**Fig. 23B**). PCA revealed 4 distinct CD45.1$^+$CD8$^+$ T cell populations: splenic and hepatic CX$_3$CR1$^+$ T cells, hepatic CXCR6^{hi} T cells after resolved infection well as CXCR6^{hi} or CXCR6^{hi}CX$_3$CR1$^+$ T cells during persistent infection, that did not form separate clusters as there were no DEGs between these populations.

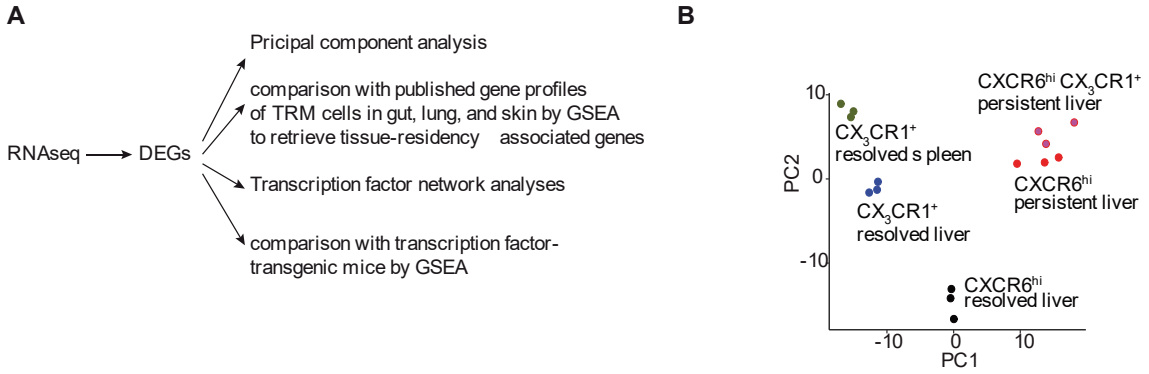

Fig. 23 RNAseq of antigen-specific CD8$^+$ T cells from the liver and spleen after resolved or during persistent Ad-GOL infection.
A Workflow of bioinformatic analysis. **B** Principal component analysis (PCA) of sorted antigen-specific CD45.1$^+$CD8$^+$ T cells from liver and spleen after resolved infection or during persistent infection. PCA: principal component analysis; 1 individual experiment with 3 biological replicates.

Next, differential gene expression was analyzed between hepatic and splenic antigen-specific CD8⁺ T cell populations. Hierarchical clustering of DEGs between splenic $CX_3CR1^+CD8^+$ T cells after resolved infection and hepatic $CXCR6^{hi}CD8^+$ T cells during persistent infection revealed 310 DEGs (**Fig. 24A,** DEGs in Table 1**,** Table 2**,** Table 4). 200 DEGs and 45 DEGs were found between splenic $CX_3CR1^+CD8^+$ T cells and hepatic $CXCR6^{hi}CD8^+$ T cells (**Fig. 24B**) and $CX_3CR1^+CD8^+$ T cells (**Fig. 24C**) after resolved infection, respectively. Hence, hepatic CD8⁺ T cells were clearly distinct from splenic $CX_3CR1^+CD8^+$ T cells. This effect was most substantial for $CXCR6^{hi}CD8^+$ T cells during persistent infection but also clearly evident for $CXCR6^{hi}CD8^+$ T cells after resolved infection. Of note, $CX_3CR1^+CD8^+$ T cells in the liver and spleen showed only minor differences in gene expression. Among the top 10 DEGs were the transcription factors *Nr4a1*, *Fos,* and *Jun* (**Fig. 24D**).

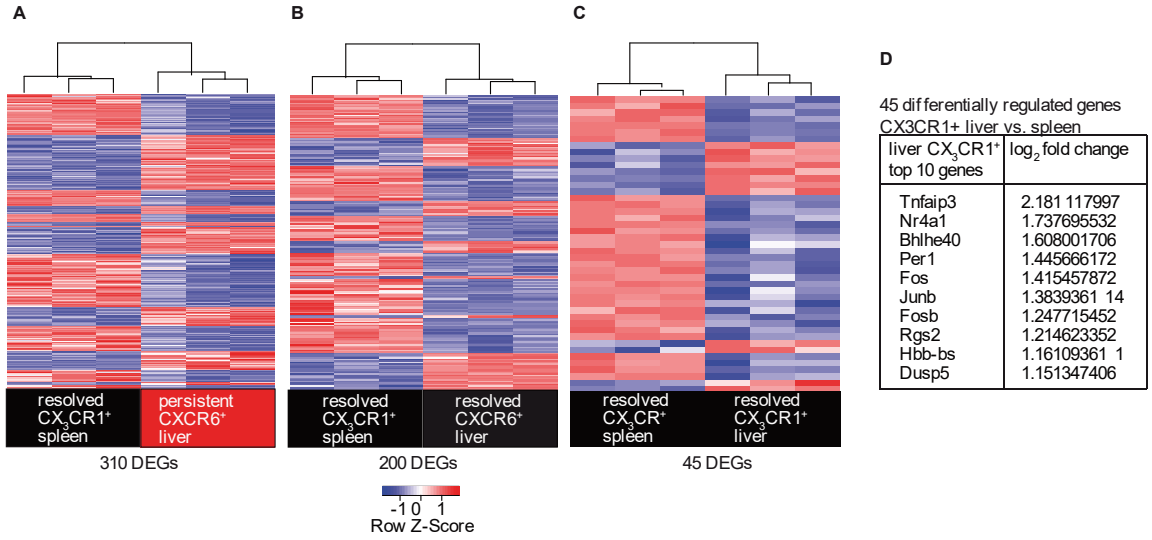

Fig. 24 Hierarchical clustering of DEGs between antigen-specific CD8⁺ T cells in the liver and spleen.
A DEGs between splenic $CX_3CR1^+CD45.1^+CD8^+$ T cells after resolved infection and hepatic $CXCR6^{hi}$ cells during persistent infection, **B** $CXCR6^{hi}$ T cells after resolved infection, **C** and CX_3CR1^+ T cells after resolved infection. **D** Top 10 regulated genes in liver CX_3R1^+ T cells when comparing liver and spleen after resolved infection. DEGs: differentially regulates genes; 1 individual experiment with 3 biological replicates; Analysis performed by Sainitin Donakonda.

2.3.2 Expression of residency-associated genes in $CXCR6^{hi}$ $CD45.1^+CD8^+$ T cells in the liver

$CXCR6^{hi}CD69^+$ $CD8^+$ T cells in the liver resembled T_{RM} cells phenotypically (**Fig. 12**) but were dysfunctional in persistently infected livers and highly functional after resolved infection (**Fig. 14** - **Fig. 19**). Using gene set enrichment analysis (GSEA), DEGs between liver $CXCR6^{hi}CD8^+$ T cells after resolved or during persistent infection, respectively, and splenic $CX_3CR1^+CD8^+$ T cells after resolved infection were compared with gene profiles published for T_{RMs} isolated from gut, lung, and skin (**Fig. 25 A, B**, Table 6 - Table 11).

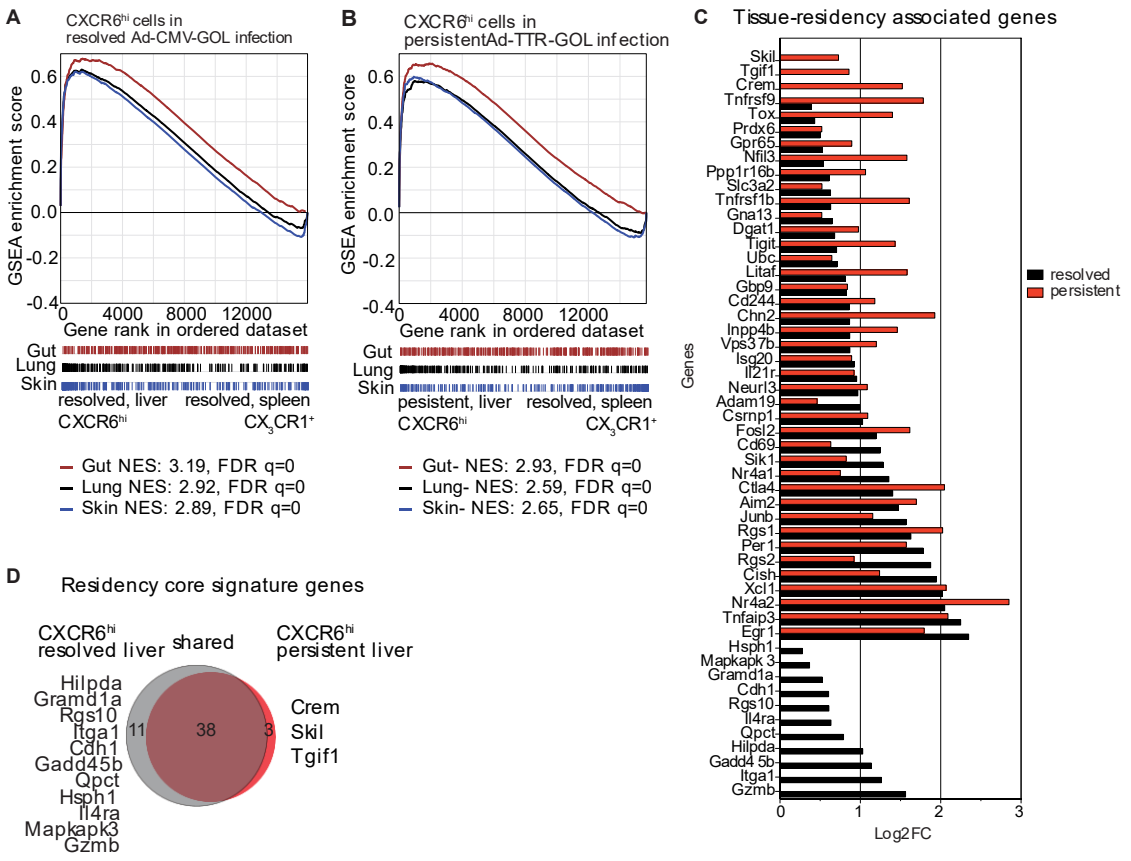

Fig. 25 Expression of tissue residency-associated genes.
A-B GSEA with gene profiles of T_{RM} cells from gut, lung, and skin[108] and DEGs between splenic CX_3CR1^+ after resolved infection and hepatic CXCR6^{hi} cells after resolved infection (**A**) and during persistent infection (**B**). **C** Expression levels of core enrichment residency-associated genes obtained in (A) in antigen-specific CXCR6^{hi}CD8$^+$ T cells after resolved and during persistent infection. **D** Venn diagram of residency-associated core-enrichment genes shared by T_{RM} cells in the liver (resolved and persistent), gut, lung, and skin as well as genes transcribed only in the reference data set and resolved or persistent liver infection, respectively. GSEA: gene set enrichment analysis, DEGs: differentially regulated genes;1 individual experiment with 3 biological replicates; analysis performed by Sainitin Donakonda.

Strikingly, transcriptomes of both functional and dysfunctional CXCR6^{hi}CD8$^+$ T cells enriched strongly in T_{RM} gene profiles. 38 genes contributed to core enrichment (**Fig. 25 C, D**), including the residency-associated transcriptions factors *Nr4a1* and *Nr4a2*[109] and G-protein signaling regulating *Rgs1* and *Rgs2*. However, 11 genes were only expressed in CXCR6^{hi}CD8$^+$ T cell after resolved infection, including *Gzmb* and *Itga1* (encoding CD49a), coinciding with their superior responsiveness. *Cdh1* (Cadherin 1) and *Qpct* (Glutaminyl-Peptide Cyclotransferase) were described before for Malaria-specific T_{RM} cells[93]. Interestingly, three genes were shared by T_{RM} cells in gut, lung, and skin and CXCR6^{hi}CD8$^+$ T cells during persistent, but not after resolved liver infection: The transcription factor *Crem* (cAMP-responsive element modulator), human T_{RM}-associated *Skil* (Smad-interacting Ski-like gene), and *Tgif1* (TGFβ-induced factor homeobox 1).

In summary, GSEA revealed the expression of residency-associated genes in both functional and dysfunctional CXCR6^{hi}CD8$^+$ T cells and corroborated the lack of effector functions observed for antigen-specific CD8$^+$ T cells during persistent infection.

2.3.3 Transcriptional differences between CXCR6^{hi} and CX$_3$CR1$^+$ CD45.1$^+$CD8$^+$ T cells in the liver after resolved infection

It was of interest to further study differences between antigen-specific CXCR6^{hi}CD8$^+$ T cells and CX$_3$CR1$^+$CD8$^+$ T cells after resolved infection, as CXCR6^{hi} T cells responded superiorly to antigen re-exposure compared to CX$_3$CR1$^+$ T cells (**Fig. 26**). 115 genes were differentially expressed between these two populations, including tissue egress-mediating *S1pr1*[89] and its regulating transcription factor *Klf2*[110] and effector T cell marker *Klrg1*[111] exclusively expressed in CX$_3$CR1$^+$ T cells (**Fig. 26 A, B,** Table 5). CXCR6^{hi} T cells expressed *Cxcr3* and *Rgs1*, both associated with T cell localization within the tissue[88], and *Dusp1*, required for T cell functionality[112].

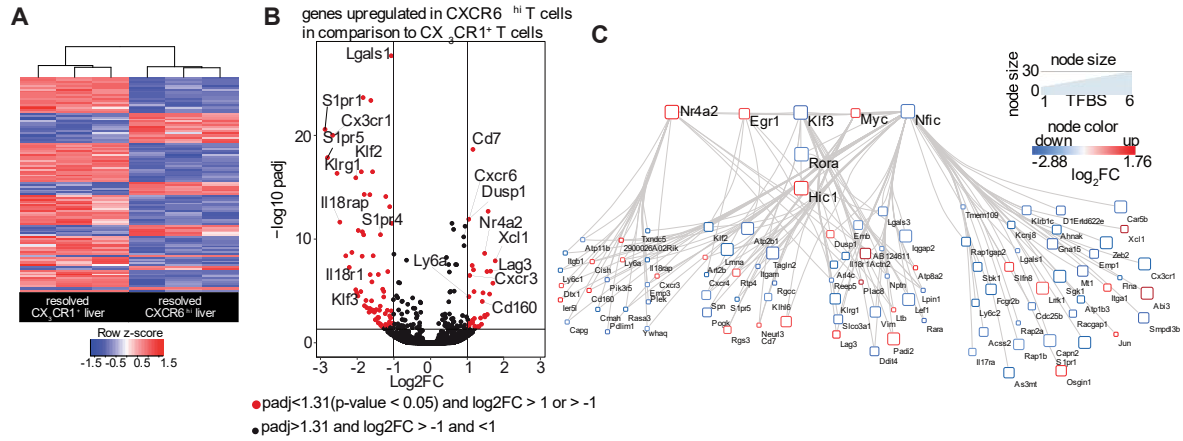

Fig. 26 Transcriptional regulation of hepatic antigen-specific CXCR6^{hi} and CX$_3$CR1$^+$ CD45.1$^+$CD8$^+$ T cells after resolved liver infection.
A Hierarchical clustering of DEGs between antigen-specific CXCR6^{hi} and CX$_3$CR1$^+$ CD45.1$^+$CD8$^+$ T cells in resolved liver infection. **B** DEGs between hepatic CXCR6^{hi} cells compared to CX$_3$CR1$^+$ cells. **C** Transcription factor network analysis of hepatic CXCR6^{hi} T cells compared to hepatic CX$_3$CR1$^+$ T cells. Regulation in CXCR6^{hi} T cells is shown. DEGs: differentially regulated genes; 1 individual experiment with 3 biological replicates; Analysis performed by Sainitin Donakonda.

Next, transcription factor network analysis revealed a vital role for the tissue residency-associated transcription factor *Nr4a2* in CXCR6^{hi} T cells and *Klf3* and *Nfic* in CX$_3$CR1$^+$ T cells.

2.3.4 Analysis of genome-wide gene expression reveals novel surface markers and a cAMP signature for dysfunctional CXCR6^{hi}CD8$^+$ T cells in the liver

Next, differences were determined between CXCR6^{hi}CD8$^+$ T cells after resolved and during persistent liver infection. Within the 127 DEGs between these T cell populations, dysfunctional CXCR6^{hi} T cells expressed more *Pdcd1* (encoding PD-1), *Il2rb* (encoding CD122), *Lag3*, and the transcription factor *Zfp36l1*, amongst others (**Fig. 27 A, B,** Table 3). The inhibitory receptors PD-1 and Lag-3 are characteristic for exhausted T cells, like the transcription factor ZPF36[113].

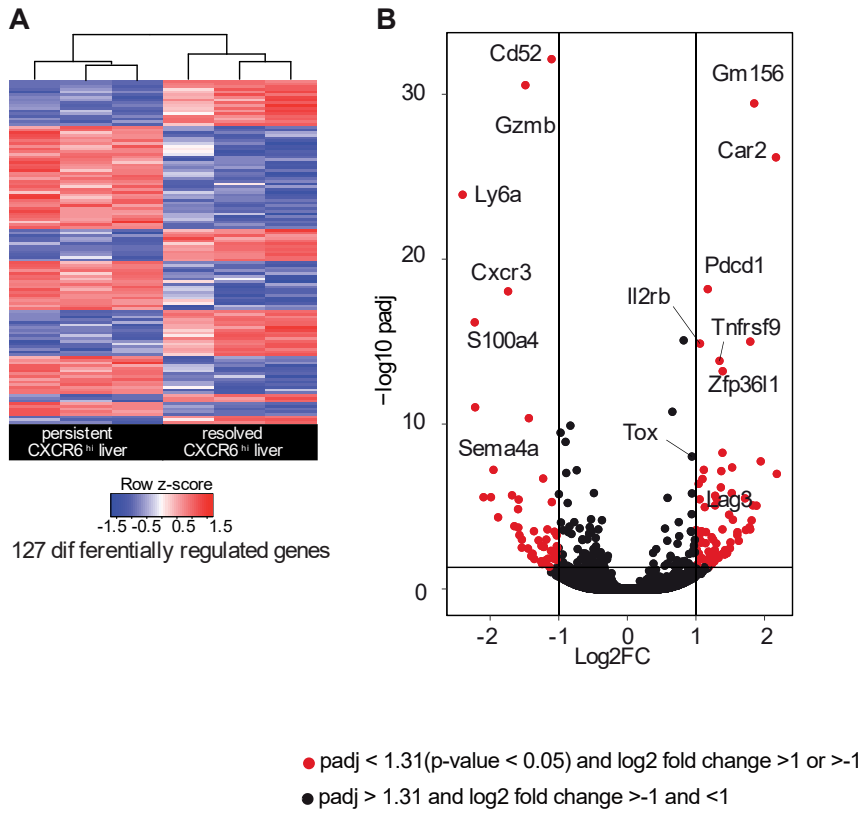

Fig. 27 Gene expression in CXCR6^{hi}CD45.1^{+}CD8^{+} T cells after resolved or during persistent infection.
A Hierarchical clustering of DEGs between CXCR6^{hi} T cells after resolved and during persistent infection. **B** Vulcano plot shows DEGs upregulated in CXCR6^{hi} T cells during persistent infection compared to resolved infection. DEGs: differentially expressed genes; 1 individual experiment with 3 biological replicates; Analysis performed by Sainitin Donakonda.

On the other side, functional CXCR6^{hi} T cells expressed more *Cd52*, *Gzmb*, *Ly6a,* and the chemokine receptors *Cxcr3*, *Ccr5*, and *Ccr2* (**Fig. 27 A, B**). Increased inhibitory receptors and lack of Gzmb expression hinted at hampered functionality. To analyze intracellular mechanisms more closely, biological processes analysis was performed (**Fig. 28 A, B,** Table 12**,** Table 13). Of note, critical functionality-related processes like the gene ontology (GO) terms signal transduction, cell adhesion, and immune effector processes were downregulated in CXCR6^{hi}CD8^{+} T cells during persistent infection (**Fig. 28A**). Besides, genes annotated to the GO term “negative regulation of cell activation” were upregulated in these cells (**Fig. 28B**).

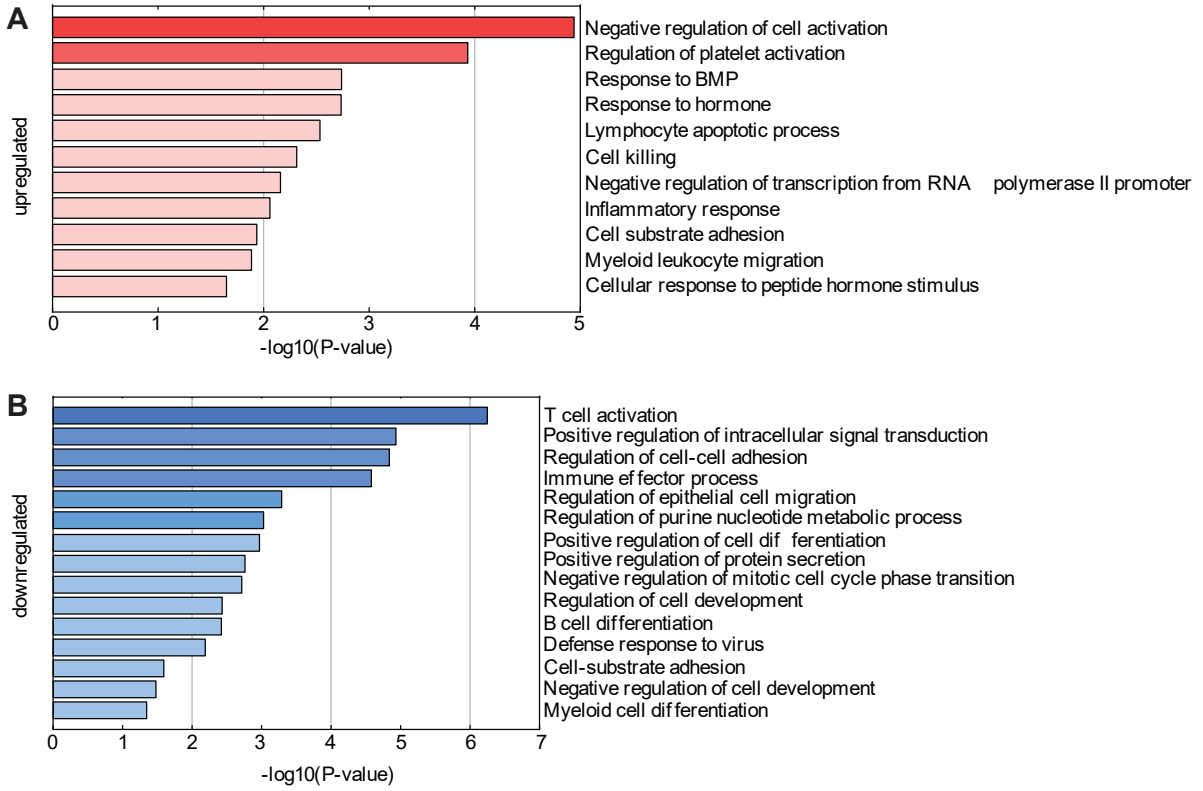

Fig. 28 Biological processes in hepatic CXCR6^{hi}CD45.1^{+}CD8^{+} T cells during persistent infection compared to resolved infection.
A-B Biological processes and GO terms in CXCR6^{hi} T cells downregulated (**A**) and upregulated (**B**) during persistent infection. GO term: gene ontology term; 1 independent experiment with 3 biological replicates; Analysis performed by Sainitin Donakonda.

Based on the DEG analysis (**Fig. 27**), it was possible to find novel surface markers to distinguish functional and dysfunctional CXCR6^{hi}CD8^{+} T cells. Therefore, genes encoding membrane proteins with a significant log2 fold change were selected. This identified increased expression of CD122, CXCR3, and Ly6a. To confirm their preferential expression on CXCR6^{hi}CD8^{+} T cells in either persistent infection (CD122) or after resolved infection (CXCR3, Ly6a), I performed tSNE analysis (**Fig. 29A**). Indeed, only CXCR6^{hi}CD8^{+} T cells after resolved infection, but not CX$_3$CR1^{+}CD8^{+} T cells or CXCR6^{hi}CD8^{+} T cells during persistent infection, co-expressed CXCR3, and Ly6a. In contrast, CD122 was preferentially expressed by CXCR6^{hi}CD8^{+} T cells during persistent infection. These results were confirmed by flow cytometry, demonstrating the expression of respective markers at the protein level in individual cells (**Fig. 29 B, C**).

Hence, CD122 was established as a marker for dysfunctional CXCR6^{hi}CD8^{+} T cells, whereas CXCR3 and Ly6a identified functional CXCR6^{hi}CD8^{+} T cells in the liver.

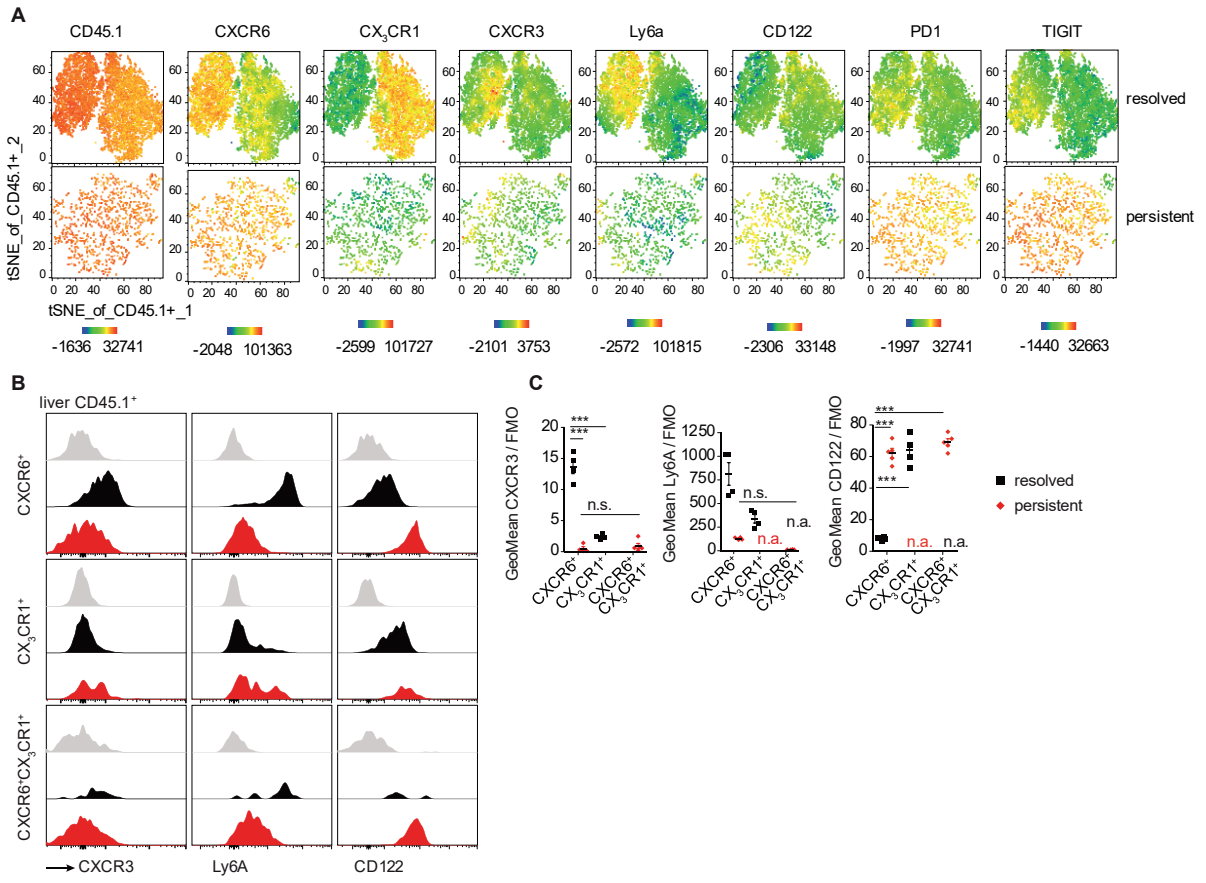

Fig. 29 Validation of novel markers for functional and dysfunctional CXCR6^{hi}CD8^{+} T cells in the liver.
A tSNE of CD45.1^{+}CD8^{+} T cells (d>30 p.i.) analyzing the markers CD45.1, CXCR6, CX3CR1, CXCR3, Ly6a, PD1, TIGIT, and CD122. Live-dead staining, CD8, and CD45.1 were used for pre-gating. T cells after resolved infection are shown in the upper row, T cells during persistent infection in the lower row. **B** Expression of surface markers to distinguish functional and dysfunctional CXCR6^{hi}CD8^{+} T cells with T cells after resolved infection in black, during persistent infection in red and FMO controls in grey. **C** Geometric means of fluorescence intensities normalized to FMO controls for markers shown in B. tSNE: t-distributed stochastic neighbor embedding.

To shed light on the transcriptional regulation of functional and dysfunctional CXCR6^{hi}CD8^{+} T cells, GSEA was performed with several transcription factor gene signatures derived from transgenic mice (**Fig. 30A**), focusing on transcription factors associated with essential roles in T cell regulation. Dysfunctional CXCR6^{hi}CD8^{+} T cells significantly enriched with the TOX gene signature, the Tbx21 (encoding T-bet) signature, and a gene signature elicited by low Eomes expression. Of note, the genes controlled by the characteristic T_{RM} transcription factors Hobit or Blimp1 were not enriched in dysfunctional CXCR6^{hi}CD8^{+} T cells during persistent infection but in their counterparts after resolved liver infection.

Next, transcriptional regulation was directly compared in functional and dysfunctional CXCR6^{hi}CD8^{+} T cells via a transcription factor network analysis (**Fig. 30B**). Strikingly, the transcription factor *Crem* (cAMP-responsive element modulator) emerged as the most dominant transcription factor in dysfunctional CXCR6^{hi}CD8^{+} T cells. Therefore, I decided to analyze Crem expression and upstream cAMP signaling in dysfunctional CXCR6^{hi}CD8^{+} T cells in detail.

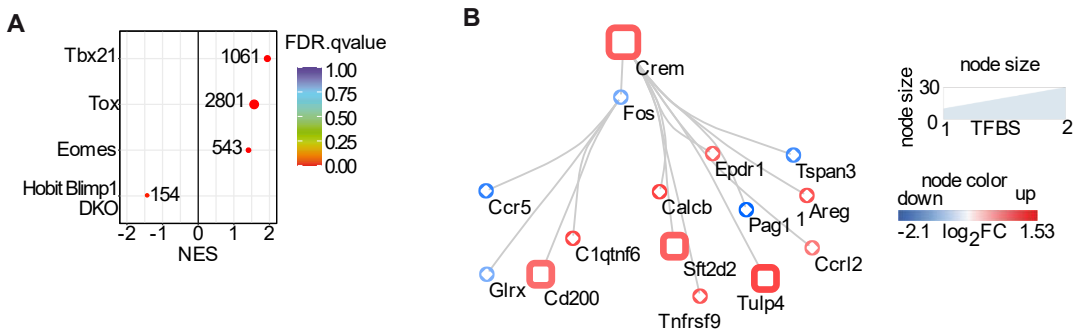

Fig. 30 Transcriptional regulation of antigen-specific CXCR6^{hi}CD8^{+} T cells after resolved and during persistent infection.
A GSEA of DEGs between CXCR6^{hi} T cells during persistent infection and resolved infection with gene sets of transcription factor signatures derived by comparing wild-type to knock-out mice (Tox, Tbx21 and Hobit-Blimp1-double knock-out) or over-expression models (Eomes), respectively. Transcription factor gene sets were published as follows: TOX[114], Tbx21[115], Eomes[116], Hobit-Blimp[117]. **B** Transcription factor network analysis of CXCR6^{hi} CD45.1^{+}CD8^{+} T cells during persistent infection compared to resolved infection. GSEA: gene set enrichment analysis; 1 independent experiment with 3 biological replicates; Analysis performed by Sainitin Donakonda.

2.4 Relevance of cAMP signaling and the transcription factor Crem in persistent liver infection in the Ad-GOL model system

The cAMP signature revealed by bioinformatic analysis was further characterized in T cells on protein level in dysfunctional antigen-specific CXCR6^{hi}CD8^{+} T cells and their functional counterparts after resolving infection. Additionally, I aimed to investigate the effects of forced cAMP signaling *ex vivo* on CXCR6^{hi}CD8^{+} T cells' functionality after resolved infection.

2.4.1 Increased expression of cAMP signaling in dysfunctional antigen-specific CXCR6^{hi}CD8^{+} T cells

First, I proved higher expression levels of Crem in dysfunctional CXCR6^{hi} CD45.1^{+}CD8^{+} T cells on protein level (**Fig. 31 A-B**), as already shown at the RNA level. Of note, only antigen-specific CD45.1^{+}CD8^{+} T cells during persistent viral infection expressed more Crem, but not polyclonal CD45.1^{neg}CD8^{+} T cells as this mixed population consists of both antigen-specific and unspecific T cells (**Fig. 31C**). Next, upstream and downstream proteins in the cAMP signaling pathway were analyzed. S114-phosphorylated protein kinase A (pPKA) upstream of Crem was elevated on CXCR6^{hi} T cells during persistent infection, as well as the Crem-target gene 4-1BB (**Fig. 31 A-B**). Compared to CXCR6^{hi} and CX$_3$CR1^{+} CD45.1^{+}CD8^{+} T cells after resolved infection, higher levels of Crem and pPKA, but not 4-1BB, were detected in CXCR6^{hi} T cells during persistent infection. The same was observed for polyclonal CD45.1^{neg}CD8^{+} T cells, indicating a specific regulation in CXCR6^{hi}CD8^{+} T cells during persistent infection.

In summary, elevated cAMP signaling suggested by bioinformatic analysis of transcriptome profiling was confirmed at the protein level selectively in antigen-specific liver CXCR6^{hi}CD8^{+} T cells during persistent Ad-GOL infection.

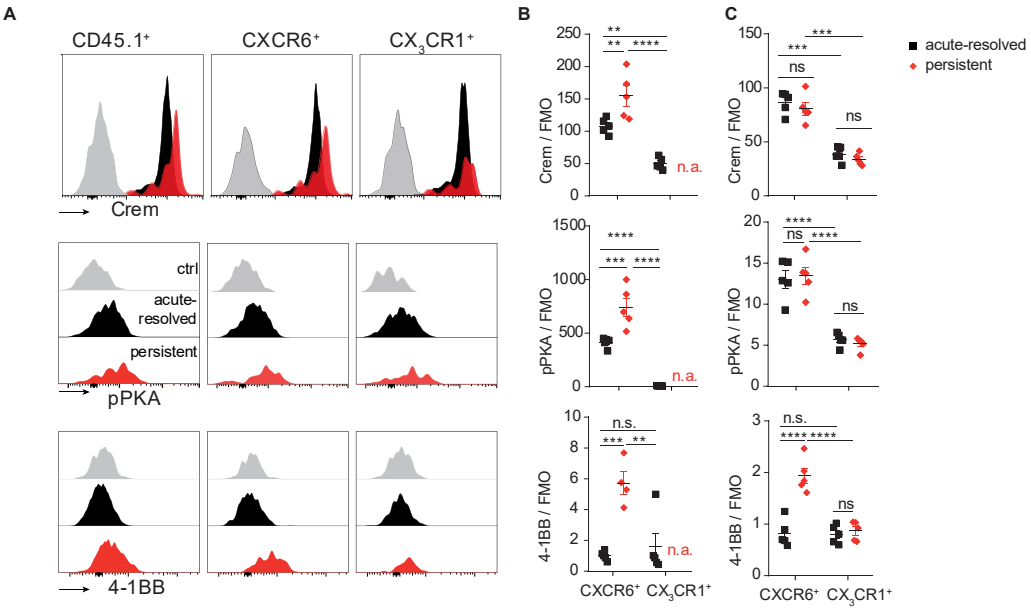

Fig. 31 cAMP signaling in antigen-specific dysfunctional CXCR6^{hi}CD8^{+} T cells.
A Representative histograms of hepatic CD45.1^{+}, CXCR6^{+}, and CX$_3$CR1^{+} CD45.1^{+}CD8^{+} T cells. **B-C** Geometric means of fluorescence intensities normalized to FMO control of CD45.1^{+} cells (**B**). and CD45.1^{neg} cells (**C**).

2.4.2 *Ex vivo* induction of cAMP signaling in functional CXCR6^{hi}CD8^{+} T cells

Since the cAMP signature revealed by bioinformatic analysis was verified on the protein level, it was next addressed whether the induction of cAMP signaling alone could dampen the functionality of CXCR6^{hi} CD45.1^{+}CD8^{+} T cells similar to the situation observed during persistent infection. To answer this question, liver T cells after resolved infection were treated with adenylate cyclase-activating forskolin. Via adenylate cyclase activation, forskolin increases intracellular cAMP levels[118]. Indeed, levels of pPKA downstream of cAMP and the Crem-target gene 4-1BB were elevated in CXCR6^{hi} CD45.1^{+}CD8^{+} T cells after forskolin treatment (**Fig. 32A**). Simultaneously, forskolin-treated CXCR6^{hi} CD45.1^{+}CD8^{+} T cells upregulated PD-1 and downregulated GzmB. Moreover, CXCR6^{hi} T cells produced less INFγ upon peptide re-stimulation after over-night treatment with forskolin (**Fig. 32B**). Strikingly, forskolin-treated CXCR6^{hi} T cells lost their highly efficient killing capacity (**Fig. 32C**). Thus, forskolin generated a phenocopy of dysfunctional CD8^{+} T cells in fully functional CXCR6^{hi}CD8^{+}.

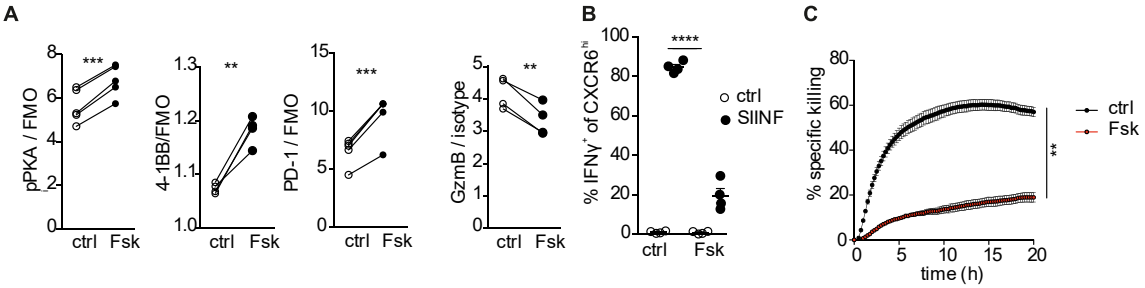

Fig. 32 Enforced *ex vivo* cAMP signaling renders CXCR6^{hi}CD45.1^{+}CD8^{+} T cells dysfunctional.
A-B Liver CXCR6^{hi}CD8^{+} T cells after resolved infection were treated *ex vivo* for 20 h with forskolin (25 µM) for phenotype analysis (**A**) or followed by 7 h peptide re-stimulation (**B**). Geometric mean of fluorescence intensities / isotype control (GzmB) or FMO control (PD-1, 4-1BB, S114-pPKA, Crem) is shown. **C** Antigen-specific sorted CXCR6^{hi}CD8^{+} T cells were treated for 20 h with 25 µM Fsk and then co-cultured with SIINFEKL-loaded or control hepatocytes to assess their specific killing capacity. Statistical analysis: paired t-test (A), two-way ANOVA (B), t-test of AUCs (C).

Next, physiologically relevant cAMP-acting agents were analyzed regarding their effect on cytokine expression in CXCR6^{hi}CD8^{+} T cells isolated from livers after resolved infection. Adenosine is a well-known regulator of T cell functionality and present at high concentrations in inflamed peripheral tissues[119], as is PGE_2, the product of cyclooxygenase activity[120]. Interestingly, PGE_2, but not adenosine, impaired cytokine production of CXCR6^{hi}CD8^{+} T cells upon re-stimulation with SIINFEKL (**Fig. 33 A-B**). However, the effect of PGE_2 was not as drastic as the effect induced by forskolin (**Fig. 33B**).

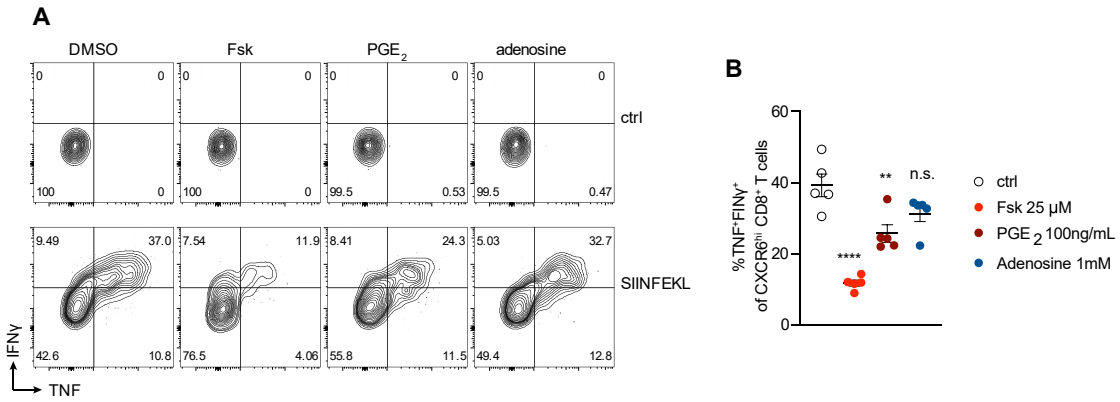

Fig. 33 Effect of cAMP activators on cytokine expression of CXCR6^{hi}CD8^{+} T cells.
A Treatment of hepatic CXCR6^{hi}CD8^{+} T cells isolated after resolved Ad-CMV-GOL infection with Fsk, PGE_2, and adenosine for 20 h followed by 7 h re-stimulation with the cognate peptide SIINFEKL. **B** Quantification of TNF^{+}IFNγ^{+} CXCR6^{hi}CD8^{+} T cells after peptide restimulation.

2.4.3 Role of the transcription factor ICER in dysfunctional CXCR6^{hi}CD8^{+} T cells

cAMP signaling does not only activate CREM via phosphorylation but also induces expression of the inducible cAMP early repressor (ICER)[40]. ICER is transcribed from an alternate internal promoter and lacks the transactivation domain required to transcribe target genes and thereby functions as a transcriptional repressor (see chapter 1.4, p. 13). Importantly, neither RNA sequencing nor labeling by the polyclonal anti-CREM antibody used in this study can discriminate the different CREM isoforms. Hence, transgenic mice with a T cell-specific knock-out for ICER were generated (ICER$^{fl/fl}$ x CD4-Cre) to elucidate the role of CREM/ICER in more detail. ICER$^{fl/fl}$ x CD4-Cre (ICER-KO) or wild-type littermates (WT) were infected with Ad-TTR-GOL to induce persistent viral infection. Infection kinetics and numbers of antigen-specific T cells were comparable in ICER-KO and WT mice (**Fig. 34 A-C**).

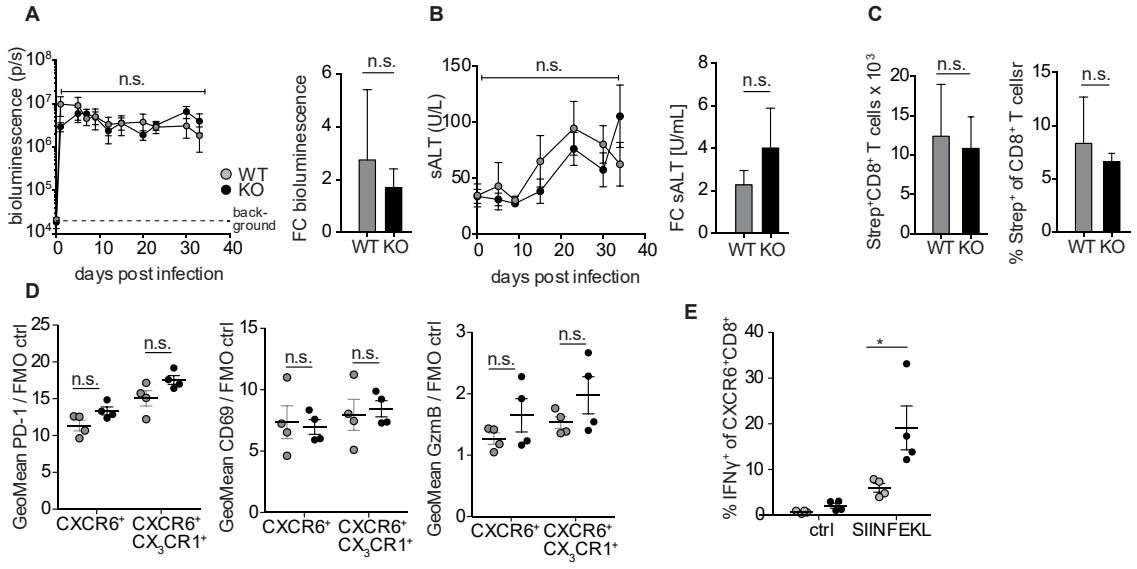

Fig. 34 Functionality of CXCR6^{hi}CD8^{+} T cells in ICER-KO mice during persistent viral infection.
A Effect of T cell-specific ICER-KO (ICER$^{fl/fl}$ x CD4-Cre; KO) compared to ICER$^{fl/fl}$ littermates (WT) on infection kinetic (fold change d34/d1 p.i.), **B** sALT levels (fold change d34/d0 p.i.), **C** antigen-specific CD8^{+} T cell distribution in the liver, **D** phenotype and **E** functionality upon peptide re-stimulation. Geometric mean of fluorescence intensities normalized to FMO control (PD-1, CD69) or isotype control (GzmB) are shown. KO: ICER$^{fl/fl}$ x CD4-Cre, WT: ICER$^{fl/fl}$, FC: fold change, Strep^{+}: H2-k^{bS8L} multimer^{+}; 1 independent experiment with 4 biological replicates.

Moreover, antigen-specific CXCR6^{hi}CD8^{+} T cells expressed similar levels of PD-1, CD69, and GzmB (**Fig. 34D**). Strikingly, more ICER-KO than ICER-WT CXCR6^{hi}CD8^{+} T cells produced IFNγ when re-stimulated *ex vivo* (**Fig. 34E**).

In summary, ICER-KO mice did not clear an Ad-TTR-GOL infection, nor did they develop more antigen-specific CXCR6^{hi}CD8^{+} T cells or CXCR6^{hi}CD8^{+} T cells with lower PD-1 expression or higher GzmB expression. However, antigen-specific CXCR6^{hi}CD8^{+} T cells showed improved *ex vivo* responsiveness to restimulation and production of cytokines compared to WT cells during persistent infection. Since improved functionality was only observed *ex vivo* but had no effect on infection kinetics *in vivo*, it raised the question of the liver microenvironment's influence on functional antigen-specific CD8^{+} T cells.

2.4.4 Influence of the liver microenvironment on antigen-specific CD8^{+} T cells

The results obtained so far suggested an inhibitory influence on antigen-specific CD8^{+} T cells of the liver microenvironment during persistent liver infection. To test this hypothesis, 9x10^{5} antigen-specific CD45.1^{+}CD45.2^{+} cytotoxic T cells generated *in vitro* were transferred into mice with either resolved or persistent liver infection on d30 p.i. (**Fig. 35A**). Of note, the CTL transfer did not reduce antigen-expression in persistently infected mice (**Fig. 35B**). However, adoptive CTL transfer increased sALT during persistent infection, indicating moderate liver damage (**Fig. 35C**). 3 days post CTL transfer, T cells were isolated from the liver and analyzed for their phenotype and function. Of note, transferred CD45.1^{+}CD45.2^{+} CTLs had migrated to the liver in higher numbers in Ad-TTR-GOL infected mice than mice with resolved Ad-CMV-GOL infection (**Fig. 35D**). 3 days after adoptive transfer in the persistently infected liver,

CD45.1$^+$CD45.2$^+$ CD8$^+$ T cells lost their ability to produce GzmB and cytokines and resembled CD45.1$^+$CD8$^+$ T cells primed and developed during persistent infection (**Fig. 35 E-F**). Contrastingly, CD45.1$^+$CD45.2$^+$ CTLs transferred into mice with resolved infection maintained their capacity to produce GzmB (**Fig. 35E**) and cytokines (**Fig. 35F**). Of note, CD45.1$^+$CD45.2$^+$CD8$^+$ T cells transferred into persistently infected mice expressed the Crem-target 4-1BB, as did CD45.1$^+$CD8$^+$ T cells developed during persistent infection (**Fig. 35G**). Hence, 3 days of persistent liver infection microenvironment and persistent antigen severely dampened functionality of *in vitro* generated CTLs.

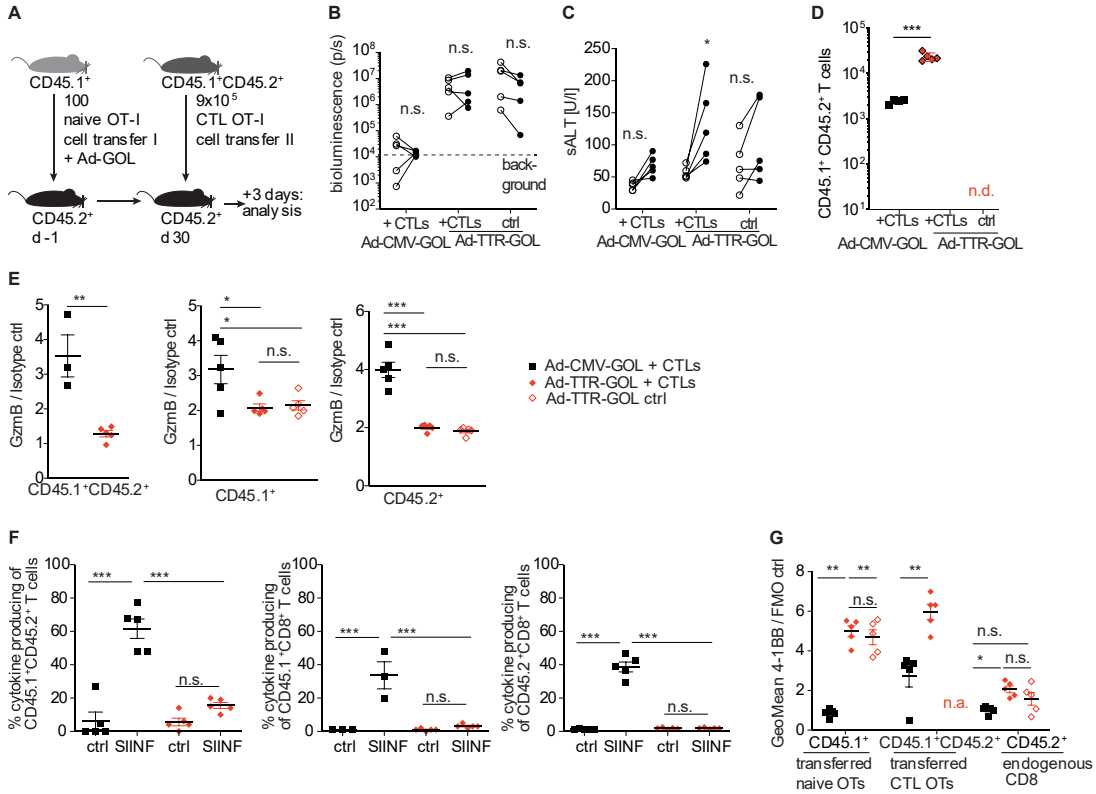

Fig. 35 Influence of the hepatic microenvironment on antigen-specific cytotoxic T lymphocytes.
Phenotype and functionality of re-isolated hepatic CD45.1$^+$CD45.2$^+$ CD8$^+$ T cells after resolved (black) or during persisting (red) infection, 3 days post CTL transfer. **A** Experimental scheme with Ad-CMV-GOL and Ad-TTR-GOL infected mice receiving CTLs or PBS (ctrl) on d30 p.i. **B** Bioluminescence and **C** sALT levels before and after CTL transfer. **D** Counts of re-isolated CTLs d3 post cell transfer II. **E** GzmB expression, **F** cytokine expression upon peptide re-stimulation for 17 h and **G** 4-1BB expression of transferred CD45.1$^+$CD45.2$^+$ CTLs, CD45.1$^+$CD45.2^{neg} T cells (transfer of naive CD8$^+$ T cells on d-1) and CD45.1^{neg}CD45.2$^+$ T cells (endogenous CD8$^+$ T cells). Geometric mean of fluorescence intensities normalized to isotype control (Gzmb) or FMO control (4-1BB) are shown.

2.5 Murine model system for Hepatitis B virus infection

Next, the question was addressed whether increased cAMP signaling in CXCR6^{hi}PD-1^{hi} CD8$^+$ T cells was not limited to persistent viral infection in an experimental infection model but whether the same mechanism regulates dysfunctional antigen-specific CD8$^+$ T cells in persistent Hepatitis B virus infection (HBV). Therefore, HBV-specific CD8$^+$ T cells were analyzed in a preclinical HBV model. This murine model system enabled me to compare CD8$^+$ T cells from the liver and spleen after resolved Adeno-HBV1.3

(AdHBV) with CD8+ T cells during persistent AdHBV infection. The findings gained in the AdHBV model are described below.

2.5.1 Infection kinetics in the AdHBV model

First, an acute-resolving and a persistent AdHBV infection model were established. In contrast to the Ad-GOL model system, the same virus was used in different doses to achieve different infection outcomes dependent on the initial infection dose.

To define viral infection doses for controlled and persistent viral AdHBV infections, mice were infected with increasing Ad-HBV-Luc doses. Ad-HBV-Luc was constructed by Dirk Wohlleber and Katrin Manske and encodes the reporter gen luciferase in addition to the 1.3-fold HBV genome. Therefore, Ad-HBV-Luc was better suited to titrate viral doses and follow the infection over time. Luciferase expression was measured daily to monitor infection kinetics (**Fig. 36A**). Of note, solely infection with 1 x 10^7 pfu Ad-HBV-Luc was controlled within the time frame monitored. In addition to the reporter luciferase, serum HBe antigen (HBeAg) levels dropped in parallel to the decrease in hepatic bioluminescence (**Fig. 36B**). Next, HBeAg levels were compared in AdHBV and Ad-HBV-Luc infections (**Fig. 36C**). HBeAg levels of AdHBV infected mice were increased compared to Ad-HBV-Luc infected mice.

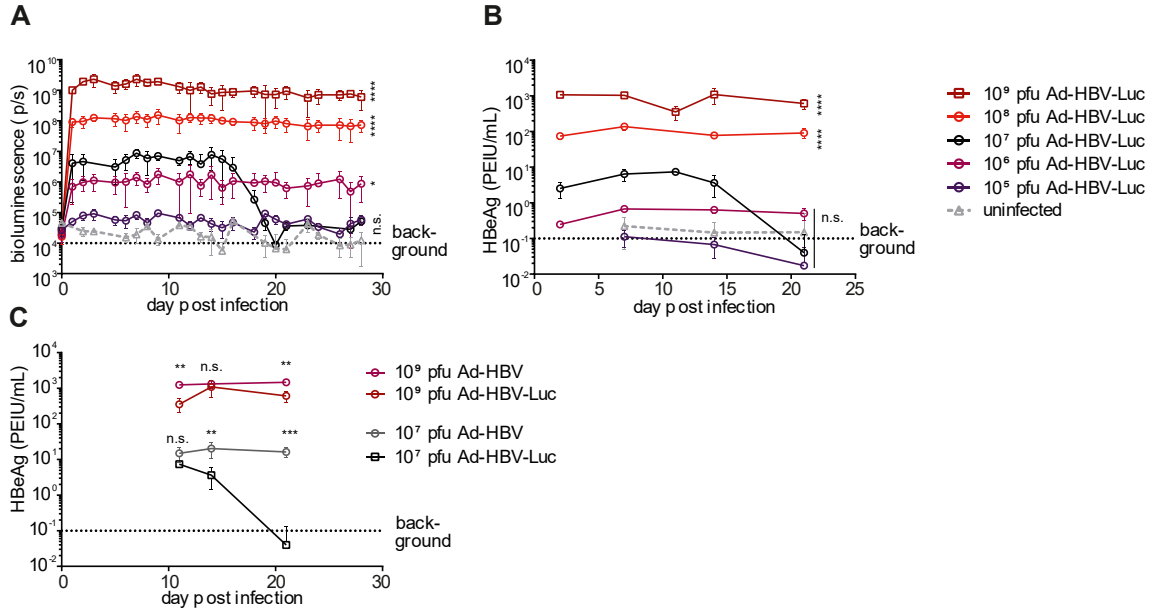

Fig. 36 Dose-dependency of an acute-resolving and persistent Ad-HBV-Luc infection.
Monitoring of **A** bioluminescence and **B** HBeAg expression during Ad-HBV-Luc infection dose kinetics. **C** Comparison of HBeAg levels between AdHBV and Ad-HBV-Luc infection.

Based on the assumption that higher viral doses were associated with the development of persistent infection and immune tolerance, different doses of AdHBV infection were tested for the outcome of antiviral immunity. Mice were infected with either 1x10^8 PFU or 7.5 x 10^6 PFU of AdHBV, and serum HBeAg levels were monitored over time (**Fig. 37A**). Indeed, mice receiving 7.5 x 10^6 PFU of AdHBV often controlled infection, i.e., in 50% of these mice, no HBeAg was detectable anymore in serum. In contrast, infection with 1x10^8 PFU of AdHBV led to persistent infection, and high HBeAg levels were

measured in serum. In these mice, slightly but statistically not significantly elevated sALT levels were found, indicating liver damage (**Fig. 37B**).

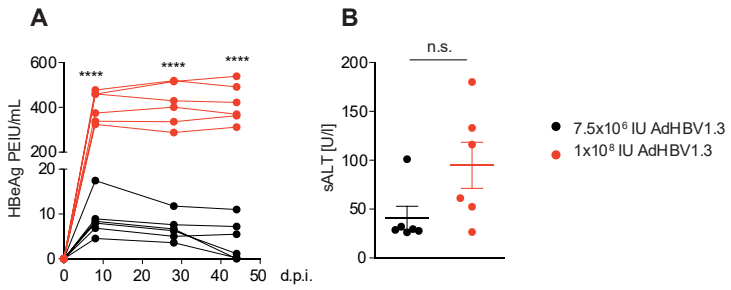

Fig. 37 Infection kinetics after low-dose or high dose AdHBV infection.
A Serum HBeAg kinetics and **B** serum ALT on day 44 p.i. were measured in mice with low dose (7.5 x 10^6 PFU) and high dose (1x10^8 PFU) AdHBV infection. PEIU: Paul-Ehrlich Institute Units/mL, PFU: plaque-forming units; Statistical analysis: t-test, n.s. p = 0.0693.

Using immunohistochemistry, it was evident that HBcore protein-positive hepatocytes were present after infection with 1 x 10^8 PFU AdHBV, whereas in mice that controlled infection and where HBeAg was negative, HBcore-expressing hepatocytes were not detected anymore (**Fig. 38**).

To study changes in HBV-specific CD8$^+$ T cells, either 1 x 10^8 PFU AdHBV (high-dose) to induce persistent infection or 7.5 x 10^6 PFU AdHBV (low-dose) to induce infection that was controlled by the immune system were employed for infection.

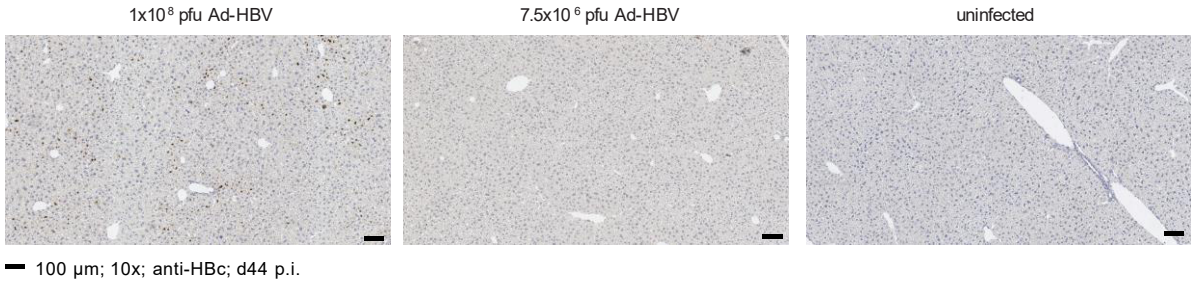

Fig. 38 HBV core protein expression in the liver.
anti-HBc staining in brown of FFPE liver tissues from mice with persistent AdHBV infection (left), controlled AdHBV infection (center), and uninfected mice. FFPE: formalin-fixed paraffin-embedded tissue.

2.5.2 Quantification of HBcore-specific CD8$^+$ T cells

After viral doses were established that led to either resolution or AdHBV infection, the antigen-specific CD8$^+$ T cells were characterized in detail. The expansion of HBV-specific CD8$^+$ T cells was analyzed using adoptive transfer of HBc93-specific TCR-tg CD45.1$^+$CD8$^+$ T cells injected one day before AdHBV infection. These cells are specific for the HBcore93 (C93) peptide MGLKFRQL presented on H-2K^b molecules. In addition to CD45.1 detection, H-2k^{bM8L} multimers detecting core-specific CD8$^+$ T cells were used to detect endogenous C93-specific CD8$^+$ T cells.

Hepatic C93-specific CD8$^+$ T cells were detected on d44 p.i. either during persistent viral infection after high-dose infection (HBeAg^{hi}) or after clearance of HBeAg^{low} low-dose infection HBeAg (HBeAg^{neg}) and (**Fig. 39A**). Both adoptively transferred HBc-specific CD45.1$^+$CD8$^+$ T cells and endogenous C93-specific multimer$^+$ CD8$^+$ T cells

were detected in the liver. When comparing mice that controlled HBV infection (HBeAg^{neg}) and persistent infection, significantly more hepatic endogenous and transferred C93-specific CD8$^+$ T cells were present in HBeAg^{neg} mice (**Fig. 39C**). Strikingly, there was no difference in HBV-specific CD8$^+$ T cells between the HBeAg^{low} and HBeAg^{hi} mice, i.e., mice with persistent infection and high or low viral load. Importantly, in the spleen, C93-specific CD8$^+$ T cells were detected only in mice that controlled infection and cleared HBeAg, but not in HBeAg^{low} or HBeAg^{hi} mice with persistent infection (**Fig. 39 B, D**).

In summary, transferred HBV-specific CD45.1$^+$CD8$^+$ T cells showed a similar behavior as the endogenous HBV-specific T cells. Both transferred and endogenous HBV-specific CD8$^+$ T cells were present in the liver after resolved and during ongoing AdHBV infection. Moreover, HBV-specific T cells were only found in the spleen when mice had cleared HBeAg. As I did not observe a difference between numbers of C93-specific T cells in HBeAg^{low} and HBeAg^{hi} mice, but more T cells after HBeAg clearance, I went for a detailed phenotype analysis next.

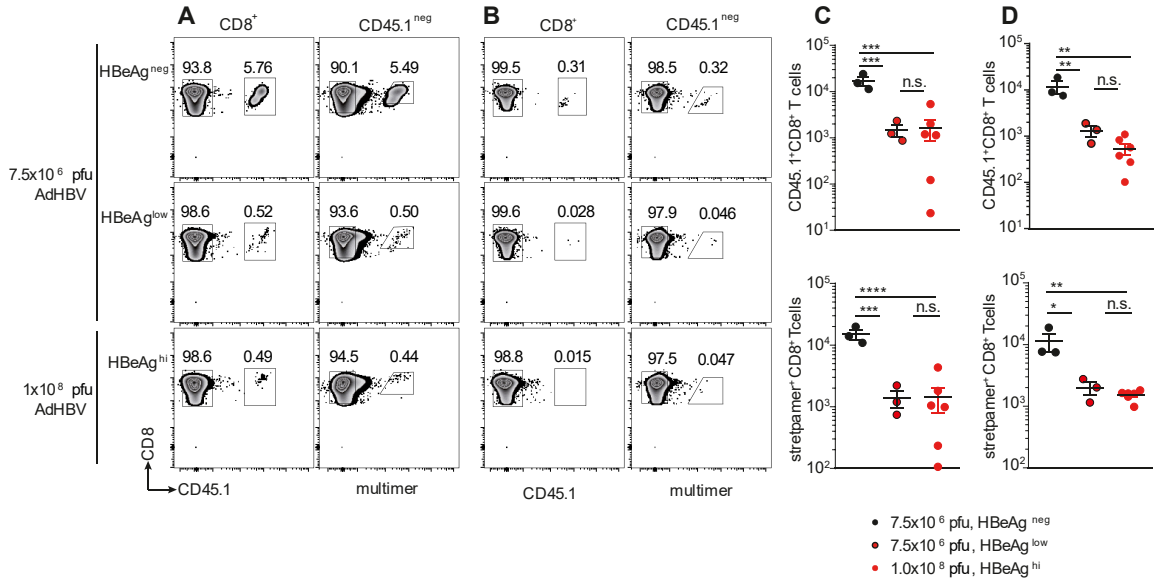

Fig. 39 Antigen-specific CD8$^+$ T cells in AdHBV infection.
CD8$^+$ T cells were isolated from mice on d44 p.i. with 7.5x10^6 PFU or 1x10^8 PFU AdHBV. Mice with 7.5x10^6 PFU AdHBV infection were stratified according to their HBeAg levels. **A** Adoptively transferred HBcore-specific TCR-tg CD45.1$^+$CD8$^+$ T cells (left) and endogenous C93(H-2^{kbM8L}) multimer-specific CD45.1^{neg}CD8$^+$ T cells (right) in liver and **B** spleen. **C** Quantification of CD45.1$^+$ and multimer-specific CD45.1^{neg}CD8$^+$ T cells in liver and **D** spleen. Ordinary one-way ANOVA with Turkey's multiple comparison test.

2.5.3 Characterization of HBcore-specific CD8$^+$ T cells in controlled and persistent infection

2.5.3.1 Expression of residency markers on HBV-specific CD8 T cells

First, it was investigated whether C93-specific CD8$^+$ T cells during the course of viral infection also separated into CXCR6^{hi} and CX$_3$CR1$^+$ populations in the AdHBV model, as observed after Ad-GOL infection described above. Therefore, T cells were isolated from the liver or spleen after mice controlled low-dose AdHBV infection (HBeAg^{neg}) and

compared these T cells to hepatic and splenic T cells in mice that failed to control low-dose AdHBV infection with low HBeAg levels (HBeAg^{low}) or high-dose AdHBV infection (HBeAg^{hi}) (**Fig. 40**).

On d44 p.i., separated hepatic CXCR6^{hi} and CX$_3$CR1$^+$ populations of CD45.1$^+$ HBV-specific CD8 T cells were found only in mice that controlled the virus and were HBeAg^{neg}. Strikingly, there was a mixed phenotype of hepatic T cells in mice that failed to clear infection (HBeAg^{low}), consisting of CXCR6^{hi}CX$_3$CR1^{neg}, CXCR6^{hi}CX$_3$CR1$^{+,}$ and CXCR6^{neg}CX$_3$CR1$^+$ CD8$^+$ T cells. During persistent high-dose AdHBV infection (HBeAg^{hi}), mainly CXCR6^{hi} cells but not CXCR6^{neg}CX$_3$CR1$^+$ CD8 T cells were found (**Fig. 40 A, C, E**). Of note, CX$_3$CR1$^+$CD8$^+$ T cells in the spleen were only found in mice that cleared HBV infection (**Fig. 40 B, D, F**).

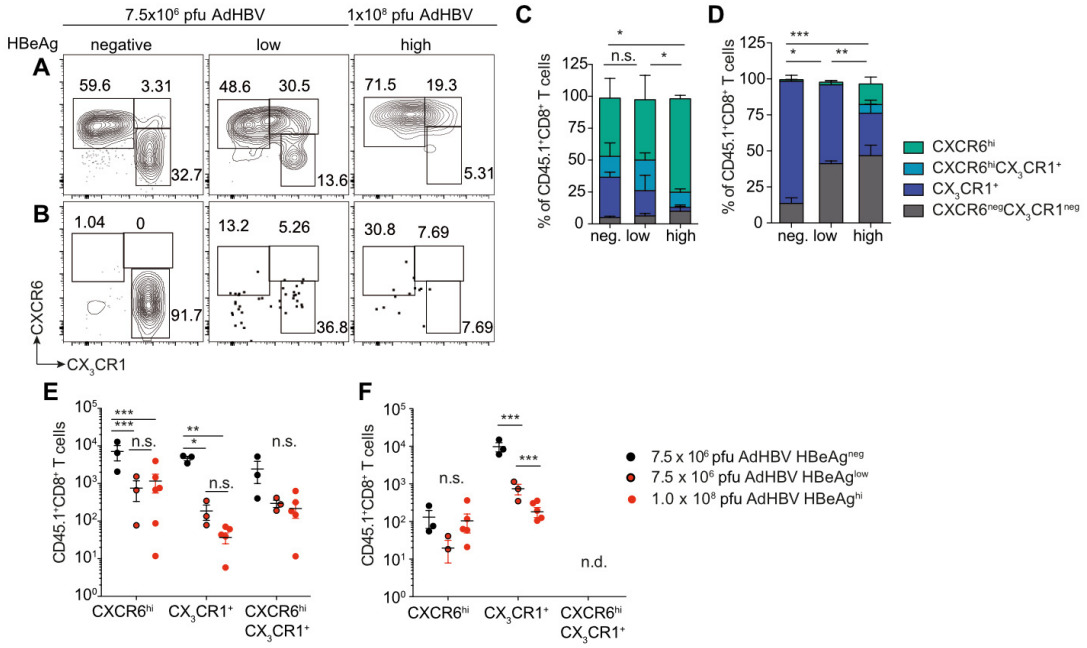

Fig. 40 Expression of tissue-residency and circulating memory marker.
C57Bl6/c mice received C93-transgenic CD45.1$^+$ CD8 T cells the day before infection with AdHBV and analysis of T cells was performed on d45 p.i., CXCR6 and CX$_3$CR1 expression on CD45.1$^+$CD8$^+$ T cells in **A** liver and **B** spleen after low-dose AdHBV infection with cleared HBeAg (left), low HBeAg levels (center) and after high-dose AdHBV infection and high HBeAg levels (right). **C** Percentages of chemokine receptor-expressing cells in **C** liver and **D** spleen. **E,F,** Quantification of CXCR6^{hi}, CX$_3$CR1$^+$ and CXCR6^{hi}CX$_3$CR1$^+$ CD45.1$^+$CD8$^+$ T cells after AdHBV infection in **E** liver and **F** spleen. Statistical Analysis: matched two-way ANOVA: HBeAg^{neg} vs. HBeAg^{hi}: CXCR6^{hi} $p < 0.05$, CX$_3$CR1$^+$ $p < 0.05$; HBeAg^{low} vs. HBeAg^{hi}: CXCR6^{hi} $p < 0.05$ (C), HBeAg^{neg} vs. HBeAg^{low}: CX$_3$CR1$^+$ $p < 0.01$, CXCR6^{neg}CX$_3$CR1^{neg} $p < 0.05$, HBeAg^{neg} vs. HBeAg^{hi}: CX$_3$CR1$^+$ $p < 0.001$, CXCR6^{neg}CX$_3$CR1^{neg} $p < 0.001$, HBeAg^{low} vs. HBeAg^{hi}: CX$_3$CR1$^+$ $p < 0.01$ (D).

As CXCR6 is expressed by liver-resident CD8$^+$ T cells, further analysis for residency markers was performed. Indeed, all HBV-specific CD45.1$^+$ CXCR6^{hi}CD8$^+$ T cells expressed higher CD69 and CD49a levels than CX$_3$CR1$^+$ cells (**Fig. 41 A, B**), consistent with tissue-residency of this population. The chemokine receptor CXCR3 was co-expressed with CXCR6 but not CX$_3$CR1 on liver CD8$^+$ T cells. CXCR6^{hi}CD8$^+$ T cells in the HBeAg^{neg} group expressed more CXCR3 than CD8$^+$ T cells in the HBeAg^{low} group that failed to control HBV infection. CD11a, which is part of the cell adhesion-promoting molecule integrin α-L, was highly expressed on liver CXCR6^{hi}CD8$^+$ T cells. However,

CXCR6^{hi}CD8^{+} T cells in mice that failed to control HBV infection (HBeAg^{hi}) expressed less CD11a than CXCR6^{hi} T cells in HBeAg^{neg} mice or HBeAg^{low} mice (**Fig. 41 A, C**). In contrast, liver CX$_3$CR1^{+}CD8^{+} T cells expressed less CD11a, but the effector molecule KLRG-1 (**Fig. 41C**, right).

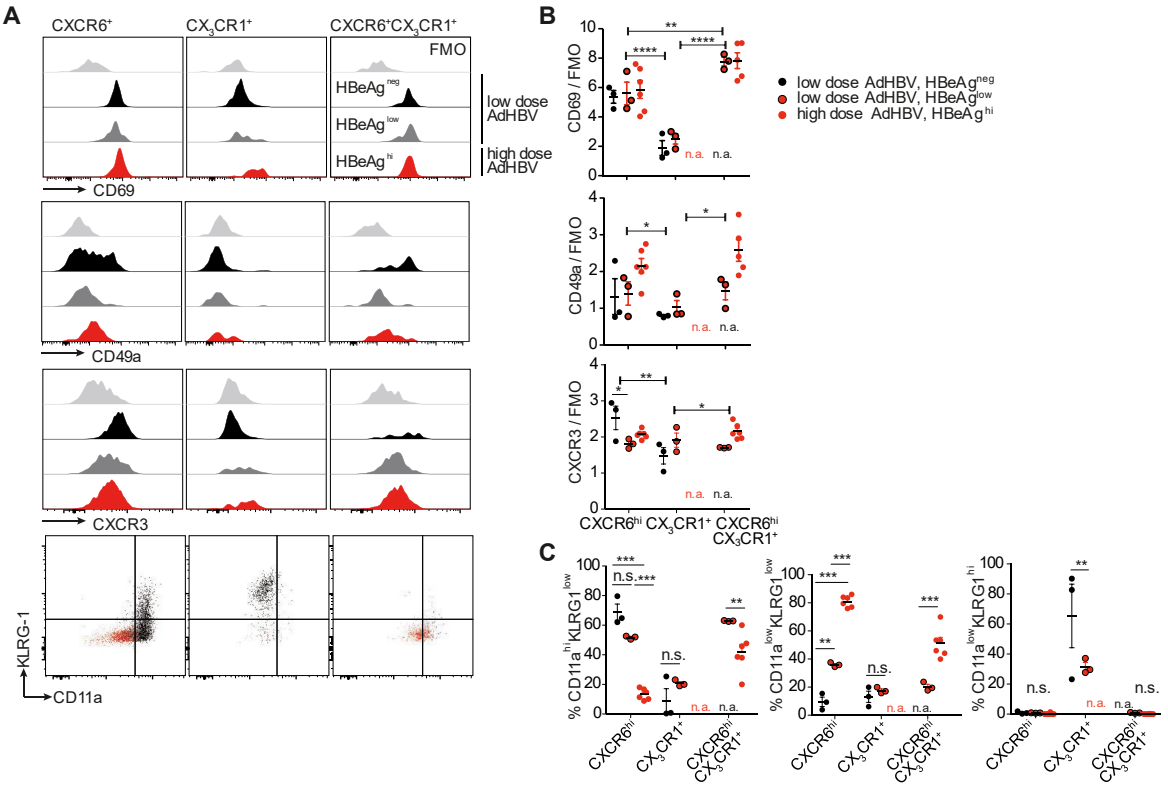

Fig. 41 Residency marker on hepatic antigen-specific CD8^{+} T cells d44 p.i.
Low-dose AdHBV infected mice were grouped according to their HBeAg levels into HBeAg^{neg} and HBeAg^{low} mice. All high-dose AdHBV infected mice were HBeAg^{hi}. **A** Expression of the residency markers CD49a, CD69, CXCR3, CD11a, and the cytotoxicity marker KLRG-1 on CXCR6^{hi}, CX$_3$CR1^{+}, and CXCR6^{hi}CX$_3$CR1^{+} T cells. **B** Geometric means of fluorescence intensities normalized to FMO controls and **C** percentages of CD11a and KLRG-1 expressing cells.

In the spleen, CX$_3$CR1^{+} HBV-specific CD8^{+} T cells were detected only in mice that controlled HBV infection, i.e., in HBeAg^{neg} mice. Of note, these cells did not express the residency markers CD69, CD49a, or CXCR3 but again showed expression of the effector cell marker KLRG1 (**Fig. 42 A-D**).

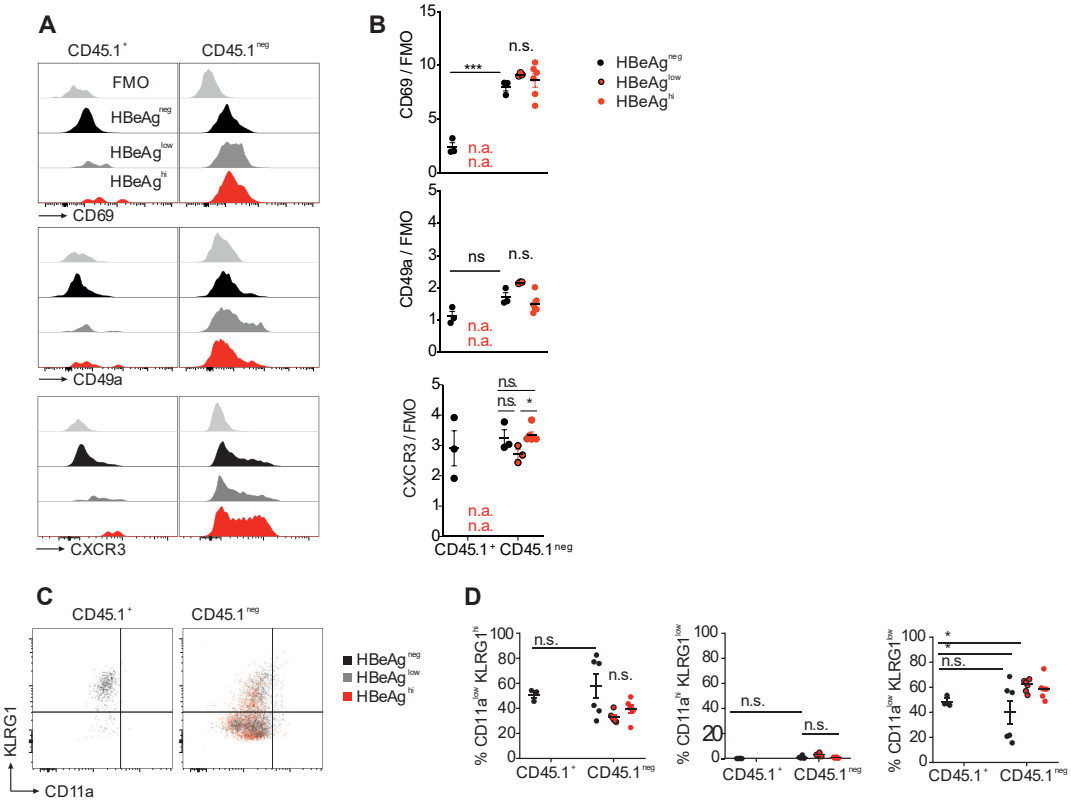

Fig. 42 Residency marker on splenic CX$_3$CR1$^+$CD8$^+$ T cells d44 p.i.
A, C Low-dose AdHBV infected mice were grouped according to their HBeAg levels into HBeAg^{neg} and HBeAg^{low} mice. All high-dose AdHBV infected mice were HBeAg^{hi}. Expression of the residency markers CD69, CD49a, CXCR3, CD11a, and the cytotoxicity marker KLRG-1 on antigen-specific CD45.1$^+$ or polyclonal CD45.1^{neg} CX$_3$CR1$^+$ CD8$^+$ T cells. **B** Geometric means of fluorescence intensities normalized to FMO controls, **D** percentages of CD11a, and KLRG-1 expressing cells.

In summary, CXCR6^{hi}CD8$^+$ T cells with a T$_{RM}$-like phenotype were found only in the liver after resolved and during persistent AdHBV infection. In contrast, effector CX$_3$CR1$^+$CD8$^+$ T cells were mainly detected in the liver and spleen after AdHBV infection was cleared and co-expressed KLRG1.

2.5.3.2 Expression of inhibitory receptors on HBc-specific CD8$^+$ T cells

HBcore-specific CXCR6^{hi}CD8$^+$ T cells are exposed continuously to their cognate antigen during persistent AdHBV infection. It was therefore analyzed whether HBeAg levels corresponded with higher inhibitory receptor expression levels. Indeed, high PD-1 expression on CXCR6^{hi} T cells coincided with high-dose AdHBV infection and high serum HBeAg (**Fig. 43 A-B**, upper panels). Although liver CXCR6^{hi}CD8$^+$ T cells after control of AdHBV infection expressed more PD-1 than CX$_3$CR1$^+$CD8$^+$ T cells, PD-1 expression was further elevated on CXCR6^{hi}CD8$^+$ T cells during persistent infection, whereas TIGIT did not show such a regulation (**Fig. 43 A-B**, lower panels).

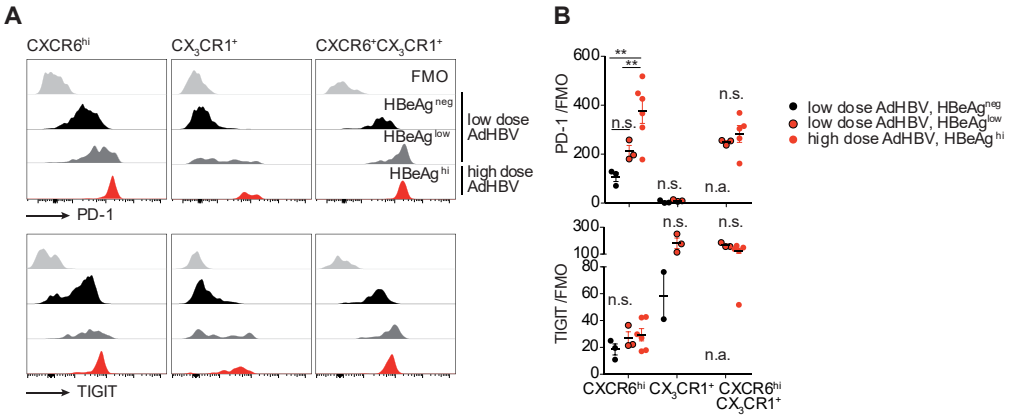

Fig. 43 Inhibitory receptor expression on C93-specific CD8⁺ T cells in the liver on d44 p.i.
Mice were infected with mice infected with low-dose or high-dose AdHBV and stratified according to their HBeAg levels. **A** Expression levels of inhibitory receptors in the liver. **B** Geometric means of fluorescence intensities normalized to FMO controls.

In the spleen, C93-specific $CX_3CR1^+CD8^+$ T cells expressed low levels of PD-1 or TIGIT after AdHBV infection was cleared (**Fig. 44 A, B**) compared to hepatic C93-specific $CD8^+$ T cells or polyclonal $CX_3CR1^+CD8^+$ T cells. As mentioned above, in low-dose AdHBV infected $HBeAg^{low}$ mice, low frequencies of C93-specific $CD8^+$ T cells were observed in the spleen.

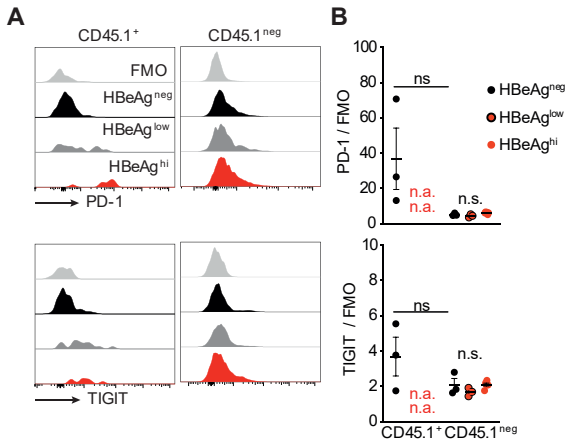

Fig. 44 Expression of inhibitory receptors on $CX_3CR1^+CD8^+$ T cells in the spleen.
A PD-1 and TIGIT expression on antigen-specific $CD45.1^+$ or polyclonal $CD45.1^{neg}$ $CX_3CR1^+CD8^+$ T cells in the spleen. **B** Geometric means of fluorescence intensities normalized to FMO controls. Statistical analysis: one-way ANOVA.

In addition to inhibitory receptors, I analyzed expression of the transcription factor TOX. In chronic LCMV infection, TOX defines exhausted $CD8^+$ T cells exposed to continuous antigen presentation[28]. In persistent AdHBV infection, only antigen-specific but not polyclonal hepatic $CXCR6^{hi}CD8^+$ T cells expressed high levels of TOX (**Fig. 45 A-B**). In the spleen, TOX expression was, in general, lower. There was no difference between antigen-specific and polyclonal $CX_3CR1^+CD8^+$ T cells regarding TOX expression.

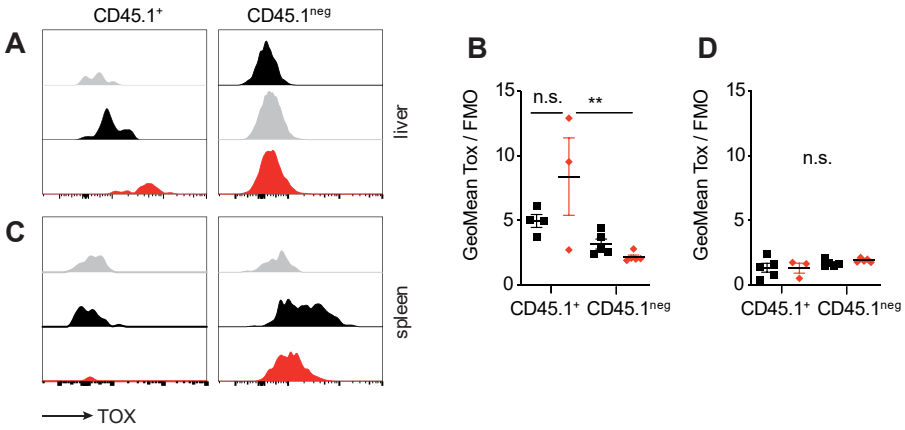

Fig. 45 Expression of the transcription factor TOX in CD8⁺ T cells on d44 p.i. with AdHBV.
A-B TOX expression levels in hepatic CXCR6^{hi}CD8⁺ T cells identified by intracellular staining and **C-D** splenic CX$_3$CR1⁺CD8⁺ T cells. **A, C** Representative histograms and **B, D** geometric means of fluorescence intensities normalized to FMO controls. Statistical analyses: one-way ANOVA.

2.5.3.3 Functionality of HBV-specific CD8⁺ T cells after resolved and during persistent infection

So far, the phenotype of C93-specific CD8⁺ T cells was analyzed after resolved and during persistent HBV infection. During persistent infection, these cells expressed tissue residency markers but also high levels of inhibitory receptors. *Bonafide* T$_{RM}$ cells are highly responsive, express high levels of GzmB and have an enormous re-stimulatory capacity. Consequently, it was addressed whether C93-specific CD8⁺ T cells during persistent AdHBV infection produced GzmB or cytokines upon antigen re-exposure.

Strikingly, HBc-specific CXCR6^{hi}CD8⁺ T cells expressed increasing levels of GzmB with decreasing HBeAg levels (**Fig. 46 A-B**). When comparing liver CXCR6^{hi} to CX$_3$CR1⁺ T cells after resolved infection, CXCR6^{hi} T cells expressed significantly more GzmB, as observed in the Ad-GOL model (see chapter 2.1.4, p. 32).

Next, hepatic C93-specific T cells' re-stimulatory capacity was evaluated through intracellular cytokine staining after exposure to the HBc peptide M8L or PMA/Ionomycin. Of note, only CXCR6^{hi} and CX3CR1⁺CD8⁺ T cells after resolved AdHBV infection produced TNF and INFγ upon re-stimulation with M8L peptide or PMA/Ionomycin (**Fig. 46 C-E**). In contrast, CXCR6^{hi}CD8⁺ T cells during persistent infection completely lacked cytokine production even after PMA/Ionomycin stimulation (**Fig. 46 D-F**), indicating induction of immune tolerance in liver HBV-specific CD8⁺ T cells during persistent HBV infection.

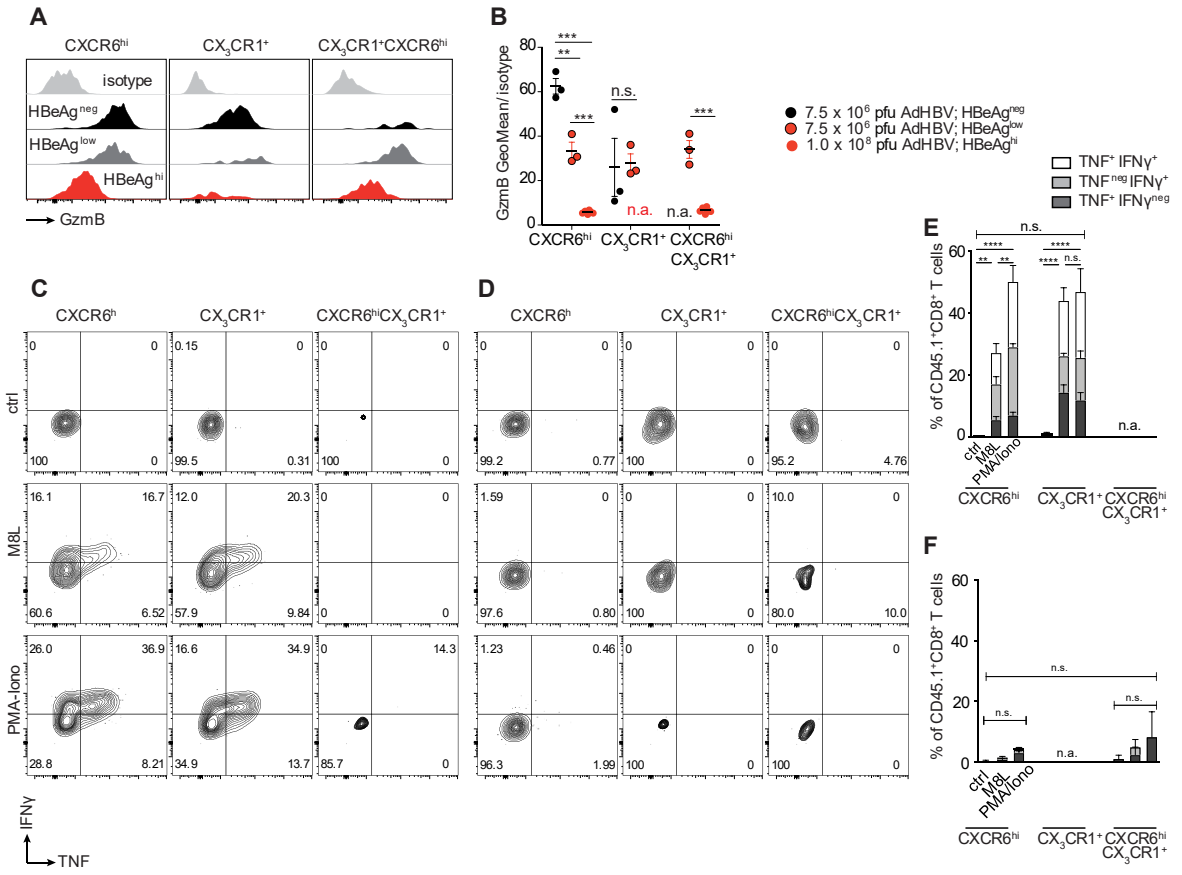

Fig. 46 Functionality of hepatic C93-specific CD8⁺ T cells in resolved and persistent AdHBV infection.
A GzmB expression in CD45.1⁺ HBc-specific CD8⁺ T cells in mice with after low-dose infection that were HBeAg^{neg} or HBeAg^{low} and mice with high-dose AdHBV infection that were HBeAg^{high}. **B** Geometric mean of GzmB fluorescence intensities normalized to isotype control. **C-F** Cytokine expression upon re-stimulation with C93-peptide (M8L) or PMA-Ionomycin in HBc-specific CD8⁺ T cells from **C, E** HBeAg^{neg} and **D, F** HBeAg^{hi} mice. Two-way ANOVA comparing CXCR6^{hi} in E and F: ctrl p>0.9999, M8L p=0.0003, PMA/Iono p < 0.0001.

Next, the functionality of splenic C93-specific CD8⁺ T cells was assessed. CD45.1⁺ C93-specific CX$_3$CR1⁺CD8⁺ T cells, which were only present in mice that cleared AdHBV infection, expressed more GzmB than polyclonal CX$_3$CR1⁺CD8⁺ T cells (**Fig. 47 A-B**). Of note, there was no difference in GzmB expression of CX$_3$CR1⁺CD8⁺ T cells between the HBeAg^{neg} and HBeAg^{low} group (**Fig. 47B**). Only HBV-specific CX$_3$CR1⁺CD8⁺ T cells in the HBeAg^{neg} group produced TNF and INFγ upon re-stimulation (**Fig. 47 C, D**), albeit at lower levels compared to hepatic CXCR6^{hi} or CX$_3$CR1⁺ T cells in the liver from mice that cleared AdHBV infection (HBeAg^{neg}) (**Fig. 47E**).

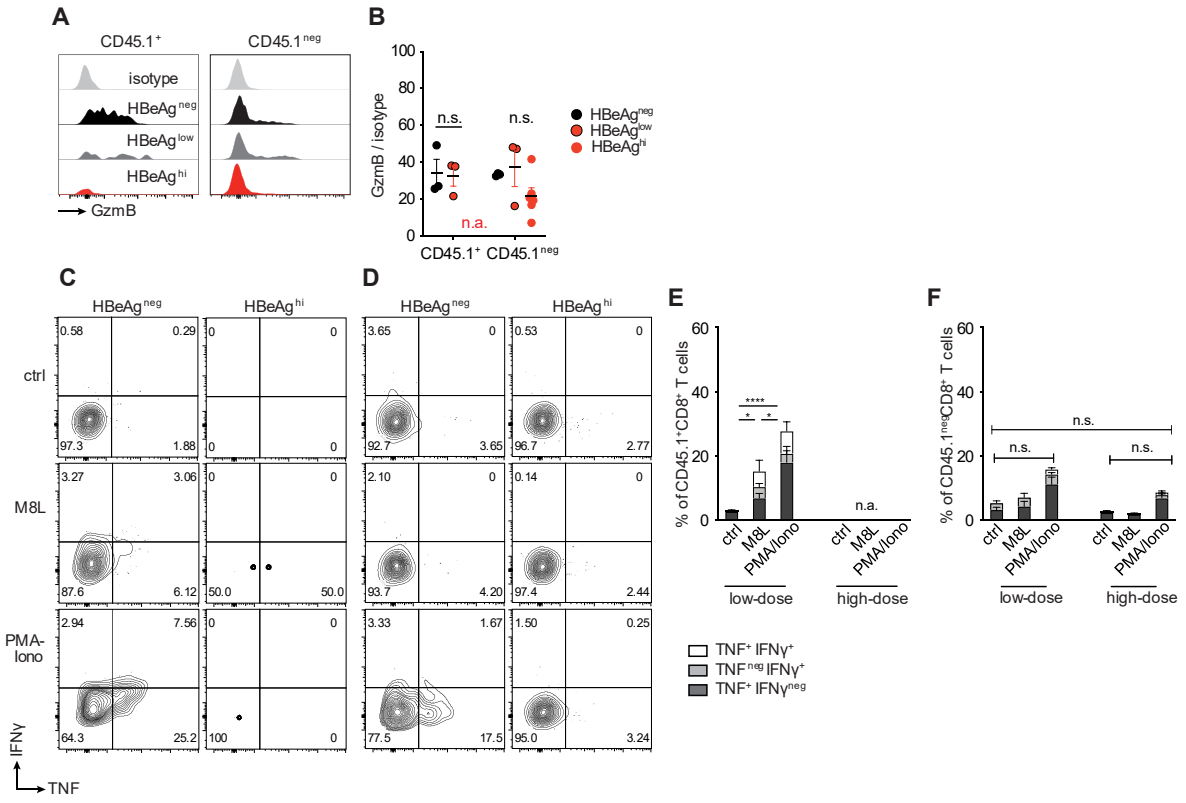

Fig. 47 splenic HBV-reactive CX$_3$CR1$^+$CD8$^+$ T cells after resolved and during persistent AdHBV infection.
A GzmB expression of antigen-specific or polyclonal CX$_3$CR1$^+$CD8$^+$ T cells. **B** Geometric means of GzmB fluorescence intensities normalized to isotype control of CX$_3$CR1$^+$CD8$^+$ T cells. **C-F** Cytokine expression upon re-stimulation with HBc-peptide (M8L) or PMA-Ionomycin of **C, E** HBc-specific or **D, F** polyclonal CX$_3$CR1$^+$CD8$^+$ T cells. Two-way ANOVA comparing the low-dose group in E and F: ctrl p=0.8755, M8L p=0.2433, PMA/Iono p=0.0570.

2.5.4 cAMP signaling in CD8$^+$ T cells during persistent AdHBV infection

In the experiments described so far, antigen-specific CXCR6^{hi}CD8$^+$ T cells in persistent AdHBV infection showed the same phenotype and functionality observed during persistent Ad-TTR-GOL infection. Therefore, it was investigated whether HBcore-specific CXCR6^{hi}CD8$^+$ T cells were regulated by the transcription factor Crem and increased cyclic AMP signaling. To test this hypothesis, I analyzed expression levels of Crem and its target gene 4-1BB in HBcore-specific CD8$^+$ T cells and the effect of induced cAMP signaling on the functionality of these cells.

At protein level, Crem expression was not significantly elevated in HBcore-specific CD45.1$^+$ T cells in persistent AdHBV infection compared to controlled infection or polyclonal CD45.1^{neg} cells in controlled or persistent infection (**Fig. 48 A-B**). Also, CXCR6^{hi}CD45.1$^+$ T cells in persistent infection did not express more Crem than polyclonal CXCR6^{hi}CD45.1$^+$ or CD45.1^{neg} T cells (**Fig. 48 C-D**).

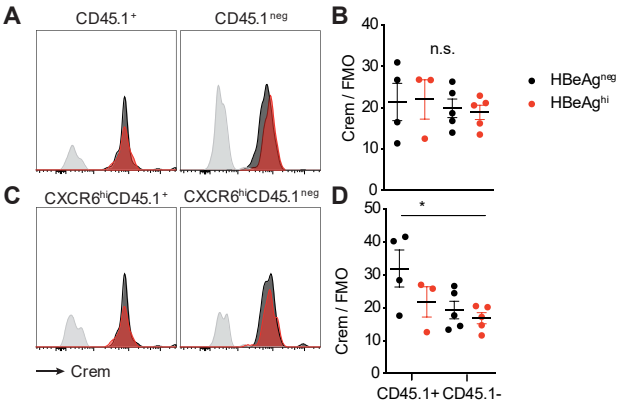

Fig. 48 Expression of the transcription factor Crem in hepatic CD8⁺ T cells.
A, C Expression of Crem after controlled low-dose AdHBV infection (HBeAg^{neg}, black) or during persistent high-dose AdHBV infection (HBeAg^{hi}, red) in **A** HBcore-specific CD45.1⁺ or polyclonal CD45.1^{neg} CD8⁺ T cells and **C** CXCR6^{hi}CD8⁺ T cells. **B, D** Geometric means of fluorescence intensities normalized to FMO control of **B** CD45.1⁺ or CD45.1^{neg} CD8⁺ T cells and **D** CXCR6^{hi}CD8⁺ T cells.

Although Crem expression was not elevated in CXCR6^{hi} cells in persistent AdHBV infection, expression levels of the Crem-target gene 4-1BB were analyzed next, as transcription factors such as Crem are not only regulated by increased expression. Interestingly, 4-1BB expression was elevated in HBcore-specific CD45.1⁺CD8⁺ T cells during persistent AdHBV infection (**Fig. 49 A-B**). Of note, only HBV-specific CXCR6^{hi} CD45.1⁺CD8⁺ T cells in mice with persistent AdHBV infection expressed more 4-1BB but not in mice that controlled AdHBV infection (**Fig. 49 C-D**).

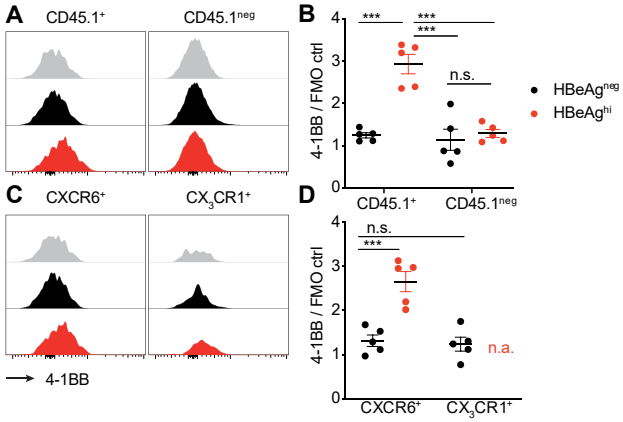

Fig. 49 Expression of the Crem-target gene 4-1BB in hepatic CD8⁺ T cells.
A, C Expression of 4-1BB after controlled low-dose AdHBV infection (HBeAg^{neg}, black) or during persistent high-dose AdHBV infection (HBeAg^{hi}, red) in **A** HBcore-specific CD45.1⁺ or polyclonal CD45.1^{neg} CD8⁺ T cells and **C** CXCR6^{hi} and CX$_3$CR1⁺ CD45.1⁺CD8⁺ T cells. **B, D** Geometric means of fluorescence intensities normalized to FMO control of **B** CD45.1⁺ or CD45.1^{neg} CD8⁺ T cells and **D** CXCR6^{hi} or CX$_3$CR1⁺ CD45.1⁺CD8⁺ T cells.

Finally, enforced cAMP signaling was analyzed regarding the functionality of hepatic CD8⁺ T cells after controlled low-dose AdHBV infection (HBeAg^{neg}), during ongoing low-dose AdHBV infection with remaining antigen (HBeAg^{low}) and compared to dysfunctional CD8⁺ T cells during persistent high-dose AdHBV infection (HBeAg^{hi}) as control. To induce cAMP signaling, hepatic T cells were treated with 25 µM adenylate cyclase-activating forskolin for 17 h. Afterward, T cells were re-stimulated with their

cognate HBcor93 peptide (M8L) to test their cytokine expression capacity. Indeed, polyclonal CXCR6^{hi} T cells from HBeAg^{low} livers completely lost their ability to produce IFNγ upon forskolin treatment and resembled cells during persistent infection (**Fig. 50 A, C**). Interestingly, TNF production was not affected by forskolin treatment. The same tendency was observed for CXCR6^{hi} cells after resolved infection. This effect, however, was not significant. CX$_3$CR1$^+$ T cells after controlled infection (HBeAg^{neg}) responded heterogeneously to forskolin treatment. Therefore, no significant effect was observed (**Fig. 50 B, D**).

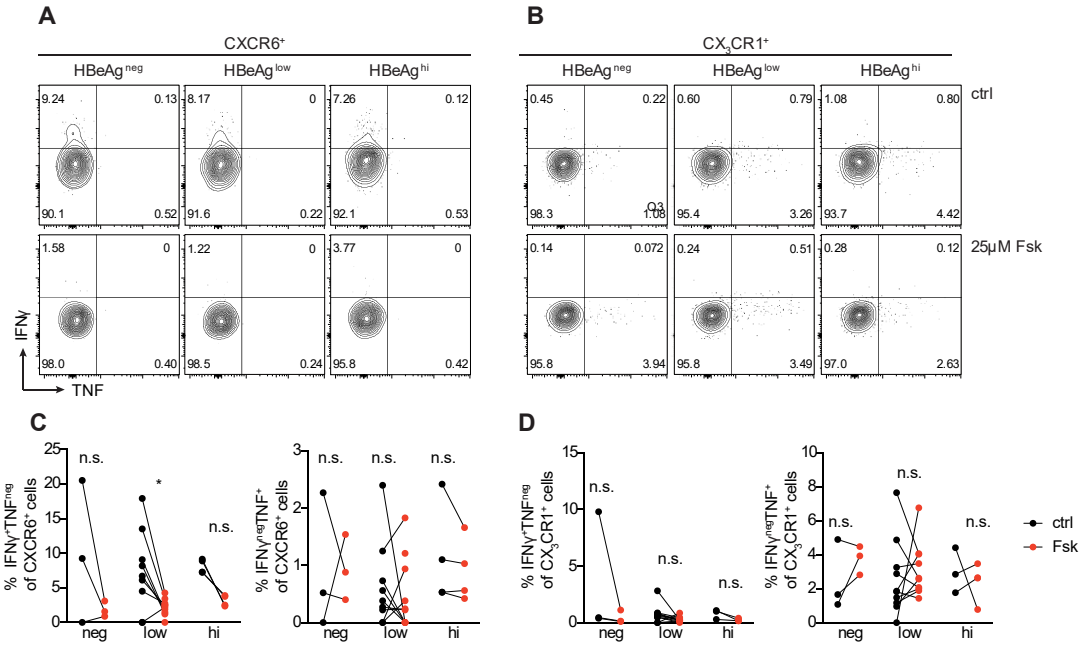

Fig. 50 Functionality of hepatic CXCR6^{hi} and CX$_3$CR1$^+$ T cells upon induced cAMP signaling.
A-B Hepatic **A** CXCR6^{hi} and **B** CX$_3$CR1$^+$ CD8$^+$ T cells were treated with 25 µM forskolin (Fsk) for 17 h and subsequently re-exposed to C93-peptide (M8L). **C-D** Percentage of INFγ$^+$TNF^{neg} and IFNγ^{neg}TNF$^+$ **C** CXCR6^{hi} and **D** CX$_3$CR1$^+$ CD8$^+$ T cells after Fsk pre-treatment.

In summary, elevated cAMP signaling dampens IFNγ production in polyclonal CXCR6^{hi}CD8$^+$ T cells in persistent liver AdHBV infection.

3 Discussion

CD8+ T cells are crucial in the immune response to viral infection and successful control of infection. In patients during self-limiting HBV infection, functional antigen-specific CD8+ T cells are abundant but are rarely detected in patients with chronic HBV infection[56]. In addition to their low abundance, T cells during a chronic HBV infection are dysfunctional and show features of exhausted cells[121,122]. Exhausted CD8+ T cells have been first described and characterized in pre-clinical infection models like the infection with different strains of LCMV, leading to acute-resolved or persistent infection. During chronic LCMV infection, antigen-specific CD8+ T cells express a multitude of inhibitory receptors and lack effector functions and are considered to be adapted to the situation of continuous exposure towards antigen[21]. Exhausted T cells (T_{EX}) are thought to be unable to resolve viral infections. However, to reinvigorate antigen-specific T cells during persistent infection to achieve infection clearance, we must understand these cells' functional characteristics. The transcriptional regulation and T_{EX} progenitor cells have been analyzed recently[123]. When analyzing the immune response during viral infections, liver-targeting viruses are of particular interest to understand how the hepatic tolerogenic environment influences virus-specific T cells[124]. During viral infections of the liver, immune tolerance-inducing liver cells such as hepatocytes and non-parenchymal cells can prime hepatic T cells[13,14,18], which might result in insufficient activation and limited effector functions[125].

In this thesis, CD8+ T cells present during viral infection of hepatocytes were analyzed to characterize their abundance, phenotype, and functionality in acute-resolved as compared to persistent infections. In particular, liver-residency of antigen-specific CD8+ T cells during persistent hepatic infection was analyzed and compared to circulating effector cells and lymphoid-tissue based memory CD8+ T cells.

3.1 Antigen-specific CD8+ T cells were not clonally deleted during persistent viral infection

Clinical studies have shown a low frequency of HBV-specific T cells in the blood of patients with chronic HBV infection[63,126]. Clinical studies are mostly limited to circulating CD8+ T cells and cannot investigate T cells in the liver, the site of infection, because liver biopsies are rarely performed. If so, little material can be allocated for research purposes beyond the diagnostic procedures. However, preclinical liver infection models allow for a refined analysis of circulating and hepatic CD8+ T cells. Considering the lessons learned from clinical situations, one would expect low numbers of antigen-specific T cells in lymphoid tissue and the liver during persistent viral Ad-GOL and AdHBV infection in mice.

However, significant numbers of antigen-specific CD8+ T cells were found in the liver but not in lymphoid tissues during persistent viral infections of the liver. Thus, virus-specific CD8+ T cells were not clonally deleted as described for T cells specific to certain epitopes during chronic LCMV infection[20]. Importantly, also HBc-specific T cells

were maintained in the liver during persistent Ad-HBV infection and not clonally deleted, as reported previously for HBeAg-specific T cells[127]. The presence of antigen-specific T cells in the liver coincided with mild liver damage, and $CD8^+$ T cell depletion abrogated liver damage[103], indicating that indeed antigen-specific $CD8^+$ T cells during persistent infection caused liver damage. Hence, these hepatic antigen-specific T cells during persistent Ad-GOL and AdHBV infection were compared to hepatic and circulating antigen-specific T cells after resolved infection.

The most evident difference between persistent and resolved viral liver infection was the distribution of antigen-specific T cells. During persistent infection, these cells were mainly found in the liver, whereas after resolved infection, they were found in liver and lymphoid tissue. Of note, effector memory T cell-defining CX_3CR1 expression[77,78] on antigen-specific T cells was limited to resolved infection. Antigen-specific CX_3CR1^+ T cells were found in the liver, the spleen, and the blood in mice that controlled the infection. In contrast, CXCR6, a marker found on liver-resident T and NKT cells[93,128,129], was detected on hepatic T cells after resolved and during persistent infection but was not expressed on $CD8^+$ T cells in lymphoid tissues.

Two issues may explain these observations: (1) $CD8^+$ T cells in the liver and lymphoid organs constitute two different entities after resolved infections: circulating CX_3CR1^+ T cells and hepatic $CXCR6^{hi}$ T cells. (2) During persistent infections, only hepatic $CXCR6^{hi}$ and very few circulating CX_3CR1^+ T cells were observed and maintained during persistent infection. Hence, the lack of CX_3CR1^+ T cells could be due to these cells' failed formation or failed maintenance. In both cases, signals required for the formation or maintenance of CX_3CR1^+ T cells seemed to be absent. During chronic LCMV infection, maintenance of antigen-specific T cells is antigen-dependent and relies on proliferation[25]. Antigen addiction would indeed explain $CXCR6^{hi}$ T cells' limitation to the liver during persistent Ad-GOL and AdHBV infection. Moreover, this concept could explain why antigen-specific T cells are rare in chronic HBV patients.

3.2 $CXCR6^{hi}$ T cells are liver-resident during persistent viral infection of the liver

$CXCR6^{hi}$ T cells were limited to the liver after resolved and during persistent Ad-GOL and AdHBV infection, raising the question of whether these cells were tissue resident. In line with most studies on tissue-resident memory T cells in mice[80,82,87] and humans[110,130], hepatic $CXCR6^{hi}$ T cells expressed the *bona fide* residency marker CD69. CD69 has been shown to prevent tissue egress *via* suppression of egress-mediating $S1P_1$[131]. However, Takamura *et al.* reported that CD69 is dispensable for T_{RM} cell maintenance in tissue damage-induced T_{RM} niches of the lung[132]. Hence, in most organs and model systems, except for some exceptions, CD69 reliably marks cells poised to stay within tissues.

For epithelial tissues like skin, gut, and the female reproductive tract, expression of the α-chain (CD103) of the $\alpha_E\beta_7$ integrin additionally marks T_{RM} cells[108]. However, CD103

was not expressed on hepatic CXCR6^{hi} T cells, in line with previous studies on liver-resident cells[93,133]. Although CD103-inducing TGF-β[108] is involved in physiological liver regeneration[134] and might be present in the liver, local concentrations might be higher in epithelial organs, and thus, CD103 is not induced on liver-resident T cells. In addition to the T_{RM} marker CD69, hepatic CXCR6^{hi} T cells after resolved, but not during persistent infection, co-expressed CD49a, the collagen-binding integrin α_1 pairing with β_1 to form VLA-1, enabling both adherence and migration of T_{RM} cells[107]. Moreover, CD49a expression might contribute to the T_{RM} cell's longevity, as VLA-1 protects T cells from apoptosis[135]. In line with the lack of CD49a on CXCR6^{hi} T cells during persistent Ad-GOL and AdHBV infection, Cheuck *et al.* reported that CD49a is preferentially expressed on IFNγ-producing T_{RM} cells in human skin[96], thus marking specifically highly functional T_{RM} cells. In addition to surface molecules mediating tissue retention, adherence, and migration, T_{RM} cells express intermediate levels of inhibitory receptors such as PD-1, Lag-3, and Tim-3[136], which was also observed for hepatic CXCR6^{hi} T cells after resolved infection. Expression of inhibitory receptors might be required to prevent tissue damage by cells poised to exert effector functions in case of a cognate challenge rapidly. However, hepatic CXCR6^{hi} T cells during persistent infection expressed high levels of inhibitory receptors associated with exhausted T cells instead[137].

When looking at transcriptomes of hepatic CXCR6^{hi} T cells compared to CX_3CR1^+ T cells after resolved infection, the T_{RM}-associated orphan nuclear receptor *Nr4a2*[84,93,138] was the top-regulated transcription factor. *Nr4a2* was reported to upregulate INFγ and IL-17 in T cells in autoimmune diseases of the central nervous system[139]. Therefore, *Nr4a2* might be required for fast responses of T_{RM} cells upon secondary infections. Additionally, after resolved Ad-GOL infection, CXCR6^{hi} but not CX_3CR1^+ hepatic T cells shared a signature of residency-associated genes with T_{RM} cells isolated from gut, lung, and skin[108], corroborating the resemblance of CXCR6^{hi} T cells with T_{RM} cells. Beura *et al.* reported a similar residency signature in female reproductive tract T_{RM}s, covering *Rgs1* and *Rgs2*, *Nr4a1*, *Ctla4,* and *Litaf*[84]. Of note, genes enriched in T_{RM} cells in gut, lung, skin, and hepatic CXCR6^{hi} T cells were also published for human T_{RM} cells[88].

In conclusion, CXCR6^{hi} T cells present in the liver after resolved viral infections expressed T_{RM} hallmarks reported in the field.

Strikingly, CXCR6^{hi} T cells during persistent Ad-TTR-GOL infection shared the residency-associated gene signature with T_{RM} cells found after resolved liver infection and published transcriptomes of T_{RM} cells in gut, lung, and skin[108]. However, these cells were dysfunctional and most likely dependent on antigen for population maintenance, rendering these cells liver-resident but probably not T_{RM} cells.

In the case of continuous antigen expression during persistent viral infection, there is another aspect to consider: Persistent TCR stimulation downregulates KLF2 expression, which in turn leads to downregulation of its target gene S1pr1, leading to

higher CD69 surface expression, as S1P1 and CD69 compete antagonistically for cell surface expression[89]. Therefore, persistent antigen expression and local antigen-presentation in the liver might drive liver residency of antigen-specific CXCR6^{hi} T cells during persistent Ad-GOL and AdHBV infection. Moreover, TCR-mediated antigen-recognition induces a migration stop signal and thereby would further assist in retaining antigen-specific CD8^{+} T cells in the liver. Leaving the liver in the presence of antigen expression would therefore require T cells to respond to signals that overcome the mechanisms mentioned above. Therefore, the accumulation of antigen-specific CXCR6^{hi}CD8^{+} T cells in the liver may result from the preferential activity of retention signals over egress signals leading to the depletion of antigen-specific CD8^{+} T cells from the circulation or lymphoid tissues.

CXCR6 was thought to be involved in liver retention since the liver sinusoidal endothelial cell-expressed CXCR6 ligand CXCL16[140] could interact with CXCR6^{hi} T cells and thereby mediate their residency. This hypothesis was tested by infecting CXCR6$^{GFP/GFP}$ mice lacking CXCR6 expression with Ad-CMV-GOL. Interestingly, numbers of antigen-specific CD8^{+} T cells were not reduced in CXCR6$^{GFP/GFP}$ mice. Furthermore, Tse *et al.* reported malaria-specific CXCR6$^{GFP/GFP}$ and wildtype CD8^{+} T cells were equally activated and migrated to the liver in comparable numbers. Lacking CXCR6 expression might be compensated by CXCR3, a chemokine receptor mediating liver recruitment that is co-expressed on hepatic T_{RM} cells in malaria[129]. CXCR6 only has one ligand, CXCL16[141], whereas CXCR3 binds to three ligands, underlining its importance for T cell trafficking[142] and potential compensation for CXCR6. CXCR3 was also expressed on CXCR6^{hi} HBV- and ovalbumin-specific T cells after resolved infection, explaining the abundance of CXCR6$^{GFP/GFP}$ T cells after resolved Ad-GOL infection.

Interestingly, expression of CXCR6 might confer certain functions to liver-resident T cells, as CXCR6$^{GFP/GFP}$ cells produced less cytokines than CXCR6$^{WT/WT}$ cells when re-stimulated with cognate peptide antigen. Hence, CXCR6 expression might be linked to the functionality of hepatic T_{RM} cells. However, Tse *et al.* did not observe hampered cytokine production upon peptide re-stimulation but an altered expression of effector and memory markers characterizing malaria-specific CXCR6$^{GFP/GFP}$ cells as short-lived effector T cells[129]. In line with the results obtained after a resolved Ad-GOL infection, Heesch *et al.* did not observe impaired clearance of infection or migration to the liver of CXCR6$^{GFP/GFP}$ cells during ovalbumin-expressing *L. monozytogenes* infection but hampered long-term maintenance of antigen-specific T cells (30 weeks p.i.)[99]. Therefore, it might be interesting to follow the maintenance of antigen-specific CXCR6$^{GFP/GFP}$ T cells in Ad-GOL infection over a prolonged time frame, as the time point analyzed in this study was 3.5 weeks p.i. Since *L. monocytogenes* can infect hepatocytes[143] and this infection leads to strong CD8^{+} T cell responses in the liver[144] as observed for adenoviral serotype 5 infections[145], it is reasonable to compare these model systems, and it is expected to find similar T cell characteristics.

In conclusion, CXCR6 expression appears to be dispensable for recruiting $CD8^+$ T cells to the liver and is not required to clear hepatic infections, as long as chemokine receptors with redundant functionality are co-expressed on the same T cell. However, CXCR6 might be required for immune surveillance by liver-resident T cells during a secondary infection, as cytokine production upon re-stimulation and long-term maintenance were lower in $CXCR6^{GFP/GFP}$ T cells. Reduced functionality might be due to a CXCR6-dependent localization to sites within the liver, where more stimulatory cytokines are available. For NK cells, such an indirect role of CXCR6 has been proposed to bolster survival[146]. Moreover, CXCR6 could be required to fine-tune resident T cells' susceptibility for further chemokine signaling, similar to the sensitization by CCL17-CCR4 interaction for DCs[147].

Future work might aim at dissecting the role of CXCR6 for T_{RM} cell functionality. On one side, the effect of the CXCR6 ligand CXCL16 on cytokine expression in $CXCR6^{hi}$ T_{RM} cells might be interesting. On the other side, examining the localization and cell-cell interactions of $CXCR6^{hi}$ T cells in the liver might help to learn more about the role of CXCR6 on liver-resident T cells.

3.3 Circulating and liver-resident memory $CD8^+$ T cells are limited to resolved infections

After resolved but not persistent infections, $CX_3CR1^+CD8^+$ T cells were present in both liver and spleen, indicating these cells circulated through the organism as demonstrated for T_{EM} cells via parabiosis studies previously[148]. As T_{EM} cells transit through non-lymphoid tissue, spleen, and blood but do not home to lymph nodes[149], CX_3CR1^+ T cells did not co-express CD62L. Instead, these cells partially co-expressed the effector marker KLRG-1, in line with observations made for circulating T_{EM} cells by Herndler-Brandstetter *et al.*[111]. Hence, the phenotype of CX_3CR1^+ T cells induced by viral liver infections matched T_{EM} cells in other infection models, such as vesicular stomatitis virus[111,148], viral infection with LCMV[150], and intracellular bacterial infection with *Listeria monocytogenes*[111].

Transcriptome analysis confirmed two distinct hepatic antigen-specific T cell populations after resolved Ad-GOL infection, as principal component analysis separated $CXCR6^{hi}$ from CX_3CR1^+ $CD8^+$ T cells. Of note, $CX_3CR1^+CD8^+$ T cells in the liver closely resembled those in the spleen. In hepatic CX_3CR1^+ T cells, *Tnfaip3* (tumor necrosis factor alpha-induced protein 3) encoding the ubiquitin-modifying enzyme A20 was the top upregulated gene. Giordano *et al.* described A20 as a “brake” on T cell anti-tumor activity in A20-deficient T cells[151]. In addition to *Tnfaip3*, the orphan nuclear receptor *Nr4a1* was increased in hepatic CX_3CR1^+ T cells. *Tnfaip3* and *Nr4a1* were previously associated with the regulation of T cell effector functions[152]. Thus, increased *Tnfaip3* and *Nr4a1* in hepatic CX_3CR1^+ T cells might control the effector functions of peripheral T cells to prevent tissue damage. On the other side, the upregulation of *Tnfaip3* and *Nr4a1* might reflect the liver’s tolerogenic imprint on CX_3CR1^+ T cells once

they are located there. Together, transiting T_{EM} cells appear to adjust their gene expression profile depending on their localization to the liver.

When comparing DEGs between hepatic CX_3CR1^+ T cells and $CXCR6^{hi}$ T cells after resolved Ad-GOL infection, the transcription factors *Klf3* and *Nfic* were upregulated in CX_3CR1^+ T cells. *Klf3* is associated with tissue egress and circulating memory T cells[153]. *Nfic* has not been described for T_{EM} cells so far. It encodes the nuclear factor 1 C-type protein belonging to the nuclear factor 1 (NF1) family. The NF1 family is involved in nucleosome remodeling and maintaining chromatin structures open for transcription[154]. Hence, investigating epigenetic regulation in peripheral T cells might be a worthwhile approach in further experiments.

Initially, the fractalkine receptor CX_3CR1 was described to identify memory $CD8^+$ T cells with effector capacities in contrast to memory T cells with proliferative potential[77]. However, hepatic and splenic CX_3CR1^+ T cells expressed less intracellular GzmB than hepatic $CXCR6^{hi}$ T cells. Hence, $CXCR6^{hi}$ T cells constitute another peripheral memory T cell population with more powerful effector functions in addition to the four subsets described originally by Böttcher *et al.*[77]. Further experiments could determine whether $CXCR6^{hi}$ T cells are more efficient in degranulation than CX_3CR1^+ T cells.

Liver $CXCR6^{hi}$ T cells showed exceptional responsiveness towards antigen-specific re-stimulation regarding target cell killing and IFNγ release, as described for T_{RM} cells before[90,155]. Of note, $CXCR6^{hi}$ T_{RM} cells and CX_3CR1^+ T_{EM} cells had significantly different killing kinetics of target cells, as $CXCR6^{hi}$ T cells significantly outpaced CX_3CR1^+ T cells, most likely due to more rapid degranulation and GzmB release. This finding demonstrates why T_{RM} cells were described as “first-responders” during re-challenges and crucial to the host’s defense in studies with depleted T_{RM} cells[82,156,157]. Moreover, hepatic $CXCR6^{hi}$ T cells killed a higher proportion of target cells than hepatic and splenic CX_3CR1^+ T cells, indicating higher cytotoxicity and meeting the cytotoxic potential required to eliminate infected parenchyma cells within the liver. Hence, the liver harbored highly functional cells after resolved infections defying its rather tolerogenic milieu described previously[158]. It is tempting to speculate that local antigen-recognition by $CD8^+$ T cells in the liver was a driver in the induction of immune tolerance and non-responsiveness towards further activation signals, explaining why memory T cells that did not see their cognate antigen anymore showed vital cytotoxic effector functions.

Direct comparison of $CXCR6^{hi}$ T cells after resolved infection to $CXCR6^{hi}$ T cells during persistent infection revealed new surface markers to discriminate functional $CXCR6^{hi}$ from dysfunctional $CXCR6^{hi}$ T cells. CXCR3 was one marker found on liver $CXCR6^{hi}CD8^+$ T cells in mice that cleared the infection. On functional cells, the chemokine receptor CXCR3 might contribute to migration to virus-infected cells early in infection[102] and thereby facilitate recruitment to the liver shortly after infection[101]. Hence, CXCR6 and CXCR3 probably fulfill the same function on liver-resident T cells. Ly6a, also termed stem cell antigen-1 (Sca-1), was another marker identifying

functional liver CXCR6^{hi} T cells in mice that cleared the infection. Ly6a is expressed on memory T cells and can be induced via IL-27 signaling, leading to higher expression of T-bet, Eomes, and Blimp-1[159]. However, a knock-out mouse model proved Ly6a expression to be dispensable for memory T cell development after clearance of viral infections, suggesting that it may serve as a surrogate marker[160]. However, a discriminatory marker tagging CXCR6^{hi} T cells during persistent infection was CD122. CD122, the IL-2 receptor β-chain (IL2Rβ) binding IL-2, and IL-15 was associated with the induction of T cell exhaustion and hampered memory development during chronic LCMV infection previously[161]. On the other hand, Pallet *et al.* demonstrated the role of IL-15 for the induction of T_{RM}-like T cells *in vitro*[97]. Hence, CD122/IL2Rβ might contribute to the survival of dysfunctional liver resident CXCR6^{hi} T cells during persistent infection of the liver.

The formation of CXCR6^{hi}CD8^{+} T cells and disappearance of CX_3CR1^{+}CD8^{+} T cells from the circulation may be part of a mechanism where local antigen-presentation in the liver caused recruitment of antigen-specific CD8^{+} T cells to the liver and where local signals allowed T cells to acquire a liver-resident phenotype. This assumption is consistent with the occurrence of CXCR6^{hi}CX_3CR1^{+} CD8^{+} T cells in mice that were about to clear AdHBV infection. The signals necessary for imprinting a liver-residency phenotype on CD8^{+} T cells remain unknown and require further investigation. Since antigen-specific CD8^{+} T cells were present but dysfunctional in the liver during persistent infection, re-invigorating effector functions in these CD8^{+} T cells might represent a strategy to overcome virus-specific immune tolerance in CD8^{+} T cells. In summary, CXCR6^{hi} T cells during persistent infection were present in the liver over a prolonged time, which might be facilitated by the expression of a residency-associated gene signature. However, these liver-resident T cells are most likely not memory cells, as they lack crucial functional capacities, have higher turnover than functional T_{RM} cells and antigen is still present.

Hence, circulating and resident memory T cells were limited to resolved liver infections: CX_3CR1^{+} T cells were functional T_{EM} cells in all settings analyzed in this study. Strikingly, liver-resident CXCR6^{hi} T cells expressed even more effector molecules and reacted significantly faster towards target cells than CX_3CR1^{+} T cells. Therefore, CXCR6^{hi} T cells represent a pillar in hepatic immune surveillance and should be considered targets for future prophylactic and therapeutic vaccine strategies. For both prophylactic and therapeutic vaccines, T cell priming in lymphoid organs could be followed by an organ-specific “pull” to seed T_{RM} cells in the virus-targeted organ as described by Fernandez-Ruiz *et al.* for a vaccine protecting against liver-stage malaria infection[93]. In their approach, local antigen is crucial to seed T_{RM} cells in the liver. Since antigen is present in the liver as well during persistent liver infection, the “prime and pull” approach could also be utilized in a therapeutic vaccination to induce hepatic T_{RM} cells. T cells could be primed in lymphoid organs and directed to the liver, where the antigen is present locally. Shin and Iwasaki suggested using local application of chemokines to attract primed T cells to the desired tissue site[162]. However, this

approach might be limited to epithelial organs. For liver-targeting viruses, iMATEs ('intrahepatic myeloid-cell aggregates for T cell population expansion')[163] could be used to enhance the accumulation of primed T cells in the liver. iMATEs might even strengthen T_{RM} cell functionality in the liver as published by Kosinska *et al.* for hepatic $CD8^+$ T cells in the context of a therapeutic protein-prime/MVA-HBcore boost vaccination scheme in AAV-HBV infected mice[164].

In conclusion, $CXCR6^{hi}$ T cells during persistent infection are dysfunctional liver-resident T cells, which represent an interesting target for re-activation to locally trigger immune effector functions, e.g., in the context of therapeutic vaccination.

3.4 Tolerance-inducing mechanisms in liver-resident $CXCR6^{hi}$ T cells during persistent viral infection

Hepatic $CXCR6^{hi}$ T cells during persistent infections expressed the residency marker CD69 and shared a set of tissue residency-associated genes with functional T_{RM} cells but lacked expression of CD49a, which marks cytotoxic T_{RM} cells[96]. At the same time, $CXCR6^{hi}$ T cells during persistent infection expressed high levels of inhibitory receptors such as PD-1, Tim-3, Lag-3, and TIGIT, which is a characteristic feature of functionally exhausted $CD8^+$ T cells[30,137]. Even more critical, these cells did not respond to antigen-specific re-stimulation regarding cytokine expression or target cell killing. The combination of residency characteristics and dysfunctionality in $CXCR6^{hi}$ T cells during persistent liver infection most likely represented an adaptation to the persistent antigen expressed in the liver. Since persistent TCR stimulation most likely drives both liver residency and functional adaptation, liver residency may represent a trap resulting in the development of dysfunctional $CXCR6^{hi}$ T cells stuck in the liver.

The transcription factor TOX is upregulated in antigen-specific T cells during persistent infection and cancer, but not in effector and memory T cells during and after resolved infection[28,114,165]. In line with these reports, TOX was significantly higher in antigen-specific $CXCR6^{hi}$ T cells during persistent infection than resolved Ad-GOL and AdHBV infection on the protein level and compatible with reduced cytokine expression. Of note, TOX is responsible for an epigenetic imprint of the dysfunctional T cell phenotype observed during persistent infection[28,114]. The chromatin structure of DNA loci associated with dysfunctionality is less accessible in TOX-KO T cells than wild-type cells. Coinciding, the chromatin of functionality-associated loci is more accessible in TOX-KO cells[165]. Taken together, TOX dampens the functionality of T cells in persistent antigen settings, which is consolidated at the level of epigenetics.

However, TOX gene expression was not significantly upregulated in $CXCR6^{hi}$ T cells during persistent Ad-GOL infections, although significant differences were observed on the protein level. Apparently, TOX had no massive impact on gene expression in dysfunctional $CXCR6^{hi}$ T cells during persistent liver infection. Instead, the cAMP-responsive element modulator (CREM) was the dominating transcription factor in these cells. The top hierarchical position of CREM in the transcription factor network analysis

hinted at elevated cAMP signaling in CXCR6^{hi} T cells during persistent viral infection of the liver. However, of the approximately 4000 Cre-responsive promotor sites in the genome, only a small number of target genes is expressed in a given cell due to chromatin accessibility and further required regulatory factors[166]. Hence, TOX might influence which genes have an open chromatin structure and are thereby sensitive to control by CREM downstream of cAMP signaling.

cAMP signaling regulates T cell functionality on several levels. First, cAMP-activated protein kinase A (PKA) impedes the activation of TCR-induced MAP kinase and thereby hampers T cell activation since MAPK is required for IL-2 production[167]. Second, PKA counteracts TCR signaling via inhibitory phosphorylation of Lck by the PKA-activated kinase Csk[168]. Third, cAMP signaling dampens T cell functionality via transcriptional regulation by the transcription factor CREM. Cytosolic CREM is activated via phosphorylation by protein kinases A and C, which are, in turn, activated by cAMP[35,40]. CREM is constitutively expressed, whereas cAMP induces expression of its isoform ICER (inducible cAMP early repressor)[39]. ICER represses CRE-binding nuclear factors in an antagonistic manner, as ICER lacks a transactivation domain. Lacking a transactivation domain, ICER cannot recruit CREB-binding protein or its homolog p300, which facilitates chromatin accessibility by histone acetyltransferase activity[169] and thus acts as a transcriptional inhibitor.

In summary, cAMP signaling can dampen T cell functionality. In line with this assumption, the cAMP signature revealed by bioinformatic analysis was verified by elevated pPKA, CREM/ICER, and one of its target genes 4-1BB in antigen-specific CXCR6^{hi} T cells during persistent Ad-GOL infection. Of note, 4-1BB expression was also upregulated in CXCR6^{hi} T cells during persistent AdHBV infection, hinting at elevated cAMP signaling in CD8^{+} T cells during experimental HBV infection. Notably, transcriptome analysis via RNA sequencing and labeling by the polyclonal anti-CREM antibody used in this study did not distinguish between the different CREM isoforms. Thus, it is unknown whether CREM isoforms containing a transactivation domain leading to target gene expression or ICER, lacking a transactivation domain[40], were expressed in CXCR6^{hi} T cells during persistent infection.

Increased cAMP signaling was verified in dysfunctional liver CXCR6^{hi} T cells. To directly assess cAMP signaling's influence on T cell effector functions, highly functional CXCR6^{hi}CD8^{+} T cells after resolved Ad-GOL or AdHBV infection were treated with the cAMP-increasing agent forskolin. Forskolin treatment resulted in a remarkable reduction of cytokine production by previously functional CXCR6^{hi} in the Ad-GOL and AdHBV model. Even more critical, target cell killing was significantly reduced in T cells isolated from Ad-GOL infected mice. This indicated chemical stimulation of the adenylyl cyclase by forskolin led to more intracellular cAMP, activating PKA via phosphorylation, which induced CREM/ICER, creating a phenocopy of dysfunctional CXCR6^{hi} T cells observed during persistent infection.

To further dissect the roles of ICER and CREM during persistent Ad-GOL infection, antigen-specific T cells were analyzed in mice with a T cell-specific ICER knock-out. Remarkably, these ICER-deficient T cells produced more IFNγ upon cognate re-stimulation compared to wild-type controls. This was in line with a study by Bodor *et al.* reporting reduced IFNγ levels in ICER-overexpressing T cells[169], suggesting ICER represses cytokine expression in T cells. This hints at ICER being the CREM isoform responsible for CXCR6^{hi} T cell dysfunctionality in persistent viral infections. Mechanistically, ICER might counteract T cell functionality by antagonistic suppression of nuclear factor of activated T cell c1 (NFATc1)[170] or of bZIP proteins like CREB[169], which are essential for T cell activation[171,172].

Recently, Crem expression in T cells has been reported in systemic lupus erythematosus. In this auto-immune disease, elevated CREM/ICER in CD4$^+$ T cells represses IL-2 transcription, hampering Treg development and activation-induced cell death of auto-reactive T cells[173]. Elevated CREM/ICER expression leading to inadequate auto-reactive T cell effector functions on one side and loss of T cell function in a persistent viral infection on the other side might seem counter-intuitive at first sight. However, in both observations, reduced cytokine expression and persistent antigen presentation were detected. In systemic lupus erythematosus, reduced IL-2 expression in CD4$^+$ T cells diminishes the Treg population, leading to increased auto-inflammation[173]. In a persistent viral infection, however, ICER suppressed IFNγ expression in dysfunctional CD8$^+$ T cells. Hence, this work proposes a role for CREM/ICER activated by cAMP signaling in driving dysfunctionality in antigen-specific CXCR6^{hi} T cells during persistent infection of the liver that acts beyond the well-characterized dysfunctionality-mediating transcription factor TOX. Future work might aim at specifically inhibiting ICER in antigen-specific T cells to rescue their functionality in the context of chronic inflammation. To further potentiate T cell functionality, ICER inhibition might be combined with checkpoint inhibitors used for immunotherapy of cancer patients[174]. Conversely, further induction of cAMP signaling and Crem expression might help attenuate autoimmunity of T cells in tissues that causes tissue damage.

So far, I have analyzed the effect of increased cAMP signaling on hepatic T cells. Going one step further, I aimed at identifying its source during persistent liver infection. In the liver, intracellular cAMP levels in T cells can be increased by adenosine[119] or PGE_2 produced by Tregs[34], Kupffer cells[2], myeloid dendritic cells[158], or liver sinusoidal endothelial cells, as shown in this study. Additionally, T cell receptor stimulation without co-stimulation via CD28 results in increased cAMP in T cells[175]. During persistent viral infections, T cells are exposed to antigen constantly, which might cause higher intracellular cAMP levels in addition to the sources mentioned above[34].

PGE_2 treatment, but not exposure to adenosine, abrogated effector functions of CXCR6^{hi} T cells isolated from mice after resolving Ad-GOL liver infection. PGE_2, in contrast to forskolin, cannot permeate cell membranes and therefore requires the expression of its receptors on the T cell's surface to induce cAMP signaling. On T cells,

EP_2 and EP_4 bind their ligand PGE_2 resulting in intracellular PKA phosphorylation[176]. Expression of EP_2 and EP_4, therefore, governs the susceptibility of T cells towards extracellular PGE_2. Since exhausted T cells during persistent viral infections upregulate EP_2 and EP_4[120], $CXCR6^{hi}$ T cells during persistent infection might be more susceptible to PGE_2 than $CXCR6^{hi}$ T cells isolated after resolved infection. This EP_2 and EP_4-dependent signal transduction might explain the difference in effect size between forskolin and PGE_2. The assays used in this study could be refined by re-exposing functional $CXCR6^{hi}$ T cells to cognate antigen first to mimic persistent antigen exposure, followed by PGE_2 treatment.

Since PGE_2 diminished T cell effector functions *ex vivo*, PGE_2 concentrations of liver homogenates were measured after resolution and during persistent liver infection to assess whether PGE2 might cause dysfunctionality of $CXCR6^{hi}$ T cells *in vivo*. However, PGE_2 levels were not significantly different. Nevertheless, localization is lost during homogenization, and PGE_2 levels measured might not represent the microenvironment of antigen-specific $CXCR6^{hi}$ T cells close to PGE_2 or cAMP-producing hepatic cell populations. In addition to PGE_2 and adenosine, glucocorticoids can also induce cAMP signaling via a G protein-coupled receptor[177]. Hence, the analysis of liver tissue for the increased presence of glucocorticoids seems to be a promising question for future work to unravel the molecular mechanisms underlying the induction of cAMP signaling.

In summary, the hepatic tolerogenic milieu combined with continuous TCR signaling and glucocorticoids might induce a cAMP signature in liver-resident T cells, causing their dysfunctionality. Hence, the following working model to understand the development of dysfunctional virus-specific $CD8^+$ T cells during persistent infection is proposed by this study: Continuous TCR stimulation is present during persistent infection and may induce chromatin-accessibility through upregulation of TOX. In parallel, the hepatic microenvironment induces CREM/ICER via cAMP signaling in $CXCR6^{hi}$ T cells. CREM/ICER may bind accessible Cre-sites, regulate gene expression, and thereby manifest the observed dysfunctionality in liver $CD8^+$ T cells. This model has implications for future T cell-based therapies of persistent viral infections: Targeting cAMP signaling in T cells, e.g. via cAMP antagonists, might be a promising re-invigoration strategy. However, cAMP signaling is a major pathway, as approx. 4000 genes have Cre-responsive sites[166] and, according to Sriram and Insel, probably most approved therapeutics in the US and the EU target cAMP signaling[178]. Hence, further work is required to determine the G-protein coupled receptors or cAMP-degrading phosphodiesterases relevant for T cells to enable specific treatment and prevent side effects. Additionally, investigating the source of elevated cAMP signaling in the liver during persistent infection is a promising strategy, as this might identify further potential molecular targets. Lastly, an approach combining antagonized cAMP signaling and increasing co-stimulatory signaling via antibody treatment might be most promising to strengthen T cell functionality during persistent viral infection of the liver.

4 Materials and Methods

4.1 Materials

4.1.1 Consumables

Product	Supplier
0.5 mL, 1.5 mL, and 2 mL reaction tubes	Sarsted
1000 µL tips	Sarsted
15 mL and 50 mL centrifugation tubes	Sarsted
96well U-Bottom plates for cell culture	TPP
96well V-bottom plates	Sarsted
96well, 48well, 24well, 12well, 6well F-Bottom plates for cell culture	TPP
Cannulas	Braun
Cell strainer 100 µm	Institute of Experimental Immunology, University of Bonn
ELISA 96well plates	BioRad
Filter tips (10 µL, 20 µL, 200µL, 1000 µL)	Sarsted
Filter tips, qPCR grade (10 µL, 20 µL, 200 µL, 1000 µL)	Sarsted
MACS separation columns	Miltenyi
Micro test titer tubes (for flow cytometry measurements)	BioRad
Omnican insulin syringes	Braun
Reflotron ALT stripes	Roche Diagnostics
Serological pipettes (2 mL, 5 mL, 10mL, 25 mL)	Sarsted
Syringes (1 mL, 2 mL, 5 mL, 10 mL)	Braun
Tip StackPacks (for 10 µL and 200 µL tips)	Sarsted

4.1.2 Chemicals and reagents

Product	Supplier
Adenosine	SigmaAldrich
Agarose	Nippon genetics
Antigenfix	DiaPath
Brefeldin A 1 mg/mL	BD Biosciences
Cell stimulation cocktail (40.5 µM Phorbol 12 myristate 13-acetate and 670 µM ionomycin)	Invitrogen
Collagen R	Serva
CountBright TM Absolute Counting Beads	Life Technologies
Dimethyl Sulfoxide (DMSO)	SigmaAldrich
DMSO	Sigma
DNA ladder 100 bp	Nippon genetics
Dynabeads	Gibco via ThermoFisher Scientific
Fetal calf serum (FCS)	PAN-Biotech

Formalin 4%	Institute of Comparative Experimental Pathology (Dr. Steiger, Technical University Munich)
Forskolin	SigmaAldrich
Glucose	Roth
Hepes 1mM	Gibco
IL-2 Proleukin	Novartis
Isoflurane (Forene® 100%)	AbbVie
L-Glutamin 200 mM	PAN-Biotech
MHC molecules and streptamers for flow cytometry	Institute for Medical Microbiology, Immunology and Hygiene, (Prof. Busch, Technical University Munich)
NaCl	Braun
Non-essential amino acids	Gibco
Penicillin/Streptomycin 10.000 mg/mL	Gibco
Percoll	GE Healthcare
PGE_2	SigmaAldrich
SIINFEKL (Ovalbumin257-264 peptide) and MGLKFRQL (HBV Core93-103 peptide)	peptides&elephants
Tissue-Tek O.C.T	Sakura Finetek
TRI-Reagent (Trizol)	Life Technologies
Trypan blue	Gibco
UltraComp eBeads	eBioscience
β-Mercaptoethanol 50 mM	Gibco

4.1.3 Buffers

Buffer	**Ingredients**
1x TAE Buffer	40 mM Tris 40 mM Acetic acid 1 mM EDTA pH 8.0 H_2O
ACK Lyse Buffer	146 mM NH_4Cl 10 mM $NaNCO_3$ 2 mM EDTA
Flow cytometry Buffer	1x PBS 1% FCS 0,01% sodium azide
GBSS	PAN Biotech
Homogenization Buffer PGE_2 ELISA (Cayman)	0.1 M phosphate pH7.4 1 mM EDTA 10 µM Ibuprofen
MACS Buffer	1x PBS 0,5% FCS 2mM EDTA
Phosphobuffered Saline (PBS), 1X	3.2 mM Na2HPO4 0.5 mM KH2PO4 1.3 mM KCl

	135 mM NaCl pH 7.4

4.1.4 Cell culture media

Medium	Ingredients
Hepatocyte attachment medium	William's E medium 10% FCS 6% Glucose 200 mM Glutamine 1 M Hepes pH 7.4 10000 U/mL Penicillin/Streptomycin 50 mg/mL Gentamycin Hydrocortisone Insulin 1.6% DMSO
Hepatocyte maintenance medium	William's E medium 6% Glucose 200 mM Glutamine 1 M Hepes pH 7.4 10000 U/mL Penicillin/Streptomycin 50 mg/mL Gentamycin Hydrocortisone Insulin 1.6% DMSO
Hepatocyte over-night medium	William's E medium 1% FCS 6% Glucose 200 mM Glutamine 1 M Hepes pH 7.4 10000 U/mL Penicillin/Streptomycin 50 mg/mL Gentamycin Hydrocortisone Insulin 1.6% DMSO
T cell medium	RPMI GlutaMAX 10% FCS 1% L-Glutamine 1% Penicillin/Streptomycin 50 µM β-Mercaptoethanol

4.1.5 Antibodies and dyes for flow cytometry

Antibody/Dye	Dilution	Clone	Manufacturer
goat anti-rabbit Alexa Fluor 647	1:500	-	Invitrogen
IgG1 isotype control APC conjugated	1:200	eBM2a	eBioscience
IgG1 isotype control PE conjugated	1:200	eBM2a	eBioscience
Live/Dead dye APC-eFluor780	1:2000	-	Invitrogen
α-human CREM polyclonal antibody	1:75	-	Invitrogen

α-human GranzymeB APC	1:200	GB11	Invitrogen
α-human GranzymeB PE	1:200	GB11	Invitrogen
α-murine 4-1BB eF450	1:200	17B5	Biolegend
α-murine CD122 PE	1:200	5H4	Biolegend
α-murine CD25 APC	1:200	PC61.5	Invitrogen
α-murine CD44 Brilliant Violet 711	1:200	IM7	Biolegend
α-murine CD44 PerCP-Cy5.5	1:200	IM7	Biolegend
α-murine CD45.1 eFluor 450	1:200	A20	Invitrogen
α-murine CD45.1 PE/Dazzle594	1:200	A20	Biolegend
α-murine CD45.1 PE-eFluor 610	1:200	A20	Invitrogen
α-murine CD69 Brilliant Violet 605	1:200	H1.2F3	Biolegend
α-murine CD69 SuperBright 600	1:200	H1.2F3	Invitrogen
α-murine CD8 Brilliant Violet 510	1:250	53-6.7	Biolegend
α-murine CD8 FITC	1:200	53-6.7	Invitrogen
α-murine CX_3CR1 Alexa Fluor 647	1:200	SA011F11	SONY Biotechnology
α-murine CX_3CR1 Alexa Fluor 700	1:200	SA011F11	SONY Biotechnology
α-murine CX_3CR1 PE	1:200	SA011F11	Biolegend
α-murine CXCR6 FITC	1:200	SA051D	Biolegend
α-murine IFNγ Brilliant Violet 711	1:200	XMG1.2	Biolegend
α-murine IFNγ PE	1:200	XMG1.2	Biolegend
α-murine pPKA Alexa Fluor 488	1:15	47/PKA	BD Biosciences
α-murine pPKA Alexa Fluor 647	1:15	47/PKA	BD Biosciences
α-murine TNFα PE-Cy7	1:200	MP6-XT22	SONY Biotechnology

4.1.6 Enzymes and Kits

Product	**Supplier**
Enzymes	
Collagenase	Worthington Biochemical Corporation
Proteinase K	Roche
RNase	Macherey-Nagel
Kits	
BrdU Flow Kit (FITC and APC)	Becton, Dickinson and Company
CD8a (Ly2) MicroBeads, mouse	Miltenyi Biotec
Foxp3/Transcription Factor Staining Buffer Set	Life Technologies
Intracellular Fixation and Permeabilization Buffer Set	Life Technologies
NucleoSpin Tissue XS, Micro kit for DNA purification	Macherey-Nagel
NucleoSpin Tissue XS, Micro kit for RNA purification	Macherey-Nagel
Prostaglandin E2 ELISA monoclonal Kit	Cayman CHEMICAL
REDTaq® ReadyMix™ PCR Reacion Mix	Sigma

Takyon™ SYBR® 2x MasterMix dTTP Blue	Eurogentec Takyon
True-nuclear transcription factor buffer set	Biolegend

4.1.7 Mice

6-week-old C67Bl/6 mice were purchased from Janvier or Charles River. H-2K^b-restricted T cell receptor transgenic CD45.1$^+$ OT-I mice (Tg(TcraTcrb)1100Mjb transgenic T cell receptor specific for ovalbumin 257-264), H-2K^b-restricted T cell receptor transgenic CD45.1$^+$ Cor93 mice (B6.Cg-Ptprca Pepcb Tg (TcraBC10, TcrbBC10) 3Chi/J transgenic T cell receptor specific for HBcore 93-100) and ICER$^{fl/fl}$ x CD4-Cre mice were bred under specific pathogen-free conditions at Translatum, Klinikum rechts der Isar. Guidelines of the Federation of Laboratory Animal Science Association were implemented for breeding and experiments.

4.1.8 Instruments

Instrument	**Supplier**
AutoMACS cell separator	Miltenyi
Cell sorter SH800	Sony Biotechnology
Easypet pipetboy	Eppendorf
ELISA-Reader	Tecan
Heat block	Eppendorf
Incubator	Heraeus Holding GmbH
IVIS Lumina In vivo imaging system	Perkin Elmer
Laminar flow cabinet	Heraeus Holding GmbH
LightCycler® 480 II	Roche Diagnostics
Microscope Axio Vert A1	Zeiss
Multifuge	Heraeus Holding GmbH
Pipettes	Eppendorf
Reflotron® Reflovet Plus; ALT measurements	Roche Diagnostics
Spectral Analyzer SP6800	Sony Biotechnology
Table-top centrifuge	Eppendorf
xCelligence RTCA	ACEA Biosciences

4.1.9 Software

Software	**Application**	**Supplier**
Microsoft Office 365	data processing	Microsoft
FlowJo	analysis of flow cytometry data	Becton, Dickinson and Company
LightCycler480	Analysis of qPCR data	Roche Diagnostics
Tecan i-control	ELISA read-out	Tecan
GraphPad Prism	statistical analysis and graphs	GraphPad Software
Image lab	analysis of gel images	BioRad
R studio	data processing	R studio
R	data processing	The R Foundation

4.2 Methods

4.2.1 Viruses and infection

Liver-targeting adenoviral constructs (Ad5ΔE1/E3) were used to deliver viral antigens to hepatocytes. Virus production and titration were done as described previously[179]. In the first course of experiments, Adenoviruses encoding for the nominal antigen ovalbumin and the reporter genes GFP and luciferase (Ad-GOL; GFP, ovalbumin, luciferase) were used for infections. Transgene expression was controlled by the CMV promoter (Ad-CMV-GOL) or by the hepatocyte-specific transthyretin promoter (Ad-TTR-GOL). Injection of $1x10^7$ PFU Ad-CMV-GOL in 100 µL NaCl i.v. into the tail vein resulted in an acute-resolving course of infection, whereas injection of $1x10^8$ - $1x10^9$ PFU Ad-TTR-GOL resulted in persistent infection as published previously[103]. For the second part of this study, the same adenoviral backbone was used to deliver the 1.3-fold overlength HBV genome (genotype D) to the liver[50]. Therefore, AdHBV1.3 in 100 µL NaCl was injected i.v. into the tail vein. All viruses used were kindly provided by PD Dr. Dirk Wohlleber and produced by Katrin Manske, Dr. Sandra Lampl, and Savvoula Michailidou.

4.2.2 Bioluminescence imaging

Expression of the virus-construct encoded reporter gene luciferase was measured with the *in vivo* imaging system (IVIS, s. 4.1.8 Instruments, S.76). To enable substrate conversion, 100 mg/kg body weight D-luciferin-K salt was injected i.p. 5 min before imaging. Imaging was performed with mice anesthetized with 2.5% isoflurane. Duration and binning were chosen depending on the expected bioluminescent signal.

4.2.3 Serum alanine transferase measurements

Hepatic tissue damage was assessed by serum alanine transaminase (sALT) measurement. 30 µL peripheral blood were withdrawn by punctuation of V. facialis and applied directly onto a Reflotron test strip. Strips were measured with the Reflotron Plus system.

4.2.4 HBeAg measurements

AdHBV1.3 infection kinetics were monitored by HBeAg measurements. Blood was withdrawn by punctuation of V. facialis. Blood was applied onto microvettes containing 500 µL Lithium heparin gel and centrifuged for 10 min at 10.000 x g. Sera were collected and stored at -80° C. Measurements were performed by Theresa Asen of the Institute of Virology (TU München, Prof. Ulrike Protzer).

4.2.5 Lymphocyte isolations

4.2.5.1 Peripheral blood cells

Peripheral blood collected by the punctuation of V. facialis was stored in microvettes containing 500 µL lithium-heparin gel. 60 µL were resuspended in 10 mL hypotonic ACK lysis buffer to lyse erythrocytes (10 min incubation at room temperature). Lysis was stopped by centrifugation at 550 x g for 5 min at 4° C. Supernatant was discarded, and cell pellets were resuspended for subsequent analysis

4.2.5.2 Splenocytes, lymph node-associated lymphocytes

Spleens or lymph nodes were mashed through 100 µm cell strainers and flushed with 30 mL cold PBS. Cells were centrifuged at 550 x g for 5 min at 4° C. Next, erythrocytes were lysed with 2 mL hypotonic ACK lysis buffer. The addition of 30 mL of PBS stopped lysis. Cell suspensions were filtered, centrifuged (same conditions), and resuspended for subsequent analysis.

4.2.5.3 Liver-associated lymphocytes

Livers were perfused with cold PBS for approx. 45 s at 5.2 mL/min velocity. Livers were then excised, weighed, and tissue samples for tissue analyses were taken and immediately frozen on dry ice. The remaining liver was weighed again and then mashed through 100 µm cell strainers using a 2 mL syringe's plunger. Strainers and plungers were flushed with 40 mL cold PBS. Homogenized livers were centrifuged at 550 x g for 5 min at 4° C. Pellets were then digested with 125 µg/mL collagenase diluted in 8 mL GBSS solution at 37° C in a rotary water bath for 10 min. The addition of 30 mL of PBS stopped digestion. Liver cells were centrifuged as described above, and cell pellets were resuspended in 3 mL 40% Percoll. Cell suspension in 40% Percoll was carefully layered on 80% Percoll in 15 mL centrifugation tubes. Gradient centrifugation was performed at 1440 x g at 20° C, acceleration was set to 7, deceleration was set to 1. Buffy coats between 40% and 80% Percoll cushions were collected and washed with PBS. Cells were centrifuged as described above and resuspended for subsequent analysis.

Lymphocyte isolations were performed with the kind help of Dr. Nina Kallin, Savvoula Michaelidou, Eric Henriss, and Ananthi Kumar.

4.2.6 T cell transfer

Single-cell suspensions of $CD8^+$ T cells were prepared in cold PBS. Concentration was adjusted to 10^2 cells/100 µL PBS for naïve OT-I T cell transfers, 10^4 cells/100 µL PBS for naïve Cor93 T cell transfers, and to 10^6 cells/100 µl PBS for CTL transfers. Single-cell suspensions were injected i.v. into the tail vein.

4.2.7 Flow cytometry (SP6800)

4.2.7.1 General procedure and surface staining

All stainings for flow cytometry were performed in 96-well V-bottom polystyrene plates. Surface stainings were performed in 30 µL flow cytometry buffer (PBS, 1% FCS, 0.01% sodium azide) per well containing the respective antibodies and fixable viability dye for 30 min at 4° C. Cells were washed 2 times at 600 x g for 3 min with 150µL flow cytometry buffer. Cells were then either filtered and transferred into flow cytometry tubes and analyzed using a spectral analyzer (SP6800) or subjected to intracellular staining.

4.2.7.2 Intracellular cytokine staining

Before intracellular cytokine staining (ICS), surface staining was prepared as described above. Cell pellets were resuspended in 100µL IC fixation buffer after the last washing step for 20 min at room temperature. Afterward, the fixation buffer was removed by centrifugation for 3 min at 600 x g. Cell pellets were resuspended in 1 x permeabilization buffer (10 x concentrate was diluted with H_2O_{dd}) and washed once. 30µL 1 x permeabilization buffer containing the respective antibodies were added to the cell pellets. ICS was incubated for 30 min at 4° C. Cells were then washed twice with 1 x permeabilization buffer. Afterward, cells were resuspended in 120µL flow cytometry buffer, filtered, and analyzed using a spectral analyzer SP6800.

4.2.7.3 Granzyme B and intranuclear staining (nuclear staining kit)

Surface staining was done as described above before granzyme B, or intranuclear staining was performed. Cell pellets were resuspended in 100µL fixation/permeabilization solution after the last washing step. The solution was prepared by mixing concentrate and diluent in a 1:4 ratio. Cells were incubated for 30 min up to 18 h at 4° C. After fixation and permeabilization, cells were washed once with 1x permeabilization buffer as described above. 30 µL 1 x permeabilization buffer containing the respective antibodies were added to the cell pellets for granzyme B staining or nuclear factor staining and incubated for 2 h. Next, cells were washed twice with 1x permeabilization buffer, resuspended in 120 µL flow cytometry buffer, and filtered before measurement with a spectral analyzer SP6800.

4.2.7.4 Methanol-based staining of nuclear factors

Surface staining was performed as described in the general procedure and surface staining. For the staining of phosphorylated PKA, cell pellets were fixed with 100 µL IC fixation buffer at 4° C for 30 min. The fixation buffer was removed by centrifugation at 600 x g for 3 min and washed once with flow cytometry buffer. First, cell pellets were resuspended in the remaining volume and second, in 100 µL ice-cold methanol. Incubation time was set to 30 min on ice. Methanol was removed by centrifugation at 700 x g for 5 min. Cells were washed twice with PBS using the same centrifugation conditions. Intranuclear staining was performed in 30 µL flow cytometry buffer containing the respective antibodies. After 2 h incubation, cells were washed twice with

flow cytometry buffer, resuspended in 120 µL flow cytometry buffer, filtered, and analyzed with a spectral analyzer SP6800.

4.2.8 Fluorescence-activated cell sorting (SH800)

The sample preparation for fluorescent activated cell sorting was done as described for the general procedure and surface staining for flow cytometry. In contrast to flow cytometry, samples for sorting were prepared under sterile conditions. Instead of sodium azide-containing flow cytometry buffer, sorting buffer (1x PBS, 0.5% FCS, 2 mM EDTA) was used. Sorted cells were collected in T cell medium (RPMI medium, 1 % L-glutamine, 1% penicillin/streptomycin, 50µM β-Mercaptoethanol) or 1x PBS containing 10% FCS.

4.2.9 Magnetically-activated cell sorting (AutoMACS)

Cells were filtered and labeled with magnetic-labeled antibodies in sorting buffer (1x PBS, 0.5% FCS, 2 mM EDTA) under sterile conditions for 5-15 min as recommended by the manufacturer. After incubation, cells were washed once with 10 mL sorting buffer at 600 x g for 5 min. Cells were then loaded on MACS columns for manual separation or the AutoMACS for automatic separation. Separation was performed according to the manufacturer's instructions. Cells were collected in sorting buffer.

4.2.10 Enzyme-linked immunosorbent assay (ELISA)

4.2.10.1 Sandwich ELISA for the quantification of IFNγ and TNF

TNF and INFγ derived from cell culture supernatant were quantified using a sandwich ELISA. All wash steps were performed with PBS + 0.05% tween. First, high protein-binding 96 well microplates were coated with 50 µL of 1 µg/mL purified anti-cytokine antibodies in coating buffer (0.1 M Na_2HPO_4, pH9) either for 2 h at room temperature or overnight at 4° C. Next, unbound antibody was removed by two wash steps. Unspecific binding was then blocked using 100 µL of 1% BSA in PBS for 30 min at room temperature. Afterward, wells were washed 3 times. 100 µL of samples and standard (recombinant cytokine dilution series starting at 40 ng/mL, dilution factor 3) were applied to the plate and incubated either at room temperature for 4 h or overnight at 4° C. After incubation, wells were washed 3 times. Then, 100µL of 0.5 µg/mL biotinylated anti-cytokine antibody in PBS were added at incubated for 1 h at room temperature. Next, wells were washed 3 times. For the detection of biotinylated antibodies, 100 µL streptavidin-coupled horseradish peroxidase were added to each well and incubated for 30 min at room temperature. Wells were washed 6 times after incubation. Next, 40 µL of TMB substrate (1-step solution ultra, ThermoFisher) solution were added to each well. After a substantial color change was observed, 40µL stop solution (0.18 M H_2SO_4) was added to each well. Absorption at 450 nm was then measured using a Tecan reader.

4.2.10.2 ELISA for the quantification of PGE_2

Prostaglandin E_2 was quantified from liver tissue and cell culture supernatant using a commercial competitive ELISA kit. Liver tissue was mechanically homogenized on ice in a hypertonic buffer based on 10x PBS containing 1 mM EDTA and 0.2 µM cyclooxygenase inhibitor ibuprofen. 1 mL homogenization buffer per 0.1 g liver tissue was used. The liver suspension was centrifuged at 8000 x g for 10 min at 4 °C. Supernatant from homogenized tissue or cell culture supernatant was measured with the ELISA as recommended by the manufacturer.

4.2.11 xCelligence kill assay

Cytotoxicity of SIINFEKL-specific $CD8^+$ T cells in liver and spleen on day >30 was assessed via *ex vivo* target-cell kill assays with xCelligence cell impedance measurement. Primary murine hepatocytes were used as target cells. Hepatocytes were isolated from uninfected C57Bl6 mice and seeded on collagenR-coated 96 well E-plates (ACEA Biosciences) as described previously[179]. 2 days after hepatocytes were seeded, lymphocytes from the liver and spleen of Ad-CMV-GOL and Ad-TTR-GOL infected mice were isolated. $CD45.1^+$ T cells were sorted with an SH800 cell sorter (Sony, s. 4.2.8 Fluorescence-activated cell sorting (SH800) S.80) into $CXCR6^{hi}$, $CX_3CR1^{+,}$ and $CXCR6^{hi}CX_3CR1^+$ populations. In the meantime, hepatocytes were pulsed with 20 mM SIINFEKL peptide for 30 min or treated as control wells. Afterward, hepatocytes were washed with medium twice to remove any unbound SIINFEKL. Sorted T cells were added to hepatocytes, and cell impedance was measured for 48 h to follow T cell-mediated cell death of hepatocytes. After the last impedance measurement, supernatants were collected, and IFN concentration was measured (s. 4.2.10.1 Sandwich ELISA for the quantification of IFNγ and TNF, S.80). % specific killing was calculated as follows: [total killing (w/ SIINFEKL – unspecific killing (w/o SIINFEKL)] x 100%.

Hepatocyte isolation was performed by Silke Hegenbarth and Annika Schneider.

4.2.12 Statistical analysis

All results were statistically analyzed with a two-way ANOVA, if not mentioned otherwise. Multiple comparisons were calculated with Tukey's test with the confidence level α set to 0.05 (95% confidence interval). P-values are indicated in graphs as follows: n.s. $p>0.05$, * $p<0.05$, ** $p<0.01$, *** $p<0.001$, **** $p<0.0001$.

All results shown are representative of at least two independent experiments with at least ten biological replicates, if not indicated otherwise.

4.2.13 Transcriptome analysis

RNA sequencing was performed in cooperation with Prof. Ruland's group (with Dr. Rupert Öllinger). Dr. Sainitin Donakoda performed transcriptome analysis.

5 References

1. Freitas-Lopes, M., Mafra, K., David, B., Carvalho-Gontijo, R. & Menezes, G. Differential Location and Distribution of Hepatic Immune Cells. *Cells* **6**, 48 (2017).

2. Crispe, I. N. The Liver as a Lymphoid Organ. *Annu. Rev. Immunol.* **27**, 147–163 (2009).

3. Wang, Y. & Zhang, C. The Roles of Liver-Resident Lymphocytes in Liver Diseases. *Front. Immunol.* **10**, 1582 (2019).

4. Protzer, U., Maini, M. K. & Knolle, P. a. Living in the liver: hepatic infections. *Nat. Rev. Immunol.* **12**, 201–213 (2012).

5. Knolle, P. A. Staying local - antigen presentation in the liver. *Curr. Opin. Immunol.* **40**, 36–42 (2016).

6. Knolle, P. A. Liver and Immune System. in *Zakim & Boyer's Hepatology: A Textbook of Liver Disease* (eds. Boyer, T. D., Manns, M. P. & Syncal, A. J.) 129–141 (Elsevier, 2011).

7. Robinson, M. W., Harmon, C. & O'Farrelly, C. Liver immunology and its role in inflammation and homeostasis. *Cell. Mol. Immunol.* **13**, 267–276 (2016).

8. Ichikawa, S., Mucida, D., Tyznik, A. J., Kronenberg, M. & Cheroutre, H. Hepatic stellate cells function as regulatory bystanders. *J. Immunol.* **186**, 5549–5555 (2011).

9. Zhang, N. & Bevan, M. J. CD8 T cells: foot soldiers of the immune system. *Immunity* **35**, 161–8 (2011).

10. Masopust, D. *et al.* Activated Primary and Memory CD8 T Cells Migrate to Nonlymphoid Tissues Regardless of Site of Activation or Tissue of Origin. *J. Immunol.* **172**, 4875–4882 (2004).

11. Cruz-Guilloty, F. *et al.* Runx3 and T-box proteins cooperate to establish the transcriptional program of effector CTLs. *J. Exp. Med.* **206**, 51–59 (2009).

12. Guidotti, L. G. *et al.* Immunosurveillance of the liver by intravascular effector CD8+ T cells. *Cell* **161**, 486–500 (2015).

13. Bertolino, P. *et al.* Early intrahepatic antigen-specific retention of naïve CD8+ T cells is predominantly ICAM-1/LFA-1 dependent in mice. *Hepatology* **42**, 1063–1071 (2005).

14. Bénéchet, A. P. *et al.* Dynamics and genomic landscape of CD8+ T cells undergoing hepatic priming. *Nature* **574**, 200–205 (2019).

15. Diehl, L. *et al.* Tolerogenic maturation of liver sinusoidal endothelial cells promotes B7-homolog 1-dependent CD8+ T cell tolerance. *Hepatology* **47**, 296–305 (2008).

16. Huang, L., Soldevila, G., Leeker, M., Flavell, R. & Crispe, I. N. The Liver Eliminates T Cells Undergoing Antigen-Triggered Apoptosis In Vivo. *Immunity* **1**, 741–749 (1994).

17. Crispe, I. N., Dao, T., Klugewitz, K., Mehal, W. Z. & Metz, D. P. The liver as a site of T-cell apoptosis: Graveyard, or killing field? *Immunol. Rev.* **174**, 47–62 (2000).

18. Böttcher, J. P. P. *et al.* Liver-Primed Memory T Cells Generated under Noninflammatory Conditions Provide Anti-infectious Immunity. *Cell Rep.* **3**, 779–795 (2013).

19. Gallimore, A. *et al.* Induction and Exhaustion of Lymphocytic Choriomeningitis Virus–specific Cytotoxic T Lymphocytes Visualized Using Soluble Tetrameric Major Histocompatibility Complex Class I–Peptide Complexes. *J. Exp. Med.* **187**, 1383–1393 (1998).

20. Zajac, A. J. *et al.* Viral Immune Evasion Due to Persistence of Activated T Cells Without Effector Function. *J. Exp. Med.* **188**, 2205–2213 (1998).

21. McLane, L. M., Abdel-Hakeem, M. S. & Wherry, E. J. CD8 T Cell Exhaustion During Chronic Viral Infection and Cancer. *Annu. Rev. Immunol.* **37**, 457–495 (2019).

22. Wherry, E. J. T cell exhaustion. *Nat. Immunol.* **131**, 492–499 (2011).

23. Matloubian, M., Concepcion, R. J. & Ahmed, R. CD4+ T cells are required to sustain CD8+ cytotoxic T-cell responses during chronic viral infection. *J. Virol.* **68**, 8056–8063 (1994).

24. Brooks, D. G. *et al.* Interleukin-10 determines viral clearance or persistence in vivo. *Nat. Med.* **12**, 1301–1309 (2006).

25. Shin, H., Blackburn, S. D., Blattman, J. N. & Wherry, E. J. Viral antigen and extensive division maintain virus-specific CD8 T cells during chronic infection. *J. Exp. Med.* **204**, 941–949 (2007).

26. Parry, R. V. *et al.* CTLA-4 and PD-1 Receptors Inhibit T-Cell Activation by Distinct Mechanisms. *Mol. Cell. Biol.* **25**, 9543–9553 (2005).

27. Crawford, A. & Wherry, E. J. The diversity of costimulatory and inhibitory receptor pathways and the regulation of antiviral T cell responses. *Curr. Opin. Immunol.* **21**, 179–186 (2009).

28. Alfei, F. *et al.* TOX reinforces the phenotype and longevity of exhausted T cells in chronic viral infection. *Nature* (2019). doi:10.1038/s41586-019-1326-9

29. Martinez, G. J. *et al.* The Transcription Factor NFAT Promotes Exhaustion of Activated CD8 + T Cells. *Immunity* **42**, 265–278 (2015).

30. Blank, C. U. *et al.* Defining 'T cell exhaustion'. *Nat. Rev. Immunol.* **19**, 665–674 (2019).

31. Wieland, D. *et al.* TCF1+ hepatitis C virus-specific CD8+ T cells are maintained after cessation of chronic antigen stimulation. *Nat. Commun.* **8**, 15050 (2017).

32. Utzschneider, D. T. *et al.* T Cell Factor 1-Expressing Memory-like CD8+ T Cells Sustain the Immune Response to Chronic Viral Infections. *Immunity* **45**, 415–427 (2016).

33. Rueda, C. M., Jackson, C. M. & Chougnet, C. A. Regulatory T-cell-mediated suppression of conventional T-cells and dendritic cells by different cAMP intracellular pathways. *Front. Immunol.* **7**, (2016).

34. Wehbi, V. L. & Taskén, K. Molecular Mechanisms for cAMP-Mediated Immunoregulation in T cells – Role of Anchored Protein Kinase A Signaling Units. *Front. Immunol.* **7**, 1–19 (2016).

35. Rauen, T., Hedrich, C. M., Tenbrock, K. & Tsokos, G. C. cAMP responsive element modulator: a critical regulator of cytokine production. *Trends Mol. Med.* **19**, 262–269 (2013).

36. Ganapathy, V., Gurlo, T., Jarstadmarken, H. O. & von Grafenstein, H. Regulation of TCR-induced IFN-γ release from islet-reactive non-obese diabetic CD8+ T cells by prostaglandin E2 receptor signaling. *Int. Immunol.* **12**, 851–860 (2000).

37. Hendricks, A., Leibold, W., Kaever, V. & Schuberth, H.-J. Prostaglandin E2 is Variably Induced by Bacterial Superantigens in Bovine Mononuclear Cells and Has a Regulatory Role for the T Cell Proliferative Response. *Immunobiology* **201**, 493–505 (2000).

38. Raker, V. K., Becker, C. & Steinbrink, K. The cAMP pathway as therapeutic target in autoimmune and inflammatory diseases. *Front. Immunol.* **7**, 1–11 (2016).

39. Molina, C. A., Foulkes, N. S., Lalli, E. & Sassone-Corsi, P. Inducibility and negative autoregulation of CREM: An alternative promoter directs the expression of ICER, an early response repressor. *Cell* **75**, 875–886 (1993).

40. Borlikova, G. & Endo, S. Inducible cAMP early repressor (ICER) and brain functions. *Mol. Neurobiol.* **40**, 73–86 (2009).

41. Bodor, J., Spetz, A. L., Strominger, J. L. & Habener, J. F. cAMP inducibility of transcriptional repressor ICER in developing and mature human T lymphocytes. *Proc. Natl. Acad. Sci.* **93**, 3536–3541 (1996).

42. Hu, J., Protzer, U. & Siddiqui, A. Revisiting Hepatitis B Virus: Challenges of Curative Therapies. *J. Virol.* **93**, 1–16 (2019).

43. World Health Organization. *Global Hepatitis Report*. *World Health Organization* (2017).

44. Maini, M. K. & Burton, A. R. Restoring, releasing or replacing adaptive immunity in chronic hepatitis B. *Nat. Rev. Gastroenterol. Hepatol.* **16**, 662–675 (2019).

45. Barker, L. F. *et al.* Transmission of Type B Viral Hepatitis to Chimpanzees. *J.*

Infect. Dis. **127**, 648–662 (1973).

46. Robinson, W. S., Clayton, D. A. & Greenman, R. L. DNA of a Human Hepatitis B Virus Candidate. *J. Virol.* **14**, 384–391 (1974).

47. Yan, H. *et al.* Sodium taurocholate cotransporting polypeptide is a functional receptor for human hepatitis B and D virus. *Elife* **1**, 1–28 (2012).

48. Seeger, C. & Mason, W. S. Molecular biology of hepatitis B virus infection. *Virology* **479–480**, 672–686 (2015).

49. Tu, T., Budzinska, M., Shackel, N. & Urban, S. HBV DNA Integration: Molecular Mechanisms and Clinical Implications. *Viruses* **9**, 75 (2017).

50. Huang, L.-R. *et al.* Transfer of HBV genomes using low doses of adenovirus vectors leads to persistent infection in immune competent mice. *Gastroenterology* **142**, 1447-1450.e3 (2012).

51. Guidotti, L. G., Isogawa, M. & Chisari, F. V. Host–virus interactions in hepatitis B virus infection. *Curr. Opin. Immunol.* **36**, 61–66 (2015).

52. Chisari, F. & Ferrari, C. Hepatitis B virus immunopathology. *Springer Semin. Immunopathol.* **17**, 261–281 (1995).

53. Chisari, F. V & Ferrari, C. Hepatitis B Virus Immunopathogenesis. *Annu. Rev. Immunol.* **13**, 29–60 (1995).

54. Luangsay, S. *et al.* Early inhibition of hepatocyte innate responses by hepatitis B virus. *J. Hepatol.* **63**, 1314–1322 (2015).

55. Cheng, X. *et al.* Hepatitis B virus evades innate immunity of hepatocytes but activates cytokine production by macrophages. *Hepatology* **66**, 1779–1793 (2017).

56. Thimme, R. *et al.* CD8+ T Cells Mediate Viral Clearance and Disease Pathogenesis during Acute Hepatitis B Virus Infection. *J. Virol.* **77**, 68–76 (2003).

57. Lucifora, J. *et al.* Specific and nonhepatotoxic degradation of nuclear hepatitis B virus cccDNA. *Science* **343**, 1221–8 (2014).

58. Xia, Y. *et al.* Interferon-γ and Tumor Necrosis Factor-α Produced by T Cells Reduce the HBV Persistence Form, cccDNA, Without Cytolysis. *Gastroenterology* **150**, 194–205 (2016).

59. Rehermann, B. & Thimme, R. Insights From Antiviral Therapy Into Immune Responses to Hepatitis B and C Virus Infection. *Gastroenterology* **156**, 369–383 (2019).

60. Rehermann, B., Ferrari, C., Pasquinelli, C. & Chisari, F. V. The hepatitis B virus persists for decades after patients' recovery from acute viral hepatitis despite active maintenance of a cytotoxic T–lymphocyte response. *Nat. Med.* **2**, 1104–1108 (1996).

61. Guidotti, L. G. Viral Clearance Without Destruction of Infected Cells During Acute HBV Infection. *Science (80-.).* **284**, 825–829 (1999).

62. Ye, B. *et al.* T-cell exhaustion in chronic hepatitis B infection: current knowledge and clinical significance. *Cell Death Dis.* **6**, e1694 (2015).

63. Boni, C. *et al.* Characterization of Hepatitis B Virus (HBV)-Specific T-Cell Dysfunction in Chronic HBV Infection. *J. Virol.* **81**, 4215–4225 (2007).

64. Schurich, A. *et al.* Role of the coinhibitory receptor cytotoxic T lymphocyte antigen-4 on apoptosis-Prone CD8 T cells in persistent hepatitis B virus infection. *Hepatology* **53**, 1494–1503 (2011).

65. Kurktschiev, P. D. *et al.* Dysfunctional CD8+ T cells in hepatitis B and C are characterized by a lack of antigen-specific T-bet induction. *J. Exp. Med.* **211**, 2047–2059 (2014).

66. Fisicaro, P. *et al.* Targeting mitochondrial dysfunction can restore antiviral activity of exhausted HBV-specific CD8 T cells in chronic hepatitis B. *Nat. Med.* **23**, 327–336 (2017).

67. Guidotti, L. G., Matzke, B., Schaller, H. & Chisari, F. V. High-level hepatitis B virus replication in transgenic mice. *J. Virol.* **69**, 6158–69 (1995).

68. Sprinzl, M., Dumortier, J. & Protzer, U. Construction of Recombinant Adenoviruses that Produce Infectious Hepatitis B Virus. in *Hepatitis B and D Protocols* **96**, 209–218 (Humana Press, 2004).

69. Sprinzl, M. F., Oberwinkler, H., Schaller, H. & Protzer, U. Transfer of Hepatitis B Virus Genome by Adenovirus Vectors into Cultured Cells and Mice : Crossing the Species Barrier Transfer of Hepatitis B Virus Genome by Adenovirus Vectors into Cultured Cells and Mice : Crossing the Species Barrier. *J. Virol.* **75**, 5108–5118 (2001).

70. Protzer, U. *et al.* Antiviral Activity and Hepatoprotection by Heme Oxygenase-1 in Hepatitis B Virus Infection. *Gastroenterology* **133**, 1156–1165 (2007).

71. John von Freyend, M. *et al.* Sequential control of hepatitis B virus in a mouse model of acute, self-resolving hepatitis B. *J. Viral Hepat.* **18**, 216–226 (2011).

72. Isogawa, M., Chung, J., Murata, Y., Kakimi, K. & Chisari, F. V. CD40 Activation Rescues Antiviral CD8+ T Cells from PD-1-Mediated Exhaustion. *PLoS Pathog.* **9**, 1–16 (2013).

73. Butz, E. A. & Bevan, M. J. Massive Expansion of Antigen-Specific CD8+ T Cells during an Acute Virus Infection. *Immunity* **8**, 167–175 (1998).

74. Lau, L. L., Jamieson, B. D., Somasundaram, T. & Ahmed, R. Cytotoxic T-cell memory without antigen. *Nature* **369**, 648–652 (1994).

75. Ahmed, R. & Gray, D. Immunological Memory and Protective Immunity: Understanding Their Relation. *Science (80-.).* **272**, 54–60 (1996).

76. Sallusto, F., Lenig, D., Förster, R., Lipp, M. & Lanzavecchia, A. Two subsets of memory T lymphocytes with distinct homing potentials and effector functions. *Nature* **401**, 708–712 (1999).

77. Böttcher, J. P. *et al.* Functional classification of memory CD8 + T cells by CX 3 CR1 expression. *Nat. Commun.* **6**, (2015).

78. Gerlach, C. *et al.* The Chemokine Receptor CX3CR1 Defines Three Antigen-Experienced CD8 T Cell Subsets with Distinct Roles in Immune Surveillance and Homeostasis. *Immunity* **45**, 1270–1284 (2016).

79. Rosato, P. C., Beura, L. K. & Masopust, D. Tissue resident memory T cells and viral immunity. *Curr. Opin. Virol.* **22**, 44–50 (2017).

80. Gebhardt, T. *et al.* Memory T cells in nonlymphoid tissue that provide enhanced local immunity during infection with herpes simplex virus. *Nat. Immunol.* **10**, 524–30 (2009).

81. Masopust, D. *et al.* Dynamic T cell migration program provides resident memory within intestinal epithelium. *J. Exp. Med.* **207**, 553–564 (2010).

82. Wu, T. *et al.* Lung-resident memory CD8 T cells (TRM) are indispensable for optimal cross-protection against pulmonary virus infection. *J. Leukoc. Biol.* **95**, 215–224 (2014).

83. Steinbach, K. *et al.* Brain-resident memory T cells represent an autonomous cytotoxic barrier to viral infection. *J. Exp. Med.* **213**, 1571–1587 (2016).

84. Beura, L. K. *et al.* Intravital mucosal imaging of CD8+ resident memory T cells shows tissue-autonomous recall responses that amplify secondary memory. *Nat. Immunol.* **19**, 173–182 (2018).

85. Tse, S.-W., Cockburn, I. A., Zhang, H., Scott, A. L. & Zavala, F. Unique transcriptional profile of liver-resident memory CD8+ T cells induced by immunization with malaria sporozoites. *Genes Immun.* **14**, 302–309 (2013).

86. Woon, H. G. *et al.* Compartmentalization of Total and Virus-Specific Tissue-Resident Memory CD8+ T Cells in Human Lymphoid Organs. *PLoS Pathog.* **12**, 1–19 (2016).

87. Mackay, L. K. *et al.* Cutting Edge: CD69 Interference with Sphingosine-1-Phosphate Receptor Function Regulates Peripheral T Cell Retention. *J. Immunol.* **194**, 2059–2063 (2015).

88. Kumar, B. V. *et al.* Human Tissue-Resident Memory T Cells Are Defined by Core Transcriptional and Functional Signatures in Lymphoid and Mucosal Sites. *Cell Rep.* **20**, 2921–2934 (2017).

89. Skon, C. N. *et al.* Transcriptional downregulation of S1pr1 is required for the establishment of resident memory CD8+ T cells. *Nat. Immunol.* **14**, 1285–93 (2013).

90. Mackay, L. K. *et al.* Long-lived epithelial immunity by tissue-resident memory T

(TRM) cells in the absence of persisting local antigen presentation. *Proc. Natl. Acad. Sci.* **109**, 7037–7042 (2012).

91. Bergsbaken, T., Bevan, M. J. & Fink, P. J. Local Inflammatory Cues Regulate Differentiation and Persistence of CD8 + Tissue-Resident Memory T Cells. *Cell Rep.* **19**, 114–124 (2017).

92. McNamara, H. A. *et al.* Up-regulation of LFA-1 allows liver-resident memory T cells to patrol and remain in the hepatic sinusoids. *Sci. Immunol.* **2**, (2017).

93. Fernandez-Ruiz, D. *et al.* Liver-Resident Memory CD8 + T Cells Form a Front-Line Defense against Malaria Liver-Stage Infection. *Immunity* **45**, 889–902 (2016).

94. Haddadi, S. *et al.* Expression and role of VLA-1 in resident memory CD8 T cell responses to respiratory mucosal viral-vectored immunization against tuberculosis. *Sci. Rep.* **7**, 9525 (2017).

95. Murray, T. *et al.* Very Late Antigen-1 Marks Functional Tumor-Resident CD8 T Cells and Correlates with Survival of Melanoma Patients. *Front. Immunol.* **7**, article 573 (2016).

96. Cheuk, S. *et al.* CD49a Expression Defines Tissue-Resident CD8 + T Cells Poised for Cytotoxic Function in Human Skin. *Immunity* **46**, 287–300 (2017).

97. Pallett, L. J. *et al.* IL-2 high tissue-resident T cells in the human liver: Sentinels for hepatotropic infection. *J. Exp. Med.* **214**, (2017).

98. Kim, C. H. *et al.* Bonzo/CXCR6 expression defines type 1-polarized T-cell subsets with extralymphoid tissue homing potential. *J. Clin. Invest.* **107**, 595–601 (2001).

99. Heesch, K. *et al.* The function of the chemokine receptor CXCR6 in the T cell response of mice against Listeria monocytogenes. *PLoS One* **9**, (2014).

100. Curbishley, S. M., Eksteen, B., Gladue, R. P., Lalor, P. & Adams, D. H. CXCR3 Activation Promotes Lymphocyte Transendothelial Migration across Human Hepatic Endothelium under Fluid Flow. *Am. J. Pathol.* **167**, 887–899 (2005).

101. Hokeness, K. L. *et al.* CXCR3-Dependent Recruitment of Antigen-Specific T Lymphocytes to the Liver during Murine Cytomegalovirus Infection. *J. Virol.* **81**, 1241–1250 (2007).

102. Hickman, H. D. *et al.* CXCR3 Chemokine Receptor Enables Local CD8+ T Cell Migration for the Destruction of Virus-Infected Cells. *Immunity* **42**, 524–537 (2015).

103. Manske, K. *et al.* Outcome of Antiviral Immunity in the Liver Is Shaped by the Level of Antigen Expressed in Infected Hepatocytes. *Hepatology* **68**, 2089–2105 (2018).

104. Rötzschke, O. *et al.* Exact prediction of a natural T cell epitope. *Eur. J. Immunol.* **21**, 2891–2894 (1991).

105. Badovinac, V. P., Haring, J. S. & Harty, J. T. Initial T Cell Receptor Transgenic Cell Precursor Frequency Dictates Critical Aspects of the CD8+ T Cell Response to Infection. *Immunity* **26**, 827–841 (2007).

106. Nolz, J. C., Starbeck-Miller, G. R. & Harty, J. T. Naive, effector and memory CD8 T-cell trafficking: parallels and distinctions. *Immunotherapy* **3**, 1223–1233 (2011).

107. Topham, D. J. & Reilly, E. C. Tissue-Resident Memory CD8+ T Cells: From Phenotype to Function. *Front. Immunol.* **9**, (2018).

108. Mackay, L. K. *et al.* The developmental pathway for CD103(+)CD8+ tissue-resident memory T cells of skin. *Nat. Immunol.* **14**, 1294–301 (2013).

109. Boddupalli, C. S. *et al.* ABC transporters and NR4A1 identify a quiescent subset of tissue-resident memory T cells. *J. Clin. Invest.* **126**, 3905–3916 (2016).

110. Stelma, F. *et al.* Human intrahepatic CD69 + CD8+ T cells have a tissue resident memory T cell phenotype with reduced cytolytic capacity. *Sci. Rep.* **7**, 6172 (2017).

111. Herndler-Brandstetter, D. *et al.* KLRG1 + Effector CD8 + T Cells Lose KLRG1, Differentiate into All Memory T Cell Lineages, and Convey Enhanced Protective Immunity. *Immunity* 1–14 (2018). doi:10.1016/j.immuni.2018.03.015

112. Zhang, Y. *et al.* MKP-1 Is Necessary for T Cell Activation and Function. *J. Biol. Chem.* **284**, 30815–30824 (2009).

113. Moore, M. J. *et al.* ZFP36 RNA-binding proteins restrain T cell activation and anti-viral immunity. *Elife* **7**, e33057 (2018).

114. Khan, O. *et al.* TOX transcriptionally and epigenetically programs CD8+ T cell exhaustion. *Nature* **571**, 211–218 (2019).

115. Xin, A. *et al.* A molecular threshold for effector CD8(+) T cell differentiation controlled by transcription factors Blimp-1 and T-bet. *Nat Immunol* **17**, 422–432 (2016).

116. Li, J., He, Y., Hao, J., Ni, L. & Dong, C. High Levels of Eomes Promote Exhaustion of Anti-tumor CD8+ T Cells. *Front. Immunol.* **9**, 2981 (2018).

117. Behr, F. M. *et al.* Blimp-1 Rather Than Hobit Drives the Formation of Tissue-Resident Memory CD8+ T Cells in the Lungs. *Front. Immunol.* **10**, (2019).

118. Seamon, K. B., Padgett, W. & Daly, J. W. Forskolin: unique diterpene activator of adenylate cyclase in membranes and in intact cells. *Proc. Natl. Acad. Sci.* **78**, 3363–3367 (1981).

119. Linnemann, C. *et al.* Adenosine regulates CD8 T-cell priming by inhibition of membrane-proximal T-cell receptor signalling. *Immunology* **128**, e728–e737 (2009).

120. Chen, J. H. *et al.* Prostaglandin E2 and programmed cell death 1 signaling

coordinately impair CTL function and survival during chronic viral infection. *Nat. Med.* **21**, 327–334 (2015).

121. Fisicaro, P. *et al.* Pathogenetic Mechanisms of T Cell Dysfunction in Chronic HBV Infection and Related Therapeutic Approaches. *Front. Immunol.* **11**, 1–16 (2020).

122. Heim, K., Neumann-Haefelin, C., Thimme, R. & Hofmann, M. Heterogeneity of HBV-Specific CD8+ T-Cell Failure: Implications for Immunotherapy. *Front. Immunol.* **10**, (2019).

123. Utzschneider, D. T. *et al.* Early precursor T cells establish and propagate T cell exhaustion in chronic infection. *Nat. Immunol.* 1–11 (2020). doi:10.1038/s41590-020-0760-z

124. Knolle, P. A., Böttcher, J. & Huang, L.-R. The role of hepatic immune regulation in systemic immunity to viral infection. 21–27 (2015). doi:10.1007/s00430-014-0371-0

125. Limmer, A. *et al.* Cross-presentation of oral antigens by liver sinusoidal endothelial cells leads to CD8 T cell tolerance. *Eur. J. Immunol.* **35**, 2970–2981 (2005).

126. Maini, M. K. *et al.* Direct ex vivo analysis of hepatitis B virus-specific CD8+ T cells associated with the control of infection. *Gastroenterology* **117**, 1386–1396 (1999).

127. Chen, M. T. *et al.* A function of the hepatitis B virus precore protein is to regulate the immune response to the core antigen. *Proc. Natl. Acad. Sci. U. S. A.* **101**, 14913–8 (2004).

128. Fan, X. & Rudensky, A. Y. Hallmarks of Tissue-Resident Lymphocytes. *Cell* **164**, 1198–1211 (2016).

129. Tse, S.-W., Radtke, A. J., Espinosa, D. A., Cockburn, I. A. & Zavala, F. The Chemokine Receptor CXCR6 Is Required for the Maintenance of Liver Memory CD8+ T Cells Specific for Infectious Pathogens. *J. Infect. Dis.* **210**, 1508–1516 (2014).

130. Sathaliyawala, T. *et al.* Distribution and Compartmentalization of Human Circulating and Tissue-Resident Memory T Cell Subsets. *Immunity* **38**, 187–197 (2013).

131. Bankovich, A. J., Shiow, L. R. & Cyster, J. G. CD69 suppresses sphingosine 1-phosophate receptor-1 (S1P1) function through interaction with membrane helix 4. *J. Biol. Chem.* **285**, 22328–22337 (2010).

132. Takamura, S. *et al.* Specific niches for lung-resident memory CD8 $^{+}$ T cells at the site of tissue regeneration enable CD69-independent maintenance. *J. Exp. Med.* **213**, 3057–3073 (2016).

133. Walk, J., Stok, J. E. & Sauerwein, R. W. Can Patrolling Liver-Resident T Cells Control Human Malaria Parasite Development ? *Trends Immunol.* **40**, 186–196

(2019).

134. Date, M., Matsuzaki, K., Tahashi, Y., Furukawa, F. & Inoue, K. Modulation of transforming growth factor beta function in hepatocytes and hepatic stellate cells in rat liver injury. *Gut* **46**, 719–724 (2000).

135. Richter, M. V. & Topham, D. J. The α 1 β 1 Integrin and TNF Receptor II Protect Airway CD8 + Effector T Cells from Apoptosis during Influenza Infection. *J. Immunol.* **179**, 5054–5063 (2007).

136. Szabo, P. A., Miron, M. & Farber, D. L. Location, location, location: Tissue resident memory T cells in mice and humans. *Sci. Immunol.* **4**, eaas9673 (2019).

137. Anderson, A. C., Joller, N. & Kuchroo, V. K. Lag-3, Tim-3, and TIGIT: Co-inhibitory Receptors with Specialized Functions in Immune Regulation. *Immunity* **44**, 989–1004 (2016).

138. Milner, J. J. & Goldrath, A. W. Transcriptional programming of tissue-resident memory CD8 + T cells. *Curr. Opin. Immunol.* **51**, 162–169 (2018).

139. Doi, Y. *et al.* Orphan nuclear receptor NR4A2 expressed in T cells from multiple sclerosis mediates production of inflammatory cytokines. *Proc. Natl. Acad. Sci.* **105**, 8381–8386 (2008).

140. Shetty, S., Lalor, P. F. & Adams, D. H. Liver sinusoidal endothelial cells — gatekeepers of hepatic immunity. *Nat. Rev. Gastroenterol. Hepatol.* **15**, 555–567 (2018).

141. Matloubian, M., David, A., Engel, S., Ryan, J. E. & Cyster, J. G. A transmembrane CXC chemokine is a ligand for HIV-coreceptor Bonzo. *Nat. Immunol.* **1**, 298–304 (2000).

142. Groom, J. R. & Luster, A. D. CXCR3 in T cell function. *Exp. Cell Res.* **317**, 620–631 (2011).

143. Bouwer, H. G. A. *et al.* Listeria monocytogenes-Infected Hepatocytes Are Targets of Major Histocompatibility Complex Class Ib-Restricted Antilisterial Cytotoxic T Lymphocytes. *Infect. Immun.* **66**, 2814–2817 (1998).

144. Pope, C. *et al.* Organ-Specific Regulation of the CD8 T Cell Response to Listeria monocytogenes Infection. *J. Immunol.* **166**, 3402–3409 (2001).

145. Kalyuzhniy, O. *et al.* Adenovirus serotype 5 hexon is critical for virus infection of hepatocytes in vivo. *Proc. Natl. Acad. Sci.* **105**, 5483–5488 (2008).

146. Paust, S. *et al.* Critical role for the chemokine receptor CXCR6 in NK cell-mediated antigen-specific memory of haptens and viruses. *Nat. Immunol.* **11**, 1127–35 (2010).

147. Stutte, S. *et al.* Requirement of CCL17 for CCR7- and CXCR4-dependent migration of cutaneous dendritic cells. *Proc. Natl. Acad. Sci. U. S. A.* **107**, 8736–8741 (2010).

148. Klonowski, K. D. *et al.* Dynamics of Blood-Borne CD8 Memory T Cell Migration In Vivo. *Immunity* **20**, 551–562 (2004).

149. Kaech, S. M. & Cui, W. Transcriptional control of effector and memory CD8+ T cell differentiation. *Nat. Rev. Immunol.* **12**, 749–761 (2012).

150. Bachmann, M. F., Wolint, P., Schwarz, K., Jäger, P. & Oxenius, A. Functional properties and lineage relationship of CD8+ T cell subsets identified by expression of IL-7 receptor alpha and CD62L. *J. Immunol.* **175**, 4686–4696 (2005).

151. Giordano, M. *et al.* The tumor necrosis factor alpha-induced protein 3 (TNFAIP3, A20) imposes a brake on antitumor activity of CD8 T cells. *Proc. Natl. Acad. Sci.* **111**, 11115–11120 (2014).

152. Liu, X. *et al.* Genome-wide analysis identifies NR4A1 as a key mediator of T cell dysfunction. *Nature* **567**, 525–529 (2019).

153. Best, J. A. *et al.* Transcriptional insights into the CD8+ T cell response to infection and memory T cell formation. *Nat. Immunol.* **14**, 404–412 (2013).

154. Chikhirzhina, G. I., Al-Shekhadat, R. I. & Chikhirzhina, E. V. Transcription factors of the NF1 family: Role in chromatin remodeling. *Mol. Biol.* **42**, 342–356 (2008).

155. Behr, F. M. *et al.* Tissue-resident memory CD8+ T cells shape local and systemic secondary T cell responses. *Nat. Immunol.* **21**, 1070–1081 (2020).

156. Khan, T. N., Mooster, J. L., Kilgore, A. M., Osborn, J. F. & Nolz, J. C. Local antigen in nonlymphoid tissue promotes resident memory CD8+ T cell formation during viral infection. *J. Exp. Med.* **213**, 951–66 (2016).

157. Zhang, N. & Bevan, M. Transforming growth factor-beta signaling controls the formation and maintenance of gut-resident memory T cells by regulating migration and retention. *Immunity* **39**, 687–696 (2013).

158. Thomson, A. W. & Knolle, P. a. Antigen-presenting cell function in the tolerogenic liver environment. *Nat. Rev. Immunol.* **10**, 753–766 (2010).

159. Liu, Z. *et al.* Interleukin-27 signalling induces stem cell antigen-1 expression in T lymphocytes in vivo. *Immunology* **152**, 638–647 (2017).

160. Whitmire, J. K., Eam, B. & Whitton, J. L. Mice deficient in stem cell antigen‐1 (Sca1, Ly‐6A/E) develop normal primary and memory CD4 + and CD8 + T‐cell responses to virus infection. *Eur. J. Immunol.* **39**, 1494–1504 (2009).

161. Beltra, J.-C. *et al.* IL2Rβ-dependent signals drive terminal exhaustion and suppress memory development during chronic viral infection. *Proc. Natl. Acad. Sci.* **113**, E5444–E5453 (2016).

162. Shin, H. & Iwasaki, A. Tissue-resident memory T cells. *Immunol. Rev.* **255**, 165–181 (2013).

163. Huang, L.-R. *et al.* Intrahepatic myeloid-cell aggregates enable local proliferation of CD8+ T cells and successful immunotherapy against chronic viral liver infection. *Nat. Immunol.* **14**, 574–583 (2013).

164. Kosinska, A. D. *et al.* Synergy of therapeutic heterologous prime-boost hepatitis B vaccination with CpG-application to improve immune control of persistent HBV infection. *Sci. Rep.* **9**, 10808 (2019).

165. Scott, A. C. *et al.* TOX is a critical regulator of tumour-specific T cell differentiation. *Nature* **571**, 270–274 (2019).

166. Zhang, X. *et al.* Genome-wide analysis of cAMP-response element binding protein occupancy, phosphorylation, and target gene activation in human tissues. *Proc. Natl. Acad. Sci.* **102**, 4459–4464 (2005).

167. Ramstad, C., Sundvold, V., Johansen, H. K. & Lea, T. cAMP-dependent protein kinase (PKA) inhibits T cell activation by phosphorylating Ser-43 of Raf-1 in the MAPK/ERK pathway. *Cell. Signal.* **12**, 557–563 (2000).

168. Ruppelt, A. *et al.* Inhibition of T Cell Activation by Cyclic Adenosine 5′-Monophosphate Requires Lipid Raft Targeting of Protein Kinase A Type I by the A-Kinase Anchoring Protein Ezrin. *J. Immunol.* **179**, 5159–5168 (2007).

169. Bodor, J. *et al.* Suppression of T-cell responsiveness by inducible cAMP early repressor (ICER). *J. Leukoc. Biol.* **69**, 1053–9 (2001).

170. Vaeth, M. *et al.* Regulatory T cells facilitate the nuclear accumulation of inducible cAMP early repressor (ICER) and suppress nuclear factor of activated T cell c1 (NFATc1). *Proc. Natl. Acad. Sci. U. S. A.* **108**, 2480–2485 (2011).

171. Wen, A. Y., Sakamoto, K. M. & Miller, L. S. The Role of the Transcription Factor CREB in Immune Function. *J. Immunol.* **185**, 6413–6419 (2010).

172. Hogan, P. G. Calcium–NFAT transcriptional signalling in T cell activation and T cell exhaustion. *Cell Calcium* **63**, 66–69 (2017).

173. Comte, D., Karampetsou, M. P. & Tsokos, G. C. T cells as a therapeutic target in SLE. *Lupus* **24**, 351–363 (2015).

174. Darvin, P., Toor, S. M., Sasidharan Nair, V. & Elkord, E. Immune checkpoint inhibitors: recent progress and potential biomarkers. *Exp. Mol. Med.* **50**, 1–11 (2018).

175. Abrahamsen, H. *et al.* TCR- and CD28-Mediated Recruitment of Phosphodiesterase 4 to Lipid Rafts Potentiates TCR Signaling. *J. Immunol.* **173**, 4847–4858 (2004).

176. Sreeramkumar, V., Fresno, M. & Cuesta, N. Prostaglandin E 2 and T cells: friends or foes? *Immunol. Cell Biol.* **90**, 579–586 (2012).

177. Nuñez, F. J. *et al.* Glucocorticoids rapidly activate cAMP production via G αs to initiate non-genomic signaling that contributes to one-third of their canonical genomic effects. *FASEB J.* **34**, 2882–2895 (2020).

178. Sriram, K. & Insel, P. A. G Protein-Coupled Receptors as Targets for Approved Drugs: How Many Targets and How Many Drugs? *Mol. Pharmacol.* **93**, 251–258 (2018).

179. Manske, K. *et al.* Outcome of Antiviral Immunity in the Liver Is Shaped by the Level of Antigen Expressed in Infected Hepatocytes. *Hepatology* **68**, 2089–2105 (2018).

180. McClary, H., Koch, R., Chisari, F. V & Guidotti, L. G. Relative sensitivity of hepatitis B virus and other hepatotropic viruses to the antiviral effects of cytokines. *J. Virol.* **74**, 2255–2264 (2000).

6 Appendix

6.1 Abbreviations

Abbreviation	Explanation
Ad	Adenovirus
Ad-CMV-GOL	Adenovirus expressing the transgenes GFP, ovalbumin, luciferase
Ad-GOL	Ad-CMV-GOL and Ad-TTR-GOL
AdHBV	Adenovirus expressing the 1.3-fold overlength HBV genome
Ad-TTR-GOL	Adenovirus expressing the transgenes GFP, ovalbumin, luciferase
ANOVA	Analysis of variance
Antigen, Ag	Antibody generator
APC	Antigen-presenting cell
AUC	Area under the curve
Blimp-1	B-lymphocyte-induced maturation protein 1
BrdU	Bromodeoxyuridine
C93	HBcore93-100 peptide (MGLKFRQL)
cAMP	Cyclic adenosine monophosphate
cccDNA	Covalently-closed circular DNA
CCR	C-C Motif Chemokine Receptor
CD	Cluster of differentiation
Cdh1	Cadherin 1
CHB	Chronic hepatitis B
CMV	cytomegalovirus
CREM	cAMP-responsive element modulator
CTL	Cytolytic T lymphocyte
Ctla4, CTLA-4	Cytotoxic T-Lymphocyte Associated Protein 4
Ctrl	control
CX_3CR1	C-X_3-C motif chemokine receptor 1
CXCL	C-X-C motif chemokine ligand
CXCL16	C-X-C motif chemokine ligand 16
CXCR3	C-X-C motif chemokine receptor 3
CXCR6	C-X-C motif chemokine receptor 6
d	day
DC	Dendritic cells
DEGs	differentially expressed genes
DNA	Desoxyribonucleic acid
Dusp1	Dual specificity phosphatase 1
ELISA	Enzyme-linked immunosorbent assay
Eomes	Eomesodermin
$EP_{2,4}$	Prostaglandin E_2 receptor 2, 4
FFPE	formalin-fixed paraffin-embedded tissue

Fig.	figure
FMO	Fluorescence minus one
Fos	Fos proto-oncogene, AP-1 transcription factor subunit
FRT	female reproductive tract
Fsk	forskolin
GeoMean	Geometric mean
GFP	Green fluorescent protein
GO	Gene ontology
GSEA	gene set enrichment analysis
GzmB	Granzyme B
h	hour
HBeAg	HBe antigen
HBsAg	HBs antigen
HBV	Hepatitis B virus
hi	high
Hobit	Homolog of blimp-1 in T cells
ICAM-I	Intercellular adhesion molecule 1
ICER	Inducible cAMP-responsive element
ICER-KO	$ICER^{fl/fl}$ x CD4-Cre
IFN	Interferon
IL	Interleukin
Il2rb	IL2 receptor beta Subunit Beta
Iono	Ionomycin
Itga1	Integrin subunit alpha 1, CD49a
IVIS	*in vivo* imaging system
Jun	Jun proto-oncogene, AP-1 transcription factor subunit
KLF2	Kruppel like factor 2
Klf3	Kruppel like factor 3
KLRG-1	Killer cell lectin-like receptor subfamily G member 1
KO	Knock-out
LAG-3	Lymphocyte activation gene 3
LCMV	Lymphocytic choriomeningitis virus
LFA-1	leukocyte adhesion glycoprotein-1
Litaf	Lipopolysaccharide-induced TNF factor
LSEC	Liver sinusoidal endothelial cell
Luc	Luciferase
Ly	Lymphocyte antigen
M8L	MGLKFRQL, amino acid sequence of the HBcore93-100 peptide
MGLKFRQL	Amino acid sequence of the HBcore93-100 peptide
n.a.	Not analyzed
n.s.	Not significant

Neg	negative
NES	Normalized enrichment score
Nfic	Nuclear factor I C
Nr4a1	Nuclear Receptor Subfamily 4 Group A Member 1
Nr4a2	Nuclear Receptor Subfamily 4 Group A Member 2
NTCP	sodium taurocholate co-transporting polypeptide
p.i.	Post infection
p/s	Photons per second
PCA	principal component analysis
PD-1, Pdcd1	Programmed cell death protein 1
PFU	Plaque-forming unit
PGE_2	Prostaglandin E_2
PMA	Phorbol 12-myristate 13-acetate
Pos	positive
pPKA, PKA	(Phosphorylated) protein kinase A
Qpct	Glutaminyl-peptide cyclotransferase
rcDNA	Relaxed circular DNA
Rgs1, 2	Regulator of G Protein signaling 1,2
RNA	Ribonucleic acid
RNAseq	RNA sequencing
$S1P_1$	sphingosine 1-phosphate receptor
S8L	SIINFEKL, amino acid sequence of the ovalbumin 257-264 peptide
sALT	Serum alanine transaminase
SIINFEKL	Amino acid sequence of ovalbumin 257-264
Skil	Smad-interacting Ski-like gene
Tbx21	T-Box transcription factor 21
TCF1	T cell factor 1, transcription factor 7
T_{CM}	Central memory T cell
TCR	T cell receptor
T_{EFF}	Effector T cell
T_{EM}	Effector memory T cells
T_{EX}	Exhausted T cell
Tg	transgenic
TGF-β	transforming growth factor beta
Tgif1	TGFβ-induced factor homeobox 1
TIGIT	T cell immunoreceptor with Ig and ITIM domains
TIM-3	T-cell immunoglobulin and mucin-domain containing-3
TNF	Tumor necrosis factor
TOX	Thymocyte selection associated high mobility group box
Treg	Regulatory T cell
T_{RM}	Tissue-resident memory T cell

t-SNE	t-distributed stochastic neighbor embedding
TTR	Transthyretin
VLA-1	Very late antigen 1, CD49a
WT	Wildtype
Zfp36l1	Zinc finger protein 36, C3H1 Type-Like 1

6.2 Tables

Table 1. Differentially regulated genes between liver CXCR6^{hi} CD45.1^{+}CD8^{+} T cells during Ad-TTR-GOL persistent infection and spleen CX_3CR1^{+} CD45.1^{+}CD8^{+} T cells after resolved Ad-CMV-GOL infection: Significantly regulated genes in CXCR6^{hi} cells (n=347)

Gene	log2FC CXCR6^{hi}	p-value	padj
2900026A02Rik	3.3678376	2.765E-15	5.625E-13
Ier5l	2.9643947	1.63E-10	2.005E-08
Nr4a2	2.8509713	2.094E-35	2.014E-32
Gm16242	2.5957381	4.203E-06	0.000226
Ikzf4	2.5606175	5.757E-06	0.0002984
Csf1	2.4936843	6.181E-08	4.946E-06
Heyl	2.4896944	1.202E-06	7.143E-05
Slc16a11	2.4434769	1.602E-08	1.421E-06
Bcl2l11	2.4203942	1.448E-09	1.595E-07
Twsg1	2.4017806	2.192E-07	1.536E-05
Glis1	2.3766024	2.742E-09	2.844E-07
Prrt1	2.3746587	2.231E-05	0.0009833
Cd200r2	2.3275067	1.304E-22	5.108E-20
Gm156	2.2791504	2.546E-41	4.489E-38
Pitpnm2	2.2750646	5.1E-06	0.0002684
Areg	2.2710043	1.821E-07	1.293E-05
Car2	2.2532575	4.286E-24	1.814E-21
Adgrg1	2.2417206	3.367E-15	6.72E-13
Cd200r1	2.1863493	2.561E-12	3.926E-10
Gm28942	2.1720106	0.0001171	0.004327
Tbc1d4	2.1634549	7.896E-09	7.807E-07
Osgin1	2.1622608	3.172E-11	4.143E-09
Cxxc5	2.1379666	1.954E-06	0.0001094
Tmprss6	2.1100527	4.549E-06	0.0002431
Trbd1	2.1009106	0.0001164	0.0043199
Ikzf2	2.0910423	3.357E-07	2.192E-05
Tnfaip3	2.0907254	1.711E-24	8.226E-22
Rnf165	2.0833498	0.0002273	0.007782
Xcl1	2.0676873	4.024E-12	5.831E-10
Mrc2	2.0666727	6.426E-05	0.002575
Ctla4	2.0472928	2.633E-05	0.0011461
Lag3	2.0373926	5.483E-05	0.0022222
Rgs1	2.0252212	1.552E-46	3.283E-43
Nrgn	2.0091727	9.286E-06	0.0004506
Arap3	1.9892243	3.903E-05	0.0016319
Epcam	1.960297	7.843E-05	0.0030618
Trbj1-2	1.9346477	0.0003987	0.0125247
Klf9	1.9300201	0.0003274	0.0105607
Chn2	1.9281465	4.954E-10	5.823E-08
Itih5	1.9031345	0.0001918	0.0067395
Tnfsf8	1.8841819	1.836E-05	0.0008194
Ppp1r3g	1.8802114	0.0009461	0.0254668
Lrrc9	1.8680091	0.0004083	0.0126659
Filip1	1.8664558	0.0001926	0.006748
Rgs16	1.8217924	0.0006541	0.0191151
Pacsin1	1.8056214	0.0006611	0.0191407
Ccdc80	1.8033258	0.0003064	0.0099741
Cd7	1.7987119	1.899E-36	2.232E-33
Egr1	1.7958318	6.825E-06	0.0003438

C2cd4b	1.7955981	0.000268	0.008916
Pdcd1	1.7887586	2.418E-39	3.654E-36
Cd200r4	1.7885152	3.164E-12	4.715E-10
Hic1	1.7862381	0.0001753	0.0062031
Tnfrsf9	1.7840013	3.332E-22	1.137E-19
Tesk2	1.780861	0.0015739	0.0385646
B4galt4	1.775069	0.0018197	0.0432595
Prelid2	1.7722632	0.0006106	0.0182096
Tacc2	1.767351	0.0003934	0.0124471
Cdc14a	1.7651326	0.0003741	0.0119208
Atp2b2	1.7627131	0.0019667	0.0459283
Lilrb4a	1.7576264	5.529E-08	4.534E-06
Cables1	1.7518373	0.0018884	0.0445075
Carmil2	1.7516889	0.001889	0.0445075
Spry1	1.7513435	0.0006813	0.0196391
Klri2	1.7433737	0.0010675	0.0280923
Slc22a15	1.7378136	0.0004614	0.0141882
Calcb	1.7363197	1.498E-08	1.39E-06
Mmd	1.7353797	1.62E-05	0.0007354
Actn2	1.7320535	7.903E-06	0.0003889
Slco4a1	1.7241511	0.0015098	0.0374065
Epdr1	1.7193064	0.0009062	0.0246644
Abcb9	1.7150772	3.592E-15	7.036E-13
Tmcc3	1.7089791	0.0015972	0.0388502
Gm4956	1.6772074	1.199E-10	1.51E-08
Ypel2	1.6672515	0.0005115	0.0155481
Spry2	1.6460673	0.0007954	0.0222615
Plscr1	1.6387367	0.0002654	0.0088582
Sh2d2a	1.6377626	2.088E-57	7.363E-54
Ccrl2	1.6364961	8.441E-09	8.192E-07
Gm15186	1.6288961	0.0006031	0.0180729
Zfp36l1	1.6272961	2.231E-16	4.918E-14
Fosl2	1.616716	6.548E-06	0.0003346
Tnfrsf1b	1.6091168	7.887E-13	1.245E-10
Gm37004	1.5916352	0.000351	0.0112535
Stk39	1.5814932	1.134E-05	0.0005406
Litaf	1.5809001	3.825E-12	5.62E-10
Nfil3	1.5793293	2.715E-07	1.841E-05
Per1	1.5717145	0.0004024	0.0125247
Fam210b	1.5706737	0.0013309	0.0334332
Fgl2	1.569386	1.746E-08	1.527E-06
Plk3	1.5656858	0.0001989	0.0069003
Ephx1	1.5524842	1.518E-09	1.655E-07
Tnfrsf1a	1.5453528	1.807E-06	0.0001019
Crem	1.5224452	7.295E-08	5.704E-06
Samsn1	1.5134951	8.75E-12	1.187E-09
Serpina3g	1.5022708	4.654E-10	5.532E-08
Dusp6	1.5022374	0.0002539	0.0085263
Jun	1.5017465	5.204E-07	3.317E-05
Myo6	1.4877583	0.0008015	0.022372
Bcl2a1b	1.4757996	6.689E-06	0.0003402
Trbj2-1	1.4713034	0.0015748	0.0385646
Cela1	1.4677681	2.142E-05	0.0009481
1810011H11Rik	1.4675338	0.000795	0.0222615

Cited4	1.4646409	0.0012971	0.0327738
Inpp4b	1.460624	0.000326	0.0105473
Casp3	1.453723	4.936E-08	4.112E-06
Bcl2	1.4383884	5.484E-12	7.535E-10
Tigit	1.432283	5.376E-06	0.0002802
Perp	1.4236065	0.0009092	0.0246644
Art2b	1.4129141	0.0001736	0.0061627
Pabpc4	1.4122463	0.0016752	0.0404616
Socs3	1.4106416	0.0008592	0.0237322
Fos	1.4077895	3.703E-06	0.000203
Ccl4	1.4068321	1.226E-38	1.622E-35
Tox	1.398898	4.689E-15	9.019E-13
Trbv12-1	1.3914762	1.02E-07	7.766E-06
Spp1	1.3813255	3.774E-06	0.0002058
Ccl3	1.3809075	5.971E-29	3.948E-26
Dusp1	1.3675994	2.678E-16	5.782E-14
Rgs3	1.3593944	3.337E-05	0.0014175
Tnfrsf18	1.3555993	6.067E-10	6.976E-08
Sdcbp2	1.3533925	6.202E-06	0.0003185
Cblb	1.351468	0.0010791	0.0283263
Trbj2-7	1.35064	4.427E-05	0.0018221
Gm19585	1.3474834	5.049E-06	0.0002671
Crbn	1.3434257	0.0004858	0.0148524
Bcl2a1d	1.3345216	0.0008935	0.0244869
Ctla2b	1.3316023	0.0009093	0.0246644
Izumo1r	1.311534	0.0001521	0.0054748
Pear1	1.2892191	0.0015304	0.0377707
Ppp1r15a	1.2840599	1.612E-08	1.421E-06
Il2rb	1.2838992	7.446E-25	3.751E-22
Cd160	1.2726626	3.543E-08	3.047E-06
Hif1a	1.2695143	0.0009568	0.025624
Cish	1.2401788	7.551E-06	0.0003745
Gsto1	1.2247715	5.428E-05	0.0022085
Nedd9	1.2027275	1.742E-05	0.0007808
Vps37b	1.200091	4.763E-12	6.654E-10
Cd38	1.1884789	0.0009081	0.0246644
Prkch	1.1851994	1.1E-06	6.699E-05
Cd244	1.1817416	3.293E-05	0.0014048
Rabgap1l	1.1786943	2.707E-05	0.0011736
Junb	1.1556149	1.185E-34	1.045E-31
Chst12	1.1536638	7.531E-06	0.0003745
Trbc1	1.1163157	2.362E-24	1.087E-21
Tiprl	1.1136546	1.381E-06	8.028E-05
Cd3e	1.1089656	8.572E-22	2.834E-19
Agfg1	1.0864521	0.0010667	0.0280923
Neurl3	1.0856075	0.0006451	0.0189749
Bhlhe40	1.0706813	2.225E-07	1.548E-05
Hist1h1c	1.0700014	0.0006622	0.0191407
Pglyrp1	1.0618686	0.0003876	0.0123124
Stat3	1.0429831	0.0001667	0.0059787
Lrmp	1.0379797	1.314E-06	7.724E-05
Ptpn11	1.029818	0.0007603	0.0214474
Padi2	1.0277983	0.0009909	0.0263394
Smc4	1.0186976	3.137E-07	2.074E-05

Ctsc	1.0179593	4.732E-08	3.973E-06
Stk17b	1.0168711	3.123E-07	2.074E-05
Chd3	-1.019963	0.0001956	0.0068286
4930523C07Rik	-1.022034	3.734E-05	0.0015773
Ppp1r12a	-1.024195	1.029E-05	0.0004948
Sike1	-1.031391	0.0018598	0.0440157
Atp2a3	-1.03787	0.0011921	0.0307579
Tbx21	-1.041669	2.678E-06	0.0001483
Rabep2	-1.043489	0.0020735	0.0481044
Lyz2	-1.054161	5.007E-05	0.0020531
Crip1	-1.082514	2.207E-21	7.074E-19
Clcn4	-1.083393	0.0011342	0.0294077
Epsti1	-1.099073	1.355E-06	7.92E-05
Ccnd3	-1.099106	1.094E-08	1.042E-06
Sp100	-1.100655	6.753E-08	5.331E-06
Kcnab2	-1.10897	9.667E-05	0.0037462
Tm9sf2	-1.141202	0.001661	0.0402103
Ccdc88c	-1.151248	0.0007882	0.0221772
Stk38	-1.158334	0.0002714	0.0090007
Prkcq	-1.165008	0.0001897	0.0066911
St3gal6	-1.167373	0.0019355	0.0453996
Tnfaip8l2	-1.213634	2.523E-05	0.0011076
Nptn	-1.237176	7.445E-06	0.0003733
Plec	-1.243314	1.156E-06	6.909E-05
Pycard	-1.255062	1.072E-10	1.367E-08
Acp5	-1.259771	1.158E-07	8.686E-06
Cdt1	-1.264846	0.0006621	0.0191407
Hopx	-1.27035	3.049E-07	2.042E-05
Thy1	-1.275403	9.462E-20	2.78E-17
Zyx	-1.305725	4.54E-14	8.28E-12
H2-K2	-1.323477	0.0013908	0.0347009
Ssh2	-1.328972	0.0004013	0.0125247
Gpr18	-1.33477	0.0021107	0.048861
Orai2	-1.349581	0.0018384	0.0436073
Dnajc15	-1.361981	8.182E-10	9.307E-08
Osbpl5	-1.383723	0.0019425	0.0454632
Map7d1	-1.386833	0.0017709	0.0422888
Tagap	-1.391425	0.0001265	0.0046296
Ly6a	-1.394392	9.492E-06	0.0004585
Rgcc	-1.415921	0.0007383	0.0209384
Txnip	-1.416665	3.641E-07	2.349E-05
Ighm	-1.420312	0.0002245	0.0077119
AI467606	-1.42605	1.064E-09	1.197E-07
Cdc42ep3	-1.436751	1.9E-07	1.34E-05
Nfic	-1.450293	0.0012182	0.0312797
Spn	-1.453063	4.289E-12	6.132E-10
Capg	-1.455839	2.372E-07	1.64E-05
Racgap1	-1.45659	0.0001035	0.0038952
Tmem37	-1.464303	0.0002592	0.0086762
Unc93b1	-1.468146	0.0002956	0.009653
Cdkn2d	-1.472421	1.239E-06	7.322E-05
Pde2a	-1.48357	0.0007404	0.0209427
Ldlrap1	-1.500525	0.0008801	0.0242459
Stard10	-1.546795	6.973E-05	0.0027629

Arid5a	-1.547904	4.211E-05	0.0017457
Emp3	-1.548544	1.123E-22	4.569E-20
Icam2	-1.553265	3.875E-05	0.0016266
Emb	-1.559109	4.034E-05	0.0016803
Cdc25b	-1.563446	0.0004	0.0125247
Tspan31	-1.568227	0.0010828	0.0283547
Anxa1	-1.587405	0.0013337	0.0334332
Gm4208	-1.590212	0.0015975	0.0388502
Ehd3	-1.613868	0.000334	0.010739
Ms4a6c	-1.61469	0.0011683	0.0302198
Atp1b3	-1.61958	2.558E-22	9.332E-20
Pik3r5	-1.630585	1.738E-07	1.259E-05
Klrk1	-1.633789	4.841E-16	1.024E-13
Sh3bp5	-1.642144	0.0009323	0.0251606
E2f2	-1.64724	0.0021634	0.04997
Il7r	-1.652805	0.000639	0.0188825
Cd24a	-1.665639	0.0008057	0.0224314
Tbxa2r	-1.689898	0.0002439	0.0082704
H2-Q10	-1.699228	5.702E-08	4.604E-06
Fgf13	-1.709567	0.0019327	0.0453996
Ccne1	-1.709906	0.0016864	0.0406395
Il17ra	-1.720593	1.765E-07	1.262E-05
Phf13	-1.729446	0.0008346	0.0231491
Siglecg	-1.74489	0.0013147	0.0331144
Glipr2	-1.778988	5.637E-08	4.587E-06
Arhgef18	-1.779499	6.736E-06	0.000341
Blk	-1.780256	0.0017873	0.0425861
Klhl6	-1.788245	3.47E-08	3.009E-06
Dkkl1	-1.792501	7.44E-05	0.0029261
S1pr4	-1.793734	4.651E-17	1.118E-14
Kcnn4	-1.795731	2.884E-07	1.943E-05
Iglj3	-1.800756	0.0015692	0.0385646
Ly86	-1.809029	0.0005477	0.0165081
Vim	-1.812759	2.095E-29	1.477E-26
Sell	-1.818991	4.208E-06	0.000226
Itgb7	-1.824678	1.753E-14	3.254E-12
Fbxl2	-1.830494	0.0012486	0.0318284
A430078G23Rik	-1.836257	0.0001006	0.0038023
Tagln2	-1.843878	4.424E-20	1.337E-17
Gm2a	-1.848324	1.567E-08	1.421E-06
Fam129b	-1.858092	0.0011105	0.0288645
Haao	-1.863041	0.0002773	0.0091105
Flna	-1.873328	1.381E-09	1.538E-07
Rasa3	-1.874826	2.519E-11	3.331E-09
Crip2	-1.891772	0.0004317	0.0133534
Ccl9	-1.904244	0.0004025	0.0125247
Apobec2	-1.91095	0.0006475	0.0189749
Apobec2	-1.91095	0.0006475	0.0189749
Tespa1	-1.913259	2.084E-05	0.0009265
Mylip	-1.913499	1.558E-05	0.0007135
Lrrc75b	-1.923253	0.0006955	0.0199393
Smad3	-1.924913	0.0002799	0.0091667
Fcmr	-1.927952	1.673E-07	1.229E-05
Vpreb3	-1.930915	0.0006592	0.0191407

1700025G04Rik	-1.942271	0.0002491	0.0083913
H2-Aa	-1.948754	4.885E-28	3.04E-25
Sema4b	-1.958884	0.0005476	0.0165081
Arl5c	-1.974085	3.202E-05	0.0013714
S100a9	-1.982196	8.749E-06	0.0004265
Gna15	-1.986684	4.781E-12	6.654E-10
Ighd	-1.993399	5.118E-09	5.206E-07
Ifitm10	-2.003893	2.716E-12	4.104E-10
Nrm	-2.010152	1.473E-05	0.0006803
Fcer2a	-2.015441	7.564E-05	0.0029638
Blnk	-2.017969	9.34E-05	0.0036328
Hid1	-2.020799	1.215E-05	0.0005711
Dok3	-2.023954	0.0001976	0.0068775
Hmga1	-2.035243	9.795E-05	0.0037817
Gprin3	-2.042572	1.15E-05	0.0005454
Tnfsf14	-2.044421	7.576E-06	0.0003745
Nck2	-2.046247	0.0002326	0.0079368
Sbk1	-2.049372	0.0001042	0.0039077
Tktl1	-2.06015	0.0002731	0.0090295
Borcs7	-2.074279	2.485E-07	1.707E-05
Iqgap2	-2.082059	1.654E-07	1.224E-05
Prdx4	-2.082105	3.742E-05	0.0015773
As3mt	-2.086164	1.608E-06	9.245E-05
Cxcr4	-2.09036	6.623E-07	4.146E-05
Emp1	-2.095019	0.0001503	0.0054463
AB124611	-2.106493	1.571E-08	1.421E-06
Il18r1	-2.117854	3.186E-07	2.094E-05
H2-Ab1	-2.122477	7.671E-32	6.243E-29
Gm10522	-2.126513	6.235E-05	0.0025079
Ahnak	-2.139985	1.531E-35	1.62E-32
Fcrla	-2.144449	1.516E-05	0.0006973
Arhgap26	-2.149148	4.085E-06	0.0002216
Rora	-2.178634	8.911E-07	5.481E-05
Lmna	-2.204856	7.974E-06	0.0003906
Cd79a	-2.209082	6.558E-05	0.0026179
Fgd2	-2.218522	9.915E-05	0.0037856
I830127L07Rik	-2.255256	1.597E-05	0.0007282
Sgk1	-2.265377	2.372E-17	5.937E-15
Tnfrsf13c	-2.268356	1.812E-06	0.0001019
Itgb1	-2.273658	2.719E-24	1.199E-21
Wdr95	-2.280227	9.44E-08	7.237E-06
Itgam	-2.29201	1.728E-05	0.0007781
Arl4c	-2.339702	1.12E-14	2.116E-12
Gm45552	-2.345452	6.218E-08	4.946E-06
Txndc5	-2.350266	3.775E-11	4.871E-09
Zeb2	-2.378561	2.675E-20	8.322E-18
Klf2	-2.386813	5.298E-57	1.401E-53
Cd22	-2.409889	6.364E-07	4.032E-05
Acss2	-2.415798	1.356E-08	1.27E-06
H2-DMb2	-2.445518	3.89E-10	4.677E-08
H2-Eb1	-2.484484	2.964E-22	1.045E-19
Ms4a1	-2.506277	5.241E-08	4.332E-06
Atp8b4	-2.513103	6.782E-09	6.768E-07
Rara	-2.523918	1.752E-07	1.261E-05

Ccr2	-2.536637	1.592E-08	1.421E-06
Iglc3	-2.553277	5.437E-13	8.849E-11
Slco3a1	-2.571268	1.121E-06	6.775E-05
Mzb1	-2.625663	3.852E-08	3.286E-06
Cmah	-2.628698	1.214E-07	9.042E-06
Cd79b	-2.682717	2.838E-18	7.901E-16
Gramd3	-2.685426	2.263E-13	3.925E-11
Pxylp1	-2.689298	4.181E-07	2.681E-05
Lef1	-2.698013	1.118E-12	1.74E-10
Spib	-2.706095	7.333E-08	5.704E-06
Ly6c2	-2.71474	1.565E-67	8.28E-64
Cd19	-2.720556	1.846E-09	1.993E-07
Iglc2	-2.756931	1.435E-16	3.229E-14
Sema4a	-2.759229	1.169E-16	2.689E-14
Kcnj8	-2.777307	4.891E-13	8.085E-11
Rap1gap2	-2.815116	1.727E-07	1.259E-05
Ly6d	-2.824615	6.218E-18	1.645E-15
Klf3	-2.830743	1.62E-22	6.123E-20
Cd74	-2.874365	6.404E-75	6.775E-71
S100a4	-2.895667	1.813E-27	1.065E-24
Cx3cr1	-2.948852	2.845E-26	1.505E-23
Fcgr2b	-2.956402	2.038E-09	2.156E-07
Pdlim1	-3.000465	4.282E-08	3.624E-06
Ly6c1	-3.132647	2.413E-17	5.937E-15
Klrg1	-3.149647	4.254E-18	1.154E-15
Il18rap	-3.163842	1.167E-19	3.336E-17
S1pr1	-3.213082	1.356E-26	7.547E-24
S1pr5	-3.965488	3.627E-31	2.74E-28

Table 2. DEGs between liver CX_3CR1^+ $CD45.1^+CD8^+$ T cells and spleen CX_3CR1^+ $CD45.1^+CD8^+$ T cells after resolved Ad-CMV-GOL infection: Significantly regulated genes in liver CX_3CR1^+ cells (n=45)

Genes	log2FC liver CX_3CR1^+	pvalue	padj
Tnfaip3	2.181118	3.08E-30	9.27E-27
Nr4a1	1.737696	1.41E-11	9.82E-09
Bhlhe40	1.608002	6.52E-18	6.55E-15
Per1	1.445666	1.56E-05	0.003363
Fos	1.415458	1.78E-07	6.47E-05
Junb	1.383936	3.53E-44	3.19E-40
Fosb	1.247715	0.000319	0.046458
Rgs2	1.214623	7.01E-06	0.001712
Hbb-bs	1.161094	7.55E-05	0.013382
Dusp5	1.151347	7.87E-06	0.001874
Ppp1r15a	1.147425	1.79E-07	6.47E-05
Zfp36l2	1.094772	9.55E-06	0.002213
Apoe	-1.10268	0.000207	0.031709
Fcer2a	-1.237773	0.000348	0.049928
Cd24a	-1.282828	0.000223	0.03364
Cd83	-1.283988	0.000108	0.017457
C1qb	-1.285256	0.000194	0.0303
Tyrobp	-1.297752	1.09E-05	0.002459
Igkj2	-1.33348	9.79E-05	0.01609

H2-Ob	-1.336795	8.4E-05	0.014614
Lyn	-1.348	8.87E-05	0.01514
H2-Oa	-1.408782	4.87E-05	0.009369
Blnk	-1.450322	2.36E-05	0.004748
Igkc	-1.53453	1.26E-08	6.35E-06
Tnfrsf13c	-1.609807	3.61E-06	0.000906
Ighm	-1.631288	3.87E-07	0.000133
Ms4a1	-1.638837	1.7E-06	0.000452
S100a9	-1.648785	1.6E-06	0.000439
Sell	-1.684145	4.39E-07	0.000142
H2-DMb2	-1.689034	1.75E-07	6.47E-05
Fcrla	-1.710354	6.91E-07	0.000208
Fcmr	-1.722636	1.13E-07	4.65E-05
Spib	-1.726435	6.77E-07	0.000208
Ighd	-1.820044	3.87E-09	2.06E-06
S100a8	-1.854983	4.49E-08	2.03E-05
Mzb1	-1.869588	7.49E-08	3.22E-05
Cd19	-1.909669	2.17E-08	1.03E-05
Iglc2	-2.072679	2.35E-12	1.77E-09
H2-Ab1	-2.152514	1.99E-34	8.98E-31
H2-Eb1	-2.257096	1.55E-19	2E-16
Iglc3	-2.314573	2.55E-13	2.1E-10
H2-Aa	-2.315858	4.89E-30	1.11E-26
Cd79b	-2.571074	3.3E-18	3.73E-15
Cd74	-2.797592	6.85E-23	1.24E-19
Ly6d	-3.087429	1.34E-22	2.02E-19

Table 3. DEGs between CXCR6^{hi} CD45.1^{+}CD8^{+} T cells during persistent Ad-TTR-GOL infection and CXCR6^{hi} CD45.1^{+}CD8^{+} T cells after resolved Ad-CMV-GOL infection: Significantly regulated genes in CXCR6^{hi} cells during persistent infection, log2FC (n=127)

Genes	log2FC CXCR6^{hi} persistent	p-value	padj
Twsg1	2.17874	3.77E-10	1.05E-07
Car2	2.16652	3.31E-30	6.70E-27
Tbc1d4	1.94433	4.96E-11	1.83E-08
Nrgn	1.88255	5.62E-08	8.92E-06
Gm156	1.84929	1.32E-33	3.57E-30
Cxxc5	1.82895	5.17E-08	8.54E-06
Heyl	1.81139	5.15E-07	6.95E-05
Cd200r2	1.79204	1.23E-18	9.99E-16
Gm16242	1.79113	2.17E-06	0.00024
Ccdc80	1.78089	1.52E-06	0.00018
C2cd4b	1.72833	2.49E-06	0.00027
Glis1	1.71577	1.70E-08	3.21E-06
Rnf165	1.62384	1.59E-05	0.0012
Tmprss6	1.60475	3.82E-06	0.00036
Arap3	1.60355	6.13E-06	0.00055
Slc16a11	1.53873	4.54E-07	6.34E-05
Cd200r1	1.52741	1.22E-10	4.28E-08
Calcb	1.52232	6.50E-09	1.53E-06
Tulp4	1.50259	2.01E-05	0.0015
C1qtnf6	1.4953	5.13E-05	0.00341
Cela1	1.48275	2.15E-07	3.17E-05

Tmcc3	1.4544	0.00012	0.0067
Mrc2	1.44649	0.00011	0.00627
Ikzf4	1.44494	0.00012	0.00697
Ncf1	1.43251	0.00012	0.00674
Ypel2	1.42453	6.96E-05	0.0044
Klri2	1.4226	0.00015	0.0078
Phactr2	1.41779	0.00016	0.0081
Zfp36l1	1.38954	9.98E-17	6.21E-14
Areg	1.38882	0.00013	0.00727
Ikzf2	1.38669	2.23E-06	0.00024
Cd200r4	1.38615	1.36E-11	5.51E-09
Gm4956	1.36921	2.38E-10	7.13E-08
Plek	1.36312	2.82E-09	6.93E-07
Tnfrsf9	1.34347	2.18E-17	1.47E-14
Nrn1	1.33037	0.00027	0.01287
Crem	1.30179	1.85E-08	3.40E-06
Swap70	1.29715	2.41E-05	0.00176
Lag3	1.2793	5.29E-08	8.57E-06
Casp3	1.27928	1.07E-08	2.22E-06
Sft2d2	1.27599	0.00014	0.00731
Gm4204	1.27513	7.07E-05	0.00444
Itih5	1.26937	0.0005	0.02115
Izumo1r	1.25025	1.25E-05	0.00102
Epdr1	1.23056	0.00081	0.03157
Bcl2l11	1.22926	8.41E-06	0.00072
Tnfsf8	1.19946	0.00025	0.0121
Tmod1	1.19548	0.00097	0.03634
Lrrc9	1.18979	0.00131	0.04555
Mmd	1.18392	8.87E-05	0.00544
Cd200	1.17609	0.00079	0.03128
Pdcd1	1.17208	4.86E-22	6.56E-19
Lyn	1.16191	0.00092	0.03483
Nap1l1	1.14589	3.67E-06	0.00035
Prr5l	1.14017	2.27E-05	0.00167
Tacc2	1.13976	0.0013	0.04555
Ptms	1.13494	0.00043	0.01869
Ephx1	1.12865	6.98E-08	1.09E-05
Ociad2	1.12185	0.00141	0.04893
Smc4	1.11492	1.86E-10	6.01E-08
Samsn1	1.09526	8.20E-10	2.14E-07
Cdkn2c	1.09002	0.00029	0.0138
Ubash3b	1.08135	3.03E-06	0.00031
1700017B05Rik	1.07646	0.00033	0.01522
Srbd1	1.07411	2.12E-05	0.00158
Spp1	1.06839	1.57E-05	0.0012
Il2rb	1.05889	1.79E-18	1.32E-15
Ccrl2	1.05478	5.32E-06	0.00048
Lrmp	1.05404	2.03E-08	3.66E-06
Stk39	1.04986	0.00021	0.01022
Irf8	1.04316	0.00013	0.00723
Abcb9	1.03918	1.68E-09	4.24E-07
Suox	1.01868	0.00086	0.03311
2900026A02Rik	1.01283	6.63E-05	0.00423
Adgrg1	1.0028	2.50E-06	0.00027

Ptger4	-1.0019	4.79E-05	0.00323
Hdac7	-1.023	4.98E-05	0.00333
Irf7	-1.0289	3.68E-05	0.00257
Chd3	-1.0307	6.46E-06	0.00057
Slfn1	-1.0349	0.00038	0.01701
Rtp4	-1.0367	0.00013	0.00713
Sit1	-1.0462	0.0003	0.01403
Glrx	-1.0482	0.00017	0.00867
Bcl11b	-1.062	3.42E-06	0.00034
Hba-a2	-1.0682	0.00013	0.00727
Glipr2	-1.0686	0.00031	0.01472
Fos	-1.1006	3.12E-08	5.37E-06
Cd52	-1.1049	9.16E-37	7.41E-33
Gadd45b	-1.1136	7.91E-05	0.00489
Ifit3	-1.137	0.00126	0.04455
Lpar6	-1.1574	0.00032	0.01474
Itgb7	-1.1651	2.19E-06	0.00024
Ifitm10	-1.1812	1.23E-05	0.00101
Slfn8	-1.1877	0.00041	0.01816
Itga1	-1.1962	0.0006	0.02479
Ly6c1	-1.2046	0.00057	0.02372
Kcnn4	-1.218	4.03E-05	0.00279
Cmtm7	-1.2191	4.15E-05	0.00284
Dnajc15	-1.2274	7.44E-10	2.01E-07
Rflnb	-1.24	0.00078	0.03092
Pmf1	-1.2497	0.0006	0.02467
Gpr132	-1.2519	3.44E-05	0.00244
Ier3	-1.2531	0.00049	0.0208
Fam78a	-1.2945	1.46E-05	0.00114
Oas3	-1.3569	0.00033	0.01522
St3gal6	-1.3614	3.09E-06	0.00031
Atp8b4	-1.3813	0.00013	0.00725
Gcnt2	-1.4005	0.0002	0.01004
Epsti1	-1.4357	8.70E-14	4.40E-11
Hid1	-1.4483	5.36E-05	0.00353
Gzmb	-1.486	6.94E-35	2.81E-31
Tspan31	-1.537	1.26E-05	0.00102
Atp8a2	-1.5393	4.57E-05	0.00311
Dkkl1	-1.5732	6.09E-06	0.00055
Dtx1	-1.5845	2.16E-08	3.81E-06
Gpr183	-1.5889	1.59E-06	0.00019
Arid5a	-1.5932	9.52E-08	1.45E-05
Ifit1bl1	-1.6475	1.23E-06	0.00016
Ccr5	-1.6809	9.81E-09	2.09E-06
Cxcr3	-1.739	7.74E-22	8.95E-19
Hmga1	-1.8842	3.13E-07	4.53E-05
Gramd3	-1.9514	1.80E-10	6.01E-08
Ccr2	-1.9884	1.37E-08	2.72E-06
Pag1	-2.0968	1.38E-08	2.72E-06
Sema4a	-2.2188	1.66E-14	9.62E-12
S100a4	-2.2248	6.70E-20	6.78E-17
Ly6a	-2.4015	7.63E-28	1.23E-24

Table 4. DEGs between liver CXCR6^{hi} CD45.1^{+}CD8^{+} T cells and spleen CX$_3$CR1^{+} CD45.1^{+}CD8^{+} T cells after resolved Ad-CMV-GOL infection: Significantly regulated genes liver CXCR6^{hi} cells (n=200)

Genes	log2FC CXCR6^{hi}	p-value	padj
Fos	2.480856853	7.06E-20	3.04E-17
Egr1	2.348582548	1.23E-10	2.01E-08
Ier5l	2.316917575	2.47E-07	2.10E-05
Actn2	2.263243597	5.26E-11	8.89E-09
Tnfaip3	2.248862007	8.65E-33	9.10E-30
Hic1	2.195003877	1.42E-07	1.26E-05
Atp8a2	2.194828861	9.59E-06	0.000639315
2900026A02Rik	2.1303442	1.09E-06	8.49E-05
Fosb	2.124801866	5.42E-07	4.38E-05
Nr4a2	2.051316017	1.81E-17	6.11E-15
Xcl1	2.018805827	3.88E-12	7.65E-10
Cish	1.945654927	1.84E-15	4.82E-13
Osgin1	1.926046542	3.83E-09	4.77E-07
Cd160	1.912658485	1.92E-20	8.63E-18
Rgs2	1.875919699	3.61E-13	7.76E-11
Jun	1.867041768	6.39E-12	1.23E-09
Prrt1	1.853652842	0.000185887	0.008538181
Lilrb4a	1.839732991	4.15E-10	6.13E-08
Dusp1	1.824919748	5.35E-35	8.43E-32
Per1	1.782930576	8.86E-06	0.000594319
Spry1	1.725305957	0.000194556	0.008850446
Ppp1r15a	1.646199817	8.05E-16	2.31E-13
Rgs1	1.629054279	1.88E-33	2.23E-30
Ptger4	1.58932909	2.31E-07	2.02E-05
Dusp2	1.58762832	1.26E-40	2.99E-37
Junb	1.569536294	1.86E-63	1.76E-59
Gzmb	1.562657765	3.85E-38	7.28E-35
D8Ertd82e	1.55973393	0.000363203	0.015342085
Fgl2	1.531831856	1.21E-08	1.36E-06
Abi3	1.472866	4.67E-06	0.000334556
Dusp6	1.416296983	0.000239179	0.010725643
Cxcr3	1.408380037	3.21E-13	7.07E-11
Bhlhe40	1.402905508	1.32E-12	2.66E-10
Plk3	1.394657869	0.000568659	0.021961843
Art2b	1.371333143	0.000123143	0.006037197
Nr4a1	1.356273264	3.80E-06	0.000276535
Rtp4	1.33073391	5.54E-05	0.00304692
Isg15	1.322592746	0.000990057	0.034189492
Socs3	1.301582833	0.001281727	0.04285406
Ccl4	1.277297683	6.79E-51	3.21E-47
Rpl36-ps3	1.262892373	0.000230302	0.010376743
Trbv12-1	1.251722529	3.86E-06	0.000279065
Cd69	1.247293094	1.08E-05	0.000705858
Cd7	1.235835931	5.02E-23	2.38E-20
Rgs3	1.234398593	0.000104986	0.005255946
Glrx	1.222840047	0.000370411	0.015577026
Coq10b	1.205641096	0.001237446	0.041520256
Fosl2	1.195447857	0.000943783	0.033094053
Hbb-bs	1.173217934	0.000837546	0.030142116
Abcb1a	1.139861232	0.000408521	0.016879589

Gadd45b	1.137853481	0.000520874	0.020621396
Adgrg1	1.131389952	0.000655387	0.02480509
Trbj2-7	1.117048804	0.000617601	0.023563487
Plcxd2	1.102480904	0.000509923	0.020358185
Socs1	1.095610788	0.000142162	0.006659074
Lrrk1	1.094512045	8.52E-05	0.004452484
Ccl3	1.08655553	2.58E-18	9.03E-16
Klf6	1.083500745	1.33E-10	2.14E-08
Zfp36l2	1.07999993	2.90E-05	0.001746872
Ly6a	1.061318895	1.06E-06	8.35E-05
Cxcr6	1.051444744	2.51E-16	7.65E-14
Traf1	1.050326807	3.73E-06	0.000273353
Ifi27l2a	1.045604493	1.32E-09	1.79E-07
Chsy1	1.011450864	0.000862753	0.030689372
Serpina3g	1.007448427	8.29E-06	0.000560031
Pnrc1	1.000762867	6.76E-12	1.28E-09
Atp2b1	-1.015438123	0.00013112	0.006300694
H2-Q10	-1.023817536	0.000261622	0.011460517
Pycard	-1.025884014	2.17E-08	2.23E-06
Apoe	-1.035956224	0.000797217	0.029120644
Kcnab2	-1.04849778	0.000127931	0.006239615
Gm8203	-1.055060534	4.58E-05	0.002611911
S1pr4	-1.061927278	2.13E-08	2.22E-06
Iqgap2	-1.063781795	0.001530932	0.04973746
Lfng	-1.081623018	7.74E-07	6.20E-05
Spn	-1.09202434	3.28E-08	3.23E-06
Tnfaip8l2	-1.092440549	0.000104394	0.005254106
Nptn	-1.105025087	6.59E-05	0.00354092
Racgap1	-1.110584694	0.000944345	0.033094053
Reep5	-1.151457901	6.03E-10	8.65E-08
Vim	-1.155677205	4.90E-15	1.22E-12
Wdr95	-1.174505275	0.001343631	0.044452586
Pik3r5	-1.174606123	1.32E-05	0.000836425
Plek	-1.175739665	1.78E-05	0.00111832
Klrk1	-1.178510859	3.73E-11	6.53E-09
Stk38	-1.19055352	0.00010893	0.005396292
Fam65b	-1.215644115	7.99E-06	0.000543737
Add3	-1.216048577	0.000205325	0.009295607
Il17ra	-1.223105126	2.80E-05	0.001709358
Atp11b	-1.236831718	1.32E-05	0.000836425
Arhgef18	-1.258942106	0.000602116	0.023065682
Rgcc	-1.28638978	0.000929748	0.032825639
Tmem109	-1.293753397	0.000336774	0.014289501
AI467606	-1.32492079	5.64E-09	6.76E-07
Gna15	-1.333379604	1.04E-07	9.59E-06
Capn2	-1.343726192	0.000128987	0.006258866
Tagln2	-1.351085437	1.39E-13	3.14E-11
H2-DMa	-1.354733901	0.000120856	0.005955925
Lpin1	-1.372545613	8.80E-05	0.004573309
Lef1	-1.374261358	7.76E-06	0.000532008
Pde2a	-1.412192943	0.000751866	0.027789665
Capg	-1.415540077	2.44E-07	2.10E-05
Sgk1	-1.421686819	1.02E-09	1.40E-07
Lyz2	-1.422342543	3.72E-09	4.69E-07

Gprin3	-1.433422958	0.000536316	0.021056523
Cxcr4	-1.470113968	8.09E-05	0.004250886
H2-Oa	-1.476711948	0.000983847	0.034099497
Cd81	-1.484936465	0.000846199	0.030214097
Klhl6	-1.501739702	8.44E-07	6.71E-05
Igkc	-1.50597908	1.25E-05	0.000805999
Ighm	-1.512715264	4.92E-05	0.002752567
Slco3a1	-1.540343577	0.000646782	0.02457772
Pxylp1	-1.543910206	0.000584453	0.022480054
Rara	-1.56425959	0.000140837	0.006629829
Ebf1	-1.569560197	0.001433966	0.046786844
Tppp3	-1.575423552	0.001076779	0.036821699
Bank1	-1.592700685	0.001323149	0.044052834
Lrrc75b	-1.598287334	0.000978566	0.034041147
Slc40a1	-1.605936243	0.001127184	0.038364792
Pkig	-1.613723936	0.000969221	0.033840488
Klrb1c	-1.618140141	0.000246559	0.010952783
Itgb1	-1.626275618	4.92E-16	1.45E-13
Ccl9	-1.628342907	0.000742948	0.027567743
Smpdl3b	-1.632370921	0.00010382	0.00525316
Ly6c1	-1.636270579	2.40E-08	2.41E-06
Ctsh	-1.63765752	0.000551824	0.021575865
Ahnak	-1.656384915	3.09E-29	2.66E-26
Sh3bp5	-1.657688137	0.000319702	0.013685175
Pld4	-1.660163612	0.000450975	0.018313859
Il6ra	-1.670832842	0.000759426	0.027959892
Klra9	-1.671310851	0.000523636	0.020644347
Rasa3	-1.686801759	3.64E-10	5.46E-08
Acss2	-1.692583064	5.70E-06	0.000402516
Ly6c2	-1.702551666	4.77E-34	6.45E-31
Nfic	-1.710492014	9.17E-05	0.004743281
Dok3	-1.728220259	0.000398002	0.016663261
Fcrla	-1.755021139	0.000132581	0.006335764
Anxa1	-1.756287857	0.000131181	0.006300694
Cd24a	-1.773111553	0.000102663	0.005222549
Arl4c	-1.78226885	6.52E-10	9.20E-08
Sema4b	-1.783113375	0.000321085	0.013685175
Apobec2	-1.78547566	0.000317452	0.013653334
Klf2	-1.792970006	2.83E-14	6.86E-12
Gm2a	-1.814023892	1.58E-08	1.72E-06
Atp1b3	-1.81473838	2.94E-26	1.74E-23
Tyrobp	-1.837322443	1.65E-08	1.77E-06
Cd83	-1.867349209	0.000133304	0.006338322
Rap1gap2	-1.878649513	4.88E-05	0.002750624
Plbd1	-1.905372629	0.000107944	0.005375634
Fcer2a	-1.909466548	4.63E-05	0.002625909
Flna	-1.912491179	2.18E-10	3.38E-08
Pdlim1	-1.935621013	3.55E-05	0.00207528
Ccr7	-1.971990888	4.12E-05	0.002376334
Blvrb	-1.97260782	5.75E-05	0.003126442
Stard10	-1.973253466	4.04E-07	3.32E-05
Fcrl1	-1.978382351	6.44E-05	0.003482652
Siglecg	-2.017312413	4.47E-05	0.002561117
H2-DMb2	-2.041240998	1.75E-08	1.84E-06

Borcs7	-2.059784536	1.13E-07	1.03E-05
Fcmr	-2.087874244	1.08E-08	1.23E-06
I830127L07Rik	-2.094310963	1.04E-05	0.000684312
Lmna	-2.096166072	6.09E-06	0.0004269
S100a8	-2.113926377	9.05E-08	8.48E-06
Igkj2	-2.131323664	1.12E-05	0.000724313
Iglc3	-2.155213693	6.07E-11	1.01E-08
Blnk	-2.165037488	6.14E-06	0.000427431
Itgam	-2.182919564	7.09E-06	0.000489704
Gm45552	-2.185409305	9.46E-08	8.78E-06
Klf3	-2.250871071	8.30E-17	2.71E-14
Zeb2	-2.265352572	1.04E-19	4.29E-17
H2-Aa	-2.27134702	7.21E-32	6.82E-29
Ms4a1	-2.282551961	3.93E-08	3.83E-06
As3mt	-2.307410111	1.28E-08	1.43E-06
Txndc5	-2.321882321	2.70E-11	4.81E-09
Cd79a	-2.32890179	2.67E-06	0.000199296
H2-Ab1	-2.334167066	9.82E-42	3.10E-38
Sell	-2.353684818	4.90E-09	6.02E-07
Il18r1	-2.378822831	3.46E-09	4.42E-07
Klrg1	-2.382078697	3.86E-14	8.92E-12
Cd79b	-2.397593215	1.24E-16	3.93E-14
Tnfrsf13c	-2.449415677	7.38E-08	7.13E-06
Cmah	-2.47546517	8.12E-08	7.76E-06
Mzb1	-2.491861591	2.28E-08	2.32E-06
Gm10522	-2.51360247	2.94E-07	2.49E-05
Iglc2	-2.513767226	1.31E-15	3.66E-13
S100a9	-2.555672611	5.40E-09	6.55E-07
Sbk1	-2.560640165	2.22E-07	1.96E-05
Cd22	-2.595308459	1.68E-08	1.79E-06
Cd19	-2.618969427	3.58E-10	5.46E-08
H2-Eb1	-2.704223718	1.76E-25	9.78E-23
Spib	-2.736349982	6.38E-09	7.45E-07
Fcgr2b	-2.815116308	7.73E-10	1.08E-07
Kcnj8	-2.895187448	3.67E-14	8.69E-12
Ighd	-2.907112863	1.70E-15	4.60E-13
Cx3cr1	-2.958415565	5.27E-27	3.33E-24
Il18rap	-2.998147738	5.84E-19	2.21E-16
S1pr1	-3.247555248	3.61E-28	2.63E-25
S1pr5	-3.399122804	8.41E-29	6.63E-26
Cd74	-3.473942778	1.05E-27	7.10E-25
Ly6d	-3.652171204	6.59E-25	3.28E-22

Table 5. DEGs between liver CX_3CR1^+ $CD45.1^+$ $CD8^+$ T cells and liver $CXCR6^{hi}$ $CD45.1^+$ $CD8^+$ T cells after resolved infection: Significantly regulated genes in $CXCR6^{hi}$ cells; FC 2 (n=115)

Genes	log2FC $CXCR6^{hi}$	pvalue	padj
Xcl1	1.7583815	6.029E-11	1.262E-08
Actn2	1.696652	1.244E-08	1.784E-06
Plac8	1.6321373	7.018E-10	1.235E-07
Abi3	1.6070334	1.707E-07	2.003E-05
Cd160	1.5658018	4.282E-16	2.073E-13

Ier5l	1.5428327	2.579E-05	0.0018665
Jun	1.5350408	7.843E-10	1.35E-07
2900026A02Rik	1.4791557	4.757E-05	0.0032035
Lag3	1.4732468	3.198E-05	0.0022722
Nr4a2	1.4716311	9.229E-12	2.383E-09
Lilrb4a	1.4269833	1.275E-07	1.543E-05
Osgin1	1.4061038	1.027E-06	0.0001033
Atp8a2	1.386201	0.0003192	0.0162623
Hic1	1.3603302	6.367E-05	0.0040783
Rflnb	1.3161297	0.0006315	0.0281108
Itga1	1.2874316	0.0006451	0.0283886
Myc	1.2047238	0.000553	0.024899
Slfn8	1.2039377	0.0010853	0.0429207
Padi2	1.1909505	7.179E-05	0.0045203
Cish	1.1821228	9.289E-08	1.16E-05
Cxcr3	1.167006	5.126E-10	9.233E-08
Cd7	1.1531577	1.729E-22	2.231E-19
Dtx1	1.1398741	0.0001134	0.0066531
Egr1	1.138766	0.0002066	0.0115128
Neurl3	1.136565	0.0001815	0.0102591
Ltb	1.1312358	1.858E-10	3.51E-08
Ifi27l2a	1.0651994	2.099E-09	3.251E-07
Rgs3	1.0588617	0.0003158	0.0161966
Rtp4	1.044273	0.0005404	0.0244765
Ly6a	1.0437417	3.243E-07	3.64E-05
Gimap1os	1.0432392	0.0002675	0.0142901
Dusp1	1.0389412	2.643E-15	1.204E-12
Lrrk1	1.0153503	0.0001017	0.0061546
Art2b	1.0034842	0.0012183	0.0476539
Ywhaq	-1.005845	2.358E-05	0.0017231
AB124611	-1.010217	0.0002904	0.0152977
Rap1b	-1.014634	6.537E-07	6.935E-05
Emb	-1.015914	0.000831	0.0351407
Il17ra	-1.02431	0.0002395	0.0129707
Klhl6	-1.025677	0.0008967	0.0367453
Emp3	-1.058072	7.782E-15	3.014E-12
Gm8203	-1.071964	1.04E-05	0.0008478
Lgals1	-1.073683	2.716E-32	2.103E-28
Spn	-1.076946	2.89E-08	4.069E-06
Atp11b	-1.087927	6.187E-05	0.0040266
Capn2	-1.095629	0.0008402	0.0351753
Lgals3	-1.113714	1.465E-16	7.564E-14
Capg	-1.114	3.733E-05	0.0025588
Iqgap2	-1.121207	0.0001682	0.0096474
Tmem109	-1.123766	0.000636	0.0281481
Rora	-1.137345	0.0003515	0.0175656
Reep5	-1.166135	8.115E-10	1.366E-07
Nptn	-1.178867	8.936E-06	0.0007363
Borcs7	-1.182159	0.001234	0.0480072
Acss2	-1.203526	0.000559	0.0250249
Vim	-1.220261	1.42E-17	7.855E-15
Cdc25b	-1.226477	0.0003394	0.0170671
Klrb1c	-1.231937	0.0010826	0.0429207
Rap2a	-1.234758	0.001071	0.0429207

Lef1	-1.23782	2.068E-05	0.0015702
Car5b	-1.260475	0.0010862	0.0429207
Fam65b	-1.275457	8.44E-08	1.108E-05
Plek	-1.27647	3.436E-07	3.802E-05
Nfic	-1.28203	0.0006684	0.0292459
Atp2b1	-1.304356	4.9E-08	6.773E-06
C230096K16Rik	-1.31063	0.0006934	0.0300307
Pogk	-1.355481	0.0004354	0.0212102
Slco3a1	-1.36532	0.0003016	0.0156763
S1pr4	-1.366267	1.226E-13	3.797E-11
Racgap1	-1.373923	3.166E-06	0.000292
Lpin1	-1.392754	8.608E-06	0.0007247
Itgam	-1.414974	0.0002279	0.0124315
D1Ertd622e	-1.416914	5.602E-05	0.0037086
Pik3r5	-1.424647	1.616E-09	2.608E-07
Pdlim1	-1.426465	0.0002151	0.0118982
Pde2a	-1.438326	5.4E-05	0.0036052
Rgcc	-1.479352	7.364E-06	0.0006408
Emp1	-1.496323	0.0001033	0.0062019
I830127L07Rik	-1.504105	9.886E-05	0.0060291
Ddit4	-1.52655	8.759E-06	0.0007295
Rara	-1.531367	1.416E-05	0.0011078
Gna15	-1.565734	1.695E-11	4.103E-09
Tagln2	-1.580813	3.501E-20	3.231E-17
Mt1	-1.589067	1.066E-05	0.0008599
Smpdl3b	-1.589834	8.049E-06	0.000685
Klf3	-1.59873	8.859E-09	1.345E-06
Cxcr4	-1.608299	8.787E-07	9.074E-05
Ahnak	-1.627409	1.649E-27	4.258E-24
Arl4c	-1.647638	1.695E-09	2.679E-07
Gm4208	-1.652504	5.661E-06	0.0004983
Itgb1	-1.654981	8.814E-18	5.251E-15
Fcgr2b	-1.677602	1.404E-05	0.0011078
Rap1gap2	-1.737673	4.542E-06	0.0004138
As3mt	-1.760988	7.946E-07	8.316E-05
Gm10522	-1.801411	2.872E-06	0.000268
Ly6c2	-1.809507	7.643E-18	4.933E-15
Rasa3	-1.823471	1.307E-13	3.892E-11
Atp1b3	-1.839666	5.83E-28	2.258E-24
Zeb2	-1.858922	6.181E-14	1.995E-11
Flna	-1.865784	1.957E-11	4.458E-09
Sgk1	-1.888706	3.755E-20	3.231E-17
Gm45552	-1.900757	9.223E-08	1.16E-05
Ly6c1	-1.971639	4.368E-14	1.471E-11
Sbk1	-1.980167	2.694E-07	3.069E-05
Cmah	-2.01014	1.326E-07	1.58E-05
Klf2	-2.037058	1.751E-19	1.233E-16
Lmna	-2.038537	5.73E-08	7.786E-06
Txndc5	-2.143871	7.245E-12	1.935E-09
Kcnj8	-2.216962	2.907E-10	5.36E-08
Il18r1	-2.310037	1.763E-11	4.138E-09
Il18rap	-2.47214	5.359E-15	2.306E-12
Klrg1	-2.549084	5.901E-20	4.57E-17
Cx3cr1	-2.668959	6.265E-24	9.705E-21

S1pr5	-2.808445	1.257E-21	1.39E-18
S1pr1	-2.876392	1.341E-24	2.596E-21

Table 6. Gene expression of Residency associated genes (identified by GSEA of DEGs between hepatic CXCR6^{hi} and splenic CX$_3$CR1$^+$ CD45.1$^+$ CD8$^+$ T cells after resolved Ad-CMV-GOL with gene profiles of T$_{RM}$ cells from gut, lung, and skin) by liver CXCR6^{hi} CD45.1$^+$ CD8$^+$ T cells and CX3CR1$^+$ CD45.1$^+$ CD8$^+$ T cells after resolved Ad-CMV-GOL liver infection (n=23)

Genes	Log2FC liver CXCR6^{hi} resolved	P-value liver CXCR6^{hi} resolved	Log2FC liver CX$_3$CR1$^+$ resolved	P-value liver CX$_3$CR1$^+$ resolved
Egr1	2.348582548	1.23204E-10	0.81426864	0.017242629
Tnfaip3	2.248862007	8.65227E-33	2.181117997	3.07577E-30
Nr4a2	2.051316017	1.80954E-17	0.446817283	0.11492332
Cish	1.945654927	1.83532E-15	0.601808147	0.0346013
Rgs2	1.875919699	3.60701E-13	1.214623352	7.00565E-06
Per1	1.782930576	8.85638E-06	1.445666172	1.56192E-05
Rgs1	1.629054279	1.88331E-33	0.645365387	7.0649E-05
Junb	1.569536294	1.85942E-63	1.383936114	3.53098E-44
Gzmb	1.562657765	3.84547E-38	0.82245555	5.77924E-11
Aim2	1.475658333	0.002795848	0.348937325	0.226411668
Nr4a1	1.356273264	3.79936E-06	1.737695532	1.41111E-11
Cd69	1.247293094	1.08169E-05	0.461633955	0.112155304
Fosl2	1.195447857	0.000943783	0.85221127	0.008714423
Gadd45b	1.137853481	0.000520874	0.379608728	0.233168968
Hilpda	1.0307553	0.001650076	0.665819666	0.031014374
Csrnp1	1.02773913	0.003892455	1.028642001	0.001020248
Vps37b	0.870691526	3.91745E-07	0.82502047	2.14956E-05
Ubc	0.710816072	1.41508E-10	0.51336175	6.0407E-05
Dgat1	0.681798965	0.152493555	0.355922495	0.298583956
Gna13	0.649073711	0.06168277	0.619073405	0.039583955
Slc3a2	0.630038891	7.76226E-05	0.333113143	0.061944964
Nfil3	0.536799186	0.11607565	0.478988348	0.122058449
Gramd1a	0.526737677	0.02546202	0.320710131	0.176922425

Table 7. Gene expression of Residency associated genes (identified by GSEA of DEGs between hepatic CXCR6^{hi} and splenic CX$_3$CR1$^+$ CD45.1$^+$ CD8$^+$ T cells after resolved Ad-CMV-GOL infection with gene profiles of T$_{RM}$ cells from gut, lung, and skin) exclusively expressed by T$_{RM}$ cells and liver CXCR6^{hi} cells after resolved liver infection (n=26)

Genes	liver CXCR6^{hi} resolved	p-value liver CXCR6^{hi} resolved
Xcl1	2.018805827	3.88323E-12
Ctla4	1.403490047	0.002774578
Sik1	1.283253122	0.005619792
Itga1	1.262928567	0.003297278
Adam19	0.99102026	0.000447945
Neurl3	0.970148533	0.001733172
Il21r	0.954837994	3.54812E-05
Isg20	0.923816414	0.015841093
Inpp4b	0.869238717	0.031388862
Chn2	0.867476716	0.010883312
Cd244	0.86076619	0.001402569
Gbp9	0.825109415	0.048676197

Litaf	0.812225815	0.000997287
Qpct	0.792271634	0.106924384
Tigit	0.705592094	0.038562875
Il4ra	0.634671957	0.137482314
Tnfrsf1b	0.631914626	0.009706186
Ppp1r16b	0.61036247	0.130254804
Rgs10	0.609189097	0.176381129
Cdh1	0.605044721	0.123722032
Gpr65	0.52577646	0.088559734
Prdx6	0.500859717	0.010553817
Tox	0.433604041	0.026069105
Tnfrsf9	0.388100015	0.092771537
Mapkapk3	0.368940773	0.17235339
Hsph1	0.281011531	0.199316165

Table 8. Gene expression of Residency associated genes (identified by GSEA of DEGs between hepatic CXCR6^{hi} and splenic CX$_3$CR1$^+$ CD45.1$^+$ CD8$^+$ T cells after resolved Ad-CMV-GOL and during persistent Ad-TTR-GOL infection with gene profiles of TRM cells from gut, lung, and skin) exclusively expressed by T_{RM} cells and liver CX$_3$CR1$^+$ CD45.1$^+$ CD8$^+$ T cells after resolved liver infection (n=3)

Genes	Log2FC liver CX$_3$CR1$^+$ resolved	p-value liver CX$_3$CR1$^+$ resolved
Skil	0.32844924	0.343827129
Cdkn1a	0.386272216	0.185947718
Tgif1	0.450883911	0.149900758

Table 9. Residency-associated genes (identified by GSEA with DEGs of CXCR6^{hi} CD45.1$^+$ CD8$^+$ T cells after resolved Ad-CMV-GOL or during persistent Ad-TTR-GOL infection compared to splenic CX$_3$CR1$^+$ T cells after resolved Ad-CMV-GOL infection with gene profiles of T_{RM} cells from gut, lung, and skin) (n=38)

Genes	Log2FC CXCR6^{hi} resolved	p-value CXCR6^{hi} resolved	padj CXCR6^{hi} resolved	Log2FC CXCR6^{hi} persistent	p-value CXCR6^{hi} persistent	padj CXCR6^{hi} persistent
Egr1	2.3485825	1.232E-10	2.01E-08	1.7958318	6.825E-06	0.0003438
Tnfaip3	2.248862	8.652E-33	9.096E-30	2.0907254	1.711E-24	8.226E-22
Nr4a2	2.051316	1.81E-17	6.115E-15	2.8509713	2.094E-35	2.014E-32
Xcl1	2.0188058	3.883E-12	7.655E-10	2.0676873	4.024E-12	5.831E-10
Cish	1.9456549	1.835E-15	4.824E-13	1.2401788	7.551E-06	0.0003745
Rgs2	1.8759197	3.607E-13	7.757E-11	0.9211367	0.0025069	0.0565476
Per1	1.7829306	8.856E-06	0.0005943	1.5717145	0.0004024	0.0125247
Rgs1	1.6290543	1.883E-33	2.227E-30	2.0252212	1.552E-46	3.283E-43
Junb	1.5695363	1.859E-63	1.759E-59	1.1556149	1.185E-34	1.045E-31
Aim2	1.4756583	0.0027958	0.0799224	1.6974803	0.0022323	0.0513382
Ctla4	1.40349	0.0027746	0.0795547	2.0472928	2.633E-05	0.0011461
Nr4a1	1.3562733	3.799E-06	0.0002765	0.7507335	0.0223967	0.301443
Sik1	1.2832531	0.0056198	0.1349606	0.8253572	0.1208145	0.8104607
Cd69	1.2472931	1.082E-05	0.0007059	0.6337284	0.0504217	0.5130746
Fosl2	1.1954479	0.0009438	0.0330941	1.616716	6.548E-06	0.0003346
Csrnp1	1.0277391	0.0038925	0.1014612	1.0932966	0.0034871	0.0729051
Adam19	0.9910203	0.0004479	0.0182692	0.46288	0.1372474	0.8461192

Neurl3	0.9701485	0.0017332	0.0548471	1.0856075	0.0006451	0.0189749
Il21r	0.954838	3.548E-05	0.0020753	0.922145	0.0001516	0.0054736
Isg20	0.9238164	0.0158411	0.2846295	0.8931686	0.0255444	0.3319833
Vps37b	0.8706915	3.917E-07	3.251E-05	1.200091	4.763E-12	6.654E-10
Inpp4b	0.8692387	0.0313889	0.4513699	1.460624	0.000326	0.0105473
Chn2	0.8674767	0.0108833	0.2237178	1.9281465	4.954E-10	5.823E-08
Cd244	0.8607662	0.0014026	0.0460802	1.1817416	3.293E-05	0.0014048
Gbp9	0.8251094	0.0486762	0.5721736	0.8392919	0.0598748	0.5665613
Litaf	0.8122258	0.0009973	0.0343139	1.5809001	3.825E-12	5.62E-10
Ubc	0.7108161	1.415E-10	2.232E-08	0.646827	8.469E-07	5.24E-05
Tigit	0.7055921	0.0385629	0.5089009	1.432283	5.376E-06	0.0002802
Dgat1	0.681799	0.1524936	0.999856	0.9762638	0.0570459	0.5481273
Gna13	0.6490737	0.0616828	0.6702022	0.5216836	0.1318915	0.8363722
Tnfrsf1b	0.6319146	0.0097062	0.2054585	1.6091168	7.887E-13	1.245E-10
Slc3a2	0.6300389	7.762E-05	0.0041032	0.523361	0.0017443	0.0418434
Ppp1r16b	0.6103625	0.1302548	0.9591214	1.0649011	0.007944	0.1413813
Nfil3	0.5367992	0.1160757	0.93473	1.5793293	2.715E-07	1.841E-05
Gpr65	0.5257765	0.0885597	0.8175143	0.8945858	0.0033826	0.0712838
Prdx6	0.5008597	0.0105538	0.2198692	0.5220087	0.0098376	0.1621052
Tox	0.433604	0.0260691	0.3965689	1.398898	4.689E-15	9.019E-13
Tnfrsf9	0.3881	0.0927715	0.8375995	1.7840013	3.332E-22	1.137E-19

Table 10. Residency-associated genes (identified by GSEA with DEGs of CXCR6^{hi} CD45.1^{+} CD8^{+} T cells after resolved Ad-CMV-GOL or during persistent Ad-TTR-GOL infection compared to splenic CX$_3$CR1^{+} T cells with gene profiles of T$_{RM}$ cells from gut, lung, and skin), genes expressed in CXCR6^{hi} CD45.1^{+} CD8^{+} T cells after resolved infection and T$_{RM}$ cells from gut, lung, and skin (n=11)

Genes	Log2FC CXCR6^{hi} resolved	p-value CXCR6^{hi} resolved	padj CXCR6^{hi} resolved
Gzmb	1.5626578	3.845E-38	7.277E-35
Itga1	1.2629286	0.0032973	0.0896518
Gadd45b	1.1378535	0.0005209	0.0206214
Hilpda	1.0307553	0.0016501	0.0529255
Qpct	0.7922716	0.1069244	0.9021894
Il4ra	0.634672	0.1374823	0.9816258
Rgs10	0.6091891	0.1763811	0.999856
Cdh1	0.6050447	0.123722	NA
Gramd1a	0.5267377	0.025462	0.3906531
Mapkapk3	0.3689408	0.1723534	0.999856
Hsph1	0.2810115	0.1993162	0.999856

Table 11. Residency-associated genes (identified by GSEA of CXCR6^{hi} CD45.1^{+} CD8^{+} T cells after resolved or during persistent Ad-TTR-GOL infection with gene profiles of T$_{RM}$ cells from gut, lung, and skin), genes expressed in CXCR6^{hi} CD45.1^{+} CD8^{+} T cells during persistent Ad-TTR-GOL infection and T$_{RM}$ cells from gut, lung, and skin (n=3)

Genes	Log2FC CXCR6^{hi} persistent	p-value CXCR6^{hi} persistent	padj CXCR6^{hi} persistent
Crem	1.5224452	7.295E-08	5.704E-06

Tgif1	0.8590905	0.0123971	0.1948715
Skil	0.7288545	0.1154619	0.7921345

Table 12. Downregulated biological processes in liver CD45.1^{+}CD8^{+} CXCR6^{hi} during persistent Ad-TTR-GOL infection in comparison to liver CD45.1^{+}CD8^{+} CXCR6^{hi} after resolved Ad-CMV-GOL infection

Term	Description	LogP	Log (q-value)	Symbols
GO:1902533	positive regulation of intracellular signal transduction	-4.9332	-1.958	Cxcr3,Gcnt2,Gadd45b,Ptger4,S100a4,Lpar6,Glrx,Itga1,Gpr183,Glipr2,Rflnb
GO:0022407	regulation of cell-cell adhesion	-4.8381	-1.956	Ccr2,Ccr5,Dtx1,Gcnt2,Slfn1,Sit1,Pag1,Itgb7,Ptger4,Gpr183,Fos
GO:0002252	immune effector process	-4.5796	-1.834	Ccr2,Gzmb,Ifit3,Ptger4,Sema4a,Irf7,Oas3,Gpr183,Ifit1bl1,Sit1,Pag1
GO:0010632	regulation of epithelial cell migration	-3.2883	-0.833	Ccr5,Sema4a,Hdac7,Glipr2,Itgb7,Cxcr3,Itga1
GO:1900542	regulation of purine nucleotide metabolic process	-3.0288	-0.630	Cxcr3,Ier3,Ptger4,Dnajc15,Fos,Gcnt2,St3gal6,Ccr5
GO:0045597	positive regulation of cell differentiation	-2.9694	-0.589	Ccr2,Ccr5,Fos,Gcnt2,Ptger4,Dkkl1,Atp8a2,Glipr2
GO:0050714	positive regulation of protein secretion	-2.7611	-0.466	Ccr5,Kcnn4,Ptger4,Glrx,Cxcr3,Ccr2,Lpar6,Slfn1,Bcl11b,Itga1,Ier3,Hdac7,Atp8a2,Gadd45b
GO:1901991	negative regulation of mitotic cell cycle phase transition	-2.7149	-0.449	Ier3,Slfn1,Gpr132,Gadd45b,Dnajc15
GO:0060284	regulation of cell development	-2.4321	-0.267	Ccr2,Ccr5,Dtx1,Atp8a2,Bcl11b,Rflnb,Gpr183,Sema4a,Itga1,Itgb7
GO:0051607	defense response to virus	-2.1894	-0.082	Ifit3,Oas3,Ifit1bl1,Ccr5,Ier3,Ptger4,Ifitm10
GO:0031589	cell-substrate adhesion	-1.5933	0.000	Gcnt2,Itgb7,Itga1,Fos,Glrx,Pag1
GO:0010721	negative regulation of cell development	-1.4797	0.000	Ccr5,Dtx1,Rflnb
GO:0030099	myeloid cell differentiation	-1.3463	0.000	Fos,Hba-a2,Gpr183

Table 13. Upregulated biological processes in liver CD45.1^{+}CD8^{+} CXCR6^{hi} during persistent Ad-TTR -GOL infection in comparison to liver CD45.1^{+}CD8^{+} CXCR6^{hi} after resolved Ad-CMV-GOL infection

Term	Description	LogP	Log(q-value)	Symbols
GO:0050866	negative regulation of cell activation	-4.9412	-0.793	Casp3,Lag3,Lyn,Cd200,Samsn1,Ubash3b,Zfp36l1,Pdcd1,Cdkn2c,Swap70,Stk39,Plek,Prr5l,Bcl2l11,Itih5,Adgrg1,Spp1,Ccdc80,Il2rb,Tnfsf8,Heyl,Mmd,Tnfrsf9
GO:0010543	regulation of platelet activation	-3.9342	-0.724	Lyn,Plek,Ubash3b,Tmprss6,Bcl2l11,Zfp36l1,Car2,Casp3,Irf8,Pdcd1,Swap70,Tnfsf8,Twsg1,Spp1,Cela1,Stk39

GO:0071772	response to BMP	-2.7382	-0.188	Heyl,Twsg1,Tmprss6,Rnf165,Zfp36l1,Casp3,Areg,Lyn,Ubash3b
GO:0009725	response to hormone	-2.7342	-0.188	Areg,Zfp36l1,Car2,Lyn,Spp1,Heyl,Tbc1d4,Irf8,Tnfrsf9,Crem,Ephx1,Bcl2l11,Adgrg1
GO:0070227	lymphocyte apoptotic process	-2.5336	-0.119	Bcl2l11,Lyn,Pdcd1
GO:0001906	cell killing	-2.3135	0.000	Bcl2l11,Lag3,Ncf1,Lyn,Swap70
GO:0000122	negative regulation of transcription from RNA polymerase II promoter	-2.1595	0.000	Crem,Irf8,Ikzf2,Cxxc5,Tmprss6,Cela1,Glis1
GO:0006954	inflammatory response	-2.0594	0.000	Lyn,Ncf1,Tnfrsf9,Stk39,Ccrl2,Cela1,Adgrg1,Irf8,Lag3,Bcl2l11,Tnfsf8
GO:0031589	cell-substrate adhesion	-1.935	0.000	Bcl2l11,Spp1,Ccdc80,Epdr1
GO:0097529	myeloid leukocyte migration	-1.8852	0.000	Lyn,Spp1,Swap70,Ccrl2,Rnf165
GO:0071375	cellular response to peptide hormone stimulus	-1.6481	0.000	Zfp36l1,Car2,Tbc1d4,Heyl

6.3 Additional figures

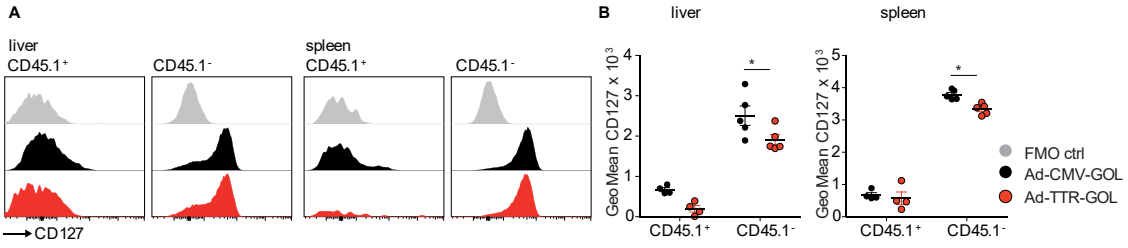

Fig. S 1 Expression of CD127 on hepatic and splenic CD8+ T cells.
A Antigen-specific CD45.1+ and polyclonal CD45.1- CD8+ T cells were analyzed for CD127 expression in liver and spleen on day 45 p.i. with Ad-CMV-GOL and Ad-TTR-GOL. **B** Geometric means of fluorescence intensities of CD127 in liver and spleen.

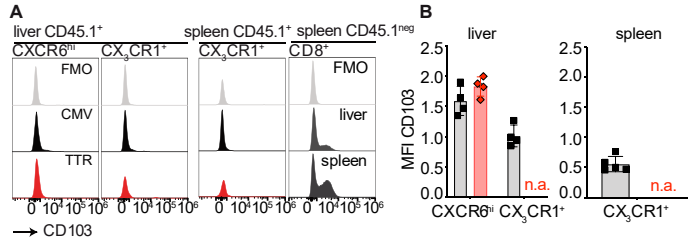

Fig. S 2 Expression of CD103 on hepatic and splenic CD8+ T cells
A Antigen-specific liver CD45.1+ CXCR6hi and CX_3CR1^+ and spleen CX_3CR1^+ CD8+ T cells on d>30 p.i. with Ad-CMV-GOL and Ad-TTR-GOL were analyzed for expression of CD103. Polyclonal spleen $CD45.1^{neg}$ CD8+ T cells were used as a staining positive control. **B** Geometric means of fluorescence intensities normalized to FMO controls.

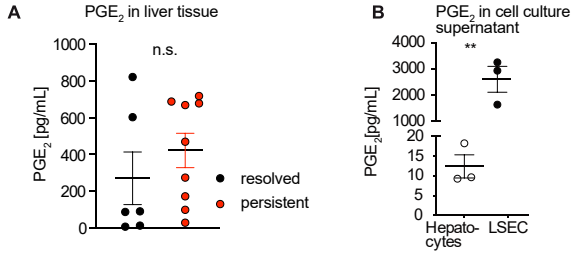

Fig. S 3 PGE_2 concentration in liver tissue and cell culture supernatant
A PGE_2 concentrations in homogenized liver tissue on d>30 p.i. with Ad-CMV-GOL (resolved) and Ad-TTR-GOL (persistent) and **B** in cell culture supernatants from primary murine hepatocytes and liver sinusoidal endothelial cells (LSEC).

6.4 List of Figures and Tables

6.4.1 List of Figures

6.4.2 List of Tables

6.4.3 List of Additional Figures

6.5 Publications

Manske, K. *et al.* Outcome of Antiviral Immunity in the Liver Is Shaped by the Level of Antigen Expressed in Infected Hepatocytes. *Hepatology* 68, 2089–2105 (2018).

6.6 Pre-Publications

Parts of this work were published at the following international conferences:

Bosch M., Manske K., Donakonda S., Wohlleber D., Knolle P., Kallin N.
„Liver-resident memory CD8 T cells develop during chronic viral infection, have reduced effector functions but can be reactivated to clear persistent viral infection of hepatocytes."
Presented at the 5th European Congress of Immunology (ECI), 2018, Amsterdam, Netherlands

Bosch M., Kallin N., Manske K., Donakonda S., Wohlleber D., Knolle P.
„Liver-resident memory $CD8^+$ T cells in chronic viral infection exhibit a unique transcriptional signature and are not terminally exhausted"
Poster presentation at the Annual Meeting of the German Association for the Study of the Liver (GASL), 2019, Heidelberg, Germany

Bosch M., Kallin N., Donakonda S., Manske S., Wohlleber D., Knolle P.
„Identification of the unique phenotype of liver-resident memory $CD8^+$ T cells in chronic viral infection"
Poster presentation at the II Joint Meeting of the German Society for Immunology and the Italian Society of Immunology, Clinical Immunology and Allergology (48th Annual Meeting of the German Society for Immunology, DGfI), 2019, Munich, Germany

Bosch M., Kallin N., Wohlleber D., Knolle P.
„Functional adaptation of the HBV-specific memory $CD8^+$ T cell response in a murine model of chronic HBV infection"
Poster presentation at the International HBV Meeting, 2019, Melbourne, Australia

7 Acknowledgments

During my time at the Institute of Molecular Immunology, I received much support and assistance.

I want to thank my supervisor Percy Knolle, who supported my project with inspiring discussions and constructive advice. I was able to work on a project of personal interest, learn new methods, was encouraged to develop my own ideas, and able to visit national and international conferences. I also want to thank my second supervisor Dietmar Zehn, who contributed to this work with helpful discussions.

I thank my mentor and the third member of my thesis advisory committee, Nina Kallin, who trained me in the lab and helped me throughout my thesis with a great deal of theoretical and practical advice. Especially at the beginning of my thesis, Nina's experience and expertise helped start this project successfully. Nina and I became a good team, and I value her work and way of working together very much. I also want to thank Dirk Wohlleber, who supported my work with great advice and discussions and granted me the use of his adenoviral model systems. Sainitin Donakonda also supported this work with all his expertise and countless analyses, provided me with R scripts, and trained me in bioinformatics, for which I am grateful. I also want to thank all other members and former members of the institute, especially Savvoula Michailidou, Silke Hegenbarth, Anna Hirschberger, Erik Henriss, Katrin Manske, Annika Schneider, Sandra Lampl, Michael Dudek, Max Lüdemann, Felix Bayerl, Philippa Meiser, and everyone else not listed here. I enjoy and value the cooperative, helpful, and friendly atmosphere at our institute and after work. I also thank my former master student Ananthi Kumar for her committed work. Ulla Protzer, Theresa Asen, and Anna Kosinska of the Institute of Virology helped me with both discussions and measurements at the diagnostic lab, for which I am very grateful.

I want to thank Nina Kallin, Annika Schneider, and Julia Bosch for proofreading this thesis.

Finally, I want to thank my family, Karin, Manfred and Julia Bosch, Irene and Ernst Manz, as well as my friends, and, above all, Chris for supporting and motivating me during difficulties and challenges. Cheering me up, having coffee with me, and running and hiking with me helped me stay positive and determined to finish this project successfully.